Design of Quantum Signal Detectors via Coherent Feedback Control

February 2019

Yu Yokotera

A Thesis for the Degree of Ph.D. in Engineering

Design of Quantum Signal Detectors via Coherent Feedback Control

February 2019

Graduate School of Science and Technology
Keio University

Yu Yokotera

Acknowledgments

This thesis summarizes the author's research works during the period of Ph.D. course at Keio University. It would not be completed without the supports of many people.

First of all, I would like to express my deepest gratitude to my supervisor, Naoki Yamamoto, for offering me many interesting research topics about engineering quantum systems, all of them interested me very much. I would like to appreciate him taking time repeatedly to discuss. His critical comments on my research always helped me to solve the problems and to improve my academic writing skills. Without his great supports, I would not have completed any of my research.

I also would like to thank the following sub-chief examiners of this thesis. Professor Shuichi Adachi (Department of Applied Physics and Physico-Informatics) gave me many detailed comments on the future directions of my research from the view of control theory. Professor Toru Namerikawa (Department of System Design Engineering) provided some control methods which will be useful for the future works of this thesis. Assistant Professor Tatsuhiko Koike (Department of Physics) gave me many valuable comments on the references which should be cited and how to write the statement of theorems.

I also thank Yuki Nojiri, who was the double degree student from Technical University of Munich (Germany). We had discussed many times the feedback control theory for quantum amplifiers. He gave me many helpful comments from the view of physics, then I had a great time thanks to him.

Moreover, I would like to thank Yuzuru Kato, who belonged to Yamamoto laboratory. He taught me how to make a presentation as easy as possible to

understand. His broad knowledge of science always interested me, and he listened to my problem about career in the future.

I also thank many lab members for having a good time together and presenting some interesting topics at lab group meeting: the present members (as of February 2019), Kohei Kobayashi, Kensuke Gallock Yoshimura, Masahide Okada, Rion Shimazu, Masaki Tanaka, Masafumi Misa, Shun Ohmura, Sho Sasaki, Yuri Tanaka, and Kentaro Tamura, and the past members (graduated by March 2018), Sanae Iida, Saki Tanaka, Yusuke Ikeda, Yuya Takahashi, Akira Sone, Yachiko Nakagawa, Jun Hirano, Kohei Akahori, Syota Sakamoto, Makito Sato, Yoshiki Kashiwamura, Ryosuke Kuroyanagi, Hideaki Nakao, Makoto Furihata, Tomoaki Mikami, Kenji Oda, Yuji Tanaka, Taishi Watanabe, Kenta Usui, Yoshiki Ohashi, and Akane Takashima.

Finally, I sincerely thank my parents for supporting and encouraging me. I could devoted myself to my research activities thanks to their supports, then they are one of the biggest contributors to my research.

Abstract

High performance signal detectors are one of the indispensable components in quantum information processing for detecting extremely weak signals, such as qubit readout and gravitational wave detection. Although some quantum detectors have been implemented in optics or superconducting circuits, the general method for enhancing their performance has not yet been sufficiently discussed. Actually, for the classical detectors, feedback control is usually used to enhance the detection performance, however its quantum version has not been investigated. This thesis provides some design theories for engineering quantum signal detectors within the framework of feedback control theory. In particular, this thesis focuses on the following key devices: quantum opto-mechanical sensor and cascaded quantum amplifier. The control problems are formulated within the framework of coherent feedback control, which does not contain any measurement component.

Chapter 1 summarizes the background of quantum signal detection and describes the purpose and contents of this thesis.

Chapter 2 is devoted to some preliminaries, describing classical linear systems, geometric control theory, feedback amplification, and open quantum systems.

Chapter 3 provides a general theory for engineering a quantum sensor achieving back-action evasion (BAE), based on the geometric control theory. Also, the general theory is used to show a physical implementation of the BAE controller. Moreover, a controller design is demonstrated for a practical situation where some experimental imperfections are present.

Chapter 4 discusses feedback methods for suppressing characteristic uncertainty of a cascaded quantum amplifier. In particular, as a most basic setup,

the following two types of feedback control methods are considered: cascade connection of feedback-controlled amplifiers, and single feedback control for cascaded amplifier. To compare the robustness of the above two feedback schemes, the sensitivity functions are defined. It is shown that the latter control method is better in the sense of sensitivity.

Chapter 5 summarizes the results of this thesis and discusses some future works.

Notation

$\mathbb{R}$	set of real numbers
$\mathbb{C}$	set of complex numbers
$\mathbb{R}^n$	set of n - dimensional real column vector
$\mathbb{C}^n$	set of n - dimensional complex column vector
$\mathbb{R}^{m\times n}$	$m \times n$ real matrix
$\mathcal{X}^\perp$	orthogonal complement of a linear space $\mathcal{X}$
I_n	$n \times n$ identity matrix
O_n	$n \times n$ zero matrix
$A = (a_{ij})$	a matrix whose (i, j) element is a_{ij}
$A^\top$	transpose of matrix A, $A^\top = (a_{ji})$
$A^\sharp$	element-wise complex conjugate, $A^\sharp = (a^*_{ji}) = (A^\dagger)^\top$
$A^\dagger$	Hermitian conjugate of matrix A, $A^\dagger = (A^*)^\top$
$\Re(\cdot)$	real part of $(\cdot)$
$\Im(\cdot)$	imaginary part of $(\cdot)$
$\mathrm{Ker}\, A$	kernel of matrix A, $\mathrm{Ker}(A) = \{x \mid Ax = 0\}$
$\mathrm{Im}\, A$	image of matrix A, $\mathrm{Im}(A) = \{y \mid y = Ax, \forall x\}$
δ_{ij}	Kronecker delta function
$\delta(t - t')$	delta function
$\mathrm{tr}A$	trace of matrix A

Contents

List of Figures

List of Tables

Chapter 1

Introduction

1.1 Background

1.1.1 Quantum Sensing

Sensing technology is quite indispensable to our daily life, because it plays a role of extracting real-world information and transferring it to a central computer system. In order to develop advanced technologies such as quantum computing, bio-imaging, and IoT(Internet of Things)-based smart system, enhancing the performance of sensing system is an important task for engineers. And recently, the use of quantum systems or quantum phenomena has attracted increasing attention for detecting extremely weak signals which are usually undetectable by the classical technologies. Actually, various kinds of quantum sensors have been studied and implemented [1], e.g., opto-mechanical oscillators for gravitational-waves [2, 3, 4], and nitrogen-vacancy centers in diamond for magnetic fields [5, 6, 7]. This research area is called *quantum metrology*, which is expected to provide a breakthrough in many areas of science. Importantly, the quantum sensing is also essential in quantum information technologies such as quantum computing and quantum communication, because the signals that appears in quantum systems are usually very weak.

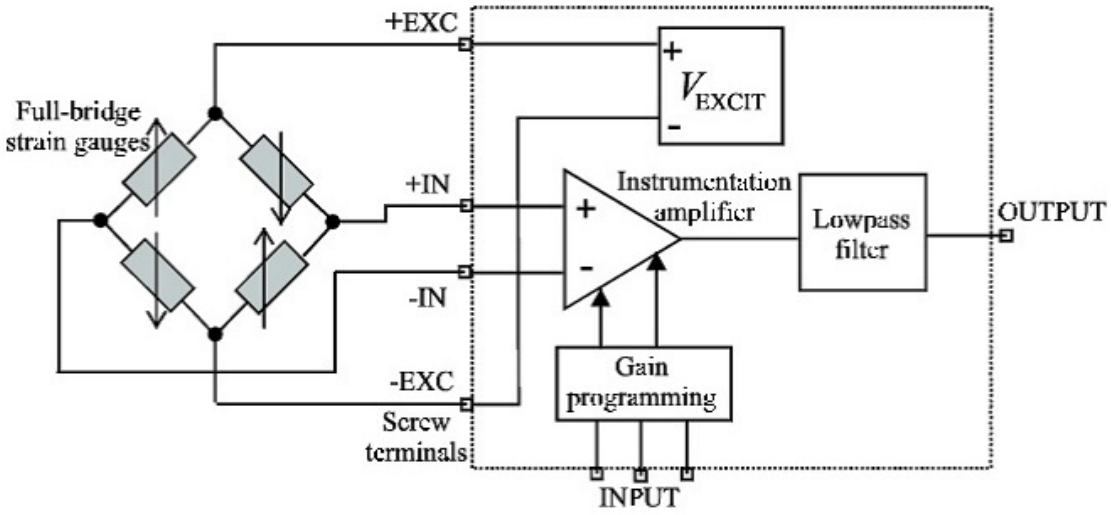

Figure 1.1: Circuit diagram of stress and pressure sensor.

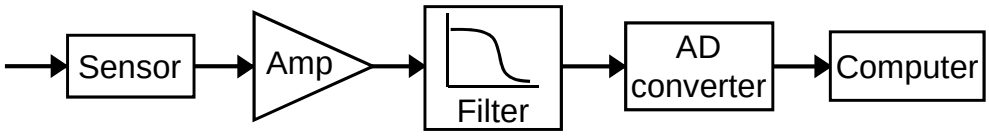

Figure 1.2: Signal flow in a classical sensing system.

1.1.2 Structure of Sensing System and Feedback

To establish a high-precise quantum sensing system, it is significant to consider how the conventional sensing system has realized the detection of target signal in practice. As an example, here focus on the simplified circuit diagram of stress and pressure sensor illustrated in Fig. 1.1 [8]. In the above system, a resistance strain gauge, which is produced from a metallic wire or a semiconductor, serves as a sensor. If the gauge is subjected to the stress, the length of the gauge wire varies which causes the change in gauge resistance. Slight changes in resistance are usually detected and converted into an electric signal by Wheatstone bridge circuit, as shown in Fig. 1.1. Because the signals from the stress gauses are very small, they should be amplified before converting them into digital signals. Also, some

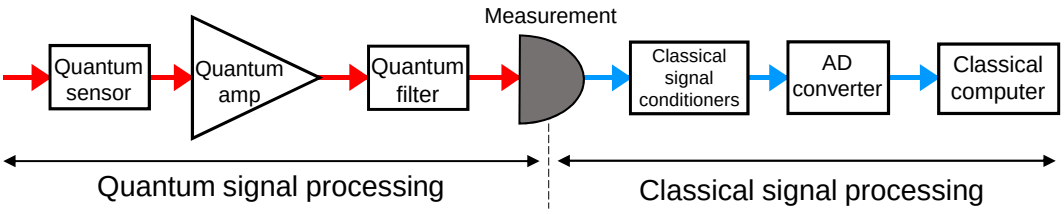

Figure 1.3: Possible structure of quantum sensing system.

unwanted noises contained in the output signals are eliminated by filter circuits. The signal flow explained above is generalized as shown in Fig. 1.2. Importantly, the whole sensing system is composed of some subsystems, and the target signal can be detected by using them in combination: not only a sensor, but also amplifiers and filters constituting the signal conditioning circuit are the key devices. The roles of the above devices are written below.

- **Sensor** is a first element of sensing system that responds to the target signal and converts it to another physical quantity.
- **Amplifier** is an active component that increases the signal level by using supplied energy.
- **Filter** is a device that selectively passes a signal with desired frequency range and removes the others.

Moreover, the notable fact is that, in the well-established sensing system, almost all the above devices are systematically engineered based on the systems and control theory, e.g., see [9, 10, 11]. More specifically, they are analyzed and designed by feedback control explicitly or implicitly, because it is a core technique that has some effects useful for system engineering, for example, noise reduction, linearity improvement, system stabilization, inverse function implementation, and so on.

Now, in the light of the fact explained above, the high-precise quantum sensing system established in the future will be composed of some key elements in the same way as the classical one. Figure 1.3 illustrates the possible structure of quantum sensing system, which includes both quantum and classical subsystems. Red and light blue lines represents the quantum and classical signal flows. At

the measurement component, the quantum signal is converted into the classical one, and it is processed by the classical circuit. Also, at the end of the sensing system, sensors, amplifiers, and filters are replaced by the quantum counterparts that work in the quantum level, i.e., quantum sensors, quantum amplifiers, and quantum filters. This thesis calls them "quantum signal detectors," meaning the key elements that will be integrated in a quantum sensing system for extracting the information of weak signals more precisely. Recently, these devices has been practically implemented in experiments. In addition to the examples of quantum sensors mentioned in the previous subsection, the signal conditioning elements at the quantum level have also been realized, e.g., quantum amplifiers in optics [12, 13] and superconducting circuits [14, 15, 16, 17], and passive optical filters (so called mode-cleaning cavities) [18, 19]. Then, along this research direction, as a next step for the practical realization of quantum sensing system, it is important to develop the systematic methods for engineering high performance quantum signal detectors. However, such general theories has not yet been sufficiently discussed in the quantum regime. Therefore, this thesis aims to develop the systematic methods for engineering each quantum signal detector. The control problems are discussed within the framework of feedback control theory. This methodology has provided many successful results in the classical regime, then if it is appropriately modified, it will be possible to extend the results to the quantum case.

1.2 Control Problems

Toward establishing the general methods for engineering quantum signal detectors, this thesis especially focuses on the quantum sensor and the quantum amplifier, because they are the first two elements in the quantum sensing system shown in Fig. 1.3 and their performance is expected to have an significant effect on the whole detection performance. For realizing ultra-precise quantum signal detection, the following control problems are fundamentally important: (i) noise decoupling for quantum sensor and (ii) stabilizing cascaded quantum amplifier. The details are explained below.

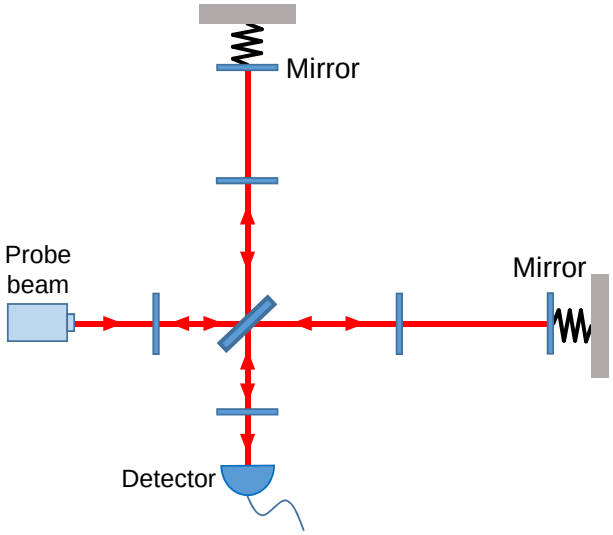

Figure 1.4: Simplified schematic setup of gravitational-wave detector based on the Michelson interferometer.

1.2.1 Noise Decoupling for Quantum Sensor

As mentioned in Subsection 1.1.1, quantum systems can be ultra-sensitive sensors because they are much more sensitive to a small perturbation (weak signal) almost inaccessible within the classical (i.e., non-quantum) regime. However they are also fragile to some unwanted external noises which limits the sensitivity of the quantum sensors, and it becomes difficult to extract the information of target signals from the output of the sensors. Then, for detecting extremely weak signals, engineering a sensor system that beats the sensitivity limitation is one of the most important subjects in quantum information science. Historically, a strong motivation to realize such an ultra-sensitive quantum sensor arises from the field of gravitational-wave detection [2, 3, 20, 21]. Gravitational-waves are ripples in spacetime propagating at the speed of light, which was predicted by Einstein in his general theory of relativity [22, 23]. First construction of detecting instruments started about fifty years ago, and in 2015, Advanced LIGO, which is the newest gravitational-wave detector of US, achieved the first direct detection of gravitational-waves from a black hole merger [24]. Figure 1.4 illustrates the

schematic setup of gravitational-wave detector based on the Michelson interferometer. At the end of the interferometer, the sensor system is composed of the moving mirror and the optical cavity, and they are coupled through the optical radiation pressure acting on the mirror. This is a well-known sensor system called the opto-mechanical oscillator. In fact, a variety of quantum sensors composed of opto-mechanical oscillators have been proposed [2, 3, 4, 25, 26, 27], and several experimental implementations of those systems have been reported not only in the kilogram-scale (used in the gravitational-wave detection), but also in various scales [28, 29, 30, 31, 32].

In general, the above quantum sensors are subjected to many types of noises. If some classical noises such as the seismic noise or the thermal noise can be suppressed by some means, there remains two types of fundamental quantum noises called the *back-action noise* and the *shot noise*. The former one, the back-action noise, comes from the uncertainty of the oscillator's position due to the radiation pressure force fluctuation. On the other hand, the latter one, the shot noise, comes from the photon number fluctuation at the photodetector. A major obstacle to detect a weak signal is that there is a trade-off between the back-action noise and the shot noise, and in a simple setup, the measurement noise power is lower bounded by the so-called *standard quantum limit (SQL)* [2, 20]. To achieve the high-precision detection of a weak signal, beating the SQL is the most significant problem. The question of whether or not it is possible to beat the SQL had been discussed [33, 34], and as a result it was theoretically shown that it is possible [35, 36]. Because the shot noise is known to be unavoidable, the SQL appears mainly due to the presence of the back-action noise. Hence, in order to realize high-precision detection below the SQL, the sensor system has to be carefully engineered so that it evades the back-action noise. That is, the present goal is to realize a *back-action evasion (BAE)* measurement by some means. In fact, many BAE methods have been developed, e.g., the variational measurement technique [37, 38, 39] or the quantum locking scheme [40, 41, 42]. Moreover, towards more accurate detection, recently some high-level approaches to design a BAE sensor can be found, based on those specific BAE methods. For instance, Ref. [43] provides

a systematic comparison of several BAE methods and gives an optimal solution. Also, systems and control theoretical methods have been developed to synthesize a BAE sensor for a specific opto-mechanical system [44, 45]; in particular, the synthesis is conducted by connecting an auxiliary system to a given plant system by *direct-interaction* [44] or *coherent feedback* [45].

Along this research direction, next it appears to be important to develop a general theory to design an auxiliary controller realizing BAE for a given sensor system. This thesis aims to solve the above problem from the view of *geometric control theory*. The details are given in Chapter 3.

1.2.2 Stabilizing Cascaded Quantum Amplifier

An amplifier is one of the most indispensable devices in modern technology [46]. Note that this device is not used in a stand-alone fashion, because its amplification gain cannot be exactly specified due to unavoidable characteristic uncertainty. Actually the amplified output signal produced from a bare amplifier can be largely distorted, and eventually the performance of signal processing is degraded. In 1920s, this issue was solved by Black [47]. He had tackled the problem of improving the performance of repeaters used for a long-distance telephone line, and as a result, proposed the method called the *negative feedback* illustrated in Fig. 1.5. e and E are input and output voltage, μ and β are gains of amplifier circuit and feedback circuit, respectively. A simple calculation leads to

$$E = \frac{\mu}{1-\mu\beta}e \approx -\frac{1}{\beta}e,$$

then, the output becomes independent of the characteristic uncertainty of amplifier. After this invention, the feedback control theory has been further investigated in depth by Blackman and Bode [48, 49]. Also, the method for analyzing the stability of feedback systems has been developed by Nyquist [50]. This feedback amplification method, This theory of feedback amplification, which is now known as one of the most successful examples of control theory, has made a significant contribution to the development of the today's electronic technologies.

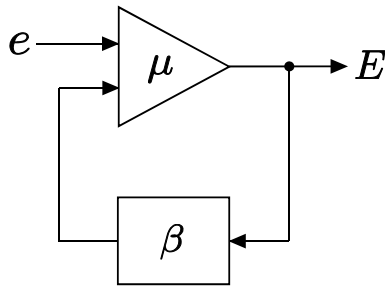

Figure 1.5: Negative feedback amplifier proposed by Black [47].

Next, consider the practical situation where amplifiers are used in a circuit network. It can be seen that some amplifiers are often cascaded to satisfy the required performance, because single amplifier does not always provide sufficient gain and bandwidth due to the gain-bandwidth constraint. Surely feedback control is needed in this case as well, however it is not obvious how to construct a feedback configuration for such a multi-component network, e.g., such problem has been discussed in Refs. [51, 52]. In particular, Ref. [51] shows the most basic sensitivity analysis of cascaded feedback amplifier. Specifically, two types of feedback structures has been considered: the case where controlled amplifiers are connected in series, and the case where a single feedback control is applied to the cascaded amplifier. Then, it has proven that the latter is better in the sense of sensitivity to the uncertainty.

Turning the attention to the quantum regime, the quantum amplifier [53, 54, 55, 56, 57, 58, 59, 60, 61] is expected to serve as a fundamental device in quantum information science, such as quantum sensing for qubit readout [16, 17] and quantum communication [62, 63, 64]. In practice, the quantum amplifier must be stabilized via feedback as in the classical case. In fact, Ref. [65] has developed the theory of feedback stabilization for a *single* quantum amplifier. Moreover, cascading quantum amplifiers has been recently studied, mainly for the enhancement of squeezing or entanglement [66, 67, 68]. Along this research direction, it is important to extend the above feedback theory to the case of cascaded quantum amplifier, which has not been yet established. The question here is how the feed-

back structure should be constructed for cascaded quantum amplifier. This control problem is further non-trivial, because the quantum amplifier is essentially a multi-input and multi-output (MIMO) device and eventually the analysis becomes much more involved than the classical case, as will be shown in Chapter 4.

1.3 Quantum Feedback Schemes

As explained above, this thesis aims to develop the design methods for quantum signal detectors based on the feedback control. Here importantly note that, in the field of quantum engineering, there are two types of feedback control schemes, which are called the *measurement-based feedback* and the *coherent feedback*. This distinction arises from the fact that, in the standard measurement setup, the measured quantum system inevitably affected by a measurement operation and non-commuting observables cannot be simultaneously measured. In the measurement-based feedback scheme, a measurement is performed on the plant system and a classical controller is designed based on the measurement results. The theory of measurement-based feedback control has been well-developed [69, 70] together with the quantum filtering theory [71, 72, 73], and many successful results in experiments can be found; e.g., see Refs. [74, 75]. On the other hand, in the coherent feedback scheme, the feedback system does not contain any measurement component and a controller is designed to be a fully quantum system [76, 77, 78, 79, 80, 81]. Recently, several works have compared the performance of the above two schemes and in some control tasks, it has been shown that the coherent feedback can outperform the measurement-based one [82, 83, 84, 85, 86].

This thesis employs a coherent feedback control because of the following reasons. In the coherent feedback scheme, the information of output from a quantum system can be fully used because of the absence of the measurement process. Thus, it can be said that there are some control tasks which are solvable only within the coherent feedback scheme. Actually, the perfect noise decoupling for linear quantum sensor cannot be solved by the measurement-based feedback scheme [45]. Also, as for the feedback control for the quantum network containing amplifiers,

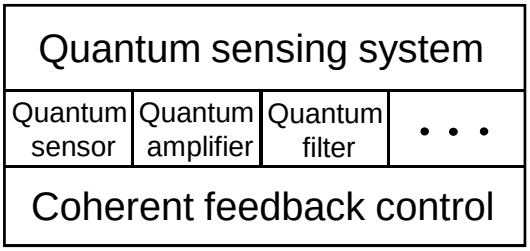

Figure 1.6: Quantum sensing system based on coherent feedback control.

the coherent feedback is a natural counterpart to the classical feedback for the amplifier, because the passive controller such as resistors and capacitors are directly connected to the operational amplifier in electric circuit [46, 51]. Summarizing, this thesis provides the design theories for engineering quantum signal detectors based on the coherent feedback, focusing on the quantum sensor and quantum amplifier. As illustrated in Fig. 1.6, the obtained results in this thesis will serve as the core techniques for realizing high-precise quantum sensing system in the future.

1.4 Organization of Thesis

The structure of this thesis is illustrated in Fig. 1.7. Chapter 2 provides some preliminaries, describing classical linear systems, geometric control theory, feedback amplification, and open quantum systems. Chapter 3 discusses a general theory for engineering a quantum sensor achieving back-action evasion (BAE), based on the geometric control theory. Also, the general theory is used to show a physical implementation of the BAE controller. Moreover, a controller design is demonstrated for a practical situation where some experimental imperfections are present. Chapter 4 studies feedback methods for suppressing characteristic uncertainty of a cascaded quantum amplifier. In particular, as a most basic setup, the following two types of feedback control methods are considered: cascade connection of feedback-controlled amplifiers, and single feedback control for cascaded amplifier. Sensitivity functions are defined to compare their performance. Moreover, for a

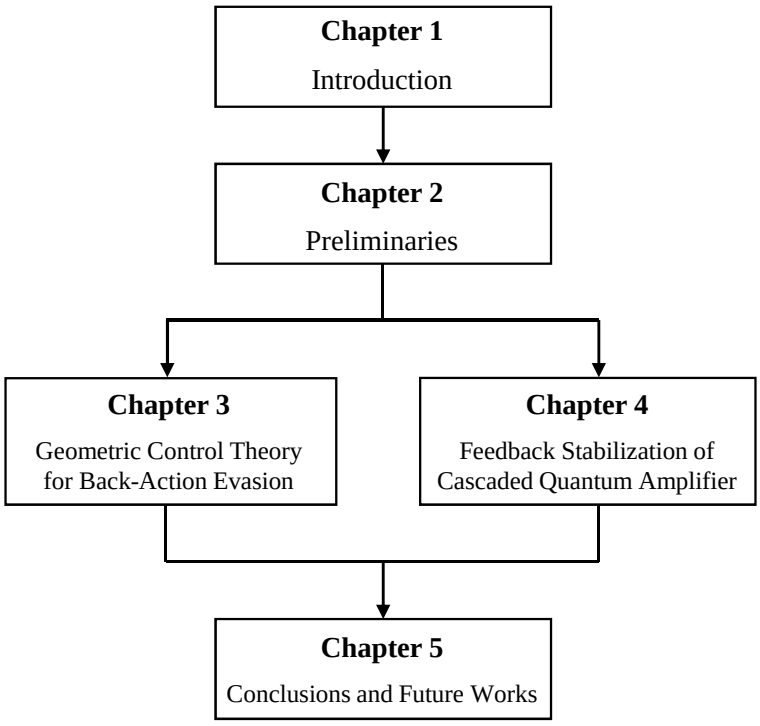

Figure 1.7: Structure of this thesis.

specific system, sensitivity and stability of the cascade feedback systems are numerically investigated. Finally, Chapter 5 summarizes the results of this thesis and discusses some future works.

Chapter 2

Preliminaries

Abstract This chapter reviews some important topics in classical control theory and provides the mathematical backgrounds for describing the dynamics of quantum systems. First, Section 2.1 summarizes the well-developed design methods for classical system engineering. Particularly, one of the most important tools is the geometric control theory, which plays a key role in engineering back-action evading linear quantum sensor, see Chapter 3. The main concepts underlying in the above control theory is so-called *invariant subspaces*; system properties are analyzed and controller synthesis is performed in terms of these subspaces. Also, the theory of feedback amplifier is introduced. The key idea is to connect an amplifier, which is unstable but high gain component, with a passive attenuator, which realizes the robust amplification. This theory will be extended to the case of cascaded quantum amplifier in Chapter 4. Moreover, Section 2.2 describes the special class of quantum systems, so-called *open quantum systems*, interacting with an external environment. The discussion begins with the assumption that, for a Markov approximation to be valid, a coupling between a system and an environment is weak, and the equations representing the time evolution of the open quantum system are shown. Also, some physical quantum devices are modeled based on the above equations.

2.1 Classical Control Theory

2.1.1 Linear Dynamical Systems

This subsection describes the *classical* linear systems. A general form of the linear time-invariant dynamical systems is given by

$$\begin{aligned} \frac{dx(t)}{dt} &= Ax(t) + Bu(t), \\ y(t) &= Cx(t) + Du(t), \end{aligned} \tag{2.1}$$

where $x(t) \in \mathcal{X} \equiv \mathbb{R}^n$ is a vector of system variables with initial condition $x(t_0) = x_0$, $u(t) \in \mathcal{U} \equiv \mathbb{R}^m$ and $y(t) \in \mathcal{Y} \equiv \mathbb{R}^l$ are vectors of input and output, respectively. A, B, C and D are real matrices with appropriate dimensions.

There is another way to describe the linear systems: Now, the Laplace transform of a time-domain function $f(t)$ is defined as

$$F(s) = \mathcal{L}[f(t)] = \int_0^\infty f(t)e^{-st}dt,$$

where s is a complex variable related to a frequency; $s = i\omega$. Then, the input-output relation of linear system (2.1) in the Laplace domain is represented by

$$Y(s) = G(s)U(s), \quad G(s) = C(sI - A)^{-1}B + D,$$

where $U(s)$ and $Y(s)$ are the Laplace transforms of $u(t)$ and $y(t)$, respectively, with the condition $x_0 = 0$. $G(s)$ is called the *transfer function*, which is a complex-valued quantity characterizing the frequency response of linear systems.

Note that the linear systems theory provides some useful concepts for system analysis and design. In particular, the following two questions are fundamentally important: for the linear system (2.1),

Q1. Is it possible to control and move the state x to any desired state by u?

Q2. Is it possible to fully estimate the state x from y?

The concepts of the *controllability* and the *observability* are related to these questions. First, the controllability, which is related to the first question, is defined as follows:

Definition 2.1.1. The linear system (2.1) is said to be *controllable* if, for any initial state $x(t_0)$ and any final state x_1, there exists a finite time $t_1 > t_0$ and input $u(t), t \in [t_0,\ t_1]$ such that $x(t_1) = x_1$. Otherwise, the linear system (2.1) is said to be *uncontrollable*.

The following theorem is useful to study the controllability of the system.

Theorem 2.1.1. The following statements are equivalent:

(1) The linear system (2.1) is controllable.

(2) The following *controllability matrix* has full row rank:

$$\mathcal{C}_u = \begin{bmatrix} B & AB & A^2B & \cdots & A^{n-1}B \end{bmatrix}.$$

(3) The following matrix is positive definite for any $t > 0$:

$$W_c(t) = \int_0^t e^{A\tau} B B^\top e^{A^\top \tau} d\tau.$$

(4) The matrix $[A - \lambda I \ B]$ has full row rank for all λ in $\mathbb{C}$.

The image of the controllability matrix, $\operatorname{Im} \mathcal{C}_u$, is called the *controllable subspace*, and $\operatorname{Ker} \mathcal{C}_u^\top = (\operatorname{Im} \mathcal{C}_u)^\perp$ is called the *uncontrollable subspace*.

On the other hand, the *observability*, which is a dual concept of the controllability, is related to the second question. The definition is given as follows:

Definition 2.1.2. The linear system (2.1) is said to be *observable* if, for any finite time $t_1 > 0$, the initial state $x(t_0) = x_0$ can be determined by the input $u(t), t \in [t_0,\ t_1]$ and the response of the output $y(t), t \in [t_0,\ t_1]$. Otherwise, the linear system (2.1) is said to be *unobservable*.

Similarly, there exists the theorem useful to study the observability of the system.

Theorem 2.1.2. The following statements are equivalent:

(1) The linear system (2.1) is *observable*.

(2) The following *observability matrix* has full column rank:

$$\mathcal{O}_y = \begin{bmatrix} C \\ CA \\ CA^2 \\ \vdots \\ CA^{n-1} \end{bmatrix}.$$

(3) The following matrix is positive definite for any $t > 0$:

$$W_o(t) = \int_0^t e^{A^\top \tau} C^\top C e^{A\tau} d\tau.$$

(4) The matrix $\begin{bmatrix} A - \lambda I \\ C \end{bmatrix}$ has full column rank for all λ in $\mathbb{C}$.

The kernel of the observability matrix, $\operatorname{Ker} \mathcal{O}_y$, is called the *unobservable subspace*, and $\operatorname{Im} \mathcal{O}_y^\top = (\operatorname{Ker} \mathcal{O}_y)^\perp$, is called the *observable subspace*.

2.1.2 Geometric Control for Disturbance Decoupling

This subsection describes the geometric control theory for the disturbance decoupling problem [87, 88, 89, 90, 91]. In this theory, the concept of *invariant subspaces* plays a key role. First, the definitions are shown as follows.

Definition 2.1.3. Let $A : \mathcal{X} \to \mathcal{X}$ be a linear map. Then, a subspace $\mathcal{V} \subseteq \mathcal{X}$ is said to be A-*invariant*, if

$$A\mathcal{V} \subseteq \mathcal{V}.$$

This means that, for any $x_0 \in \mathcal{V}$, it follows that $x(t, x_0) \in \mathcal{V}$ for all $t > 0$, and that A-invariant subspace $\mathcal{V}$ is spanned by the eigenvectors of A.

Definition 2.1.4. Given a linear map $A : \mathcal{X} \to \mathcal{X}$ and a subspace $\operatorname{Im} B \subseteq \mathcal{X}$, a subspace $\mathcal{V} \subseteq \mathcal{X}$ is said to be (A, B)-*(controlled) invariant*, if

$$A\mathcal{V} \subseteq \mathcal{V} \oplus \operatorname{Im} B.$$

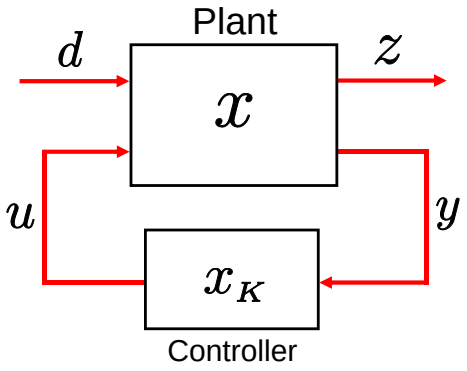

Figure 2.1: General configuration for the disturbance decoupling via a dynamical feedback controller.

Definition 2.1.5. Given a linear map $A : \mathcal{X} \to \mathcal{X}$ and a subspace $\mathrm{Ker}\, C \subseteq \mathcal{X}$, a subspace $\mathcal{V} \subseteq \mathcal{X}$ is said to be (C, A)-*(conditioned) invariant*, if

$$A(\mathcal{V} \cap \mathrm{Ker}\, C) \subseteq \mathcal{V}.$$

Definition 2.1.6. Assume that $\mathcal{V}_1$ is (C, A)-invariant, $\mathcal{V}_2$ is (A, B)-invariant, and $\mathcal{V}_1 \subseteq \mathcal{V}_2$. Then, $(\mathcal{V}_1, \mathcal{V}_2)$ is said to be a (C, A, B)-pair.

Now, from Definition 2.1.4 and 2.1.5, the following lemmas can be obtained.

Lemma 2.1.1. $\mathcal{V} \subseteq \mathcal{X}$ is (A, B)-invariant if and only if there exists a matrix F such that

$$F \in \mathcal{F}(\mathcal{V}) \equiv \{F : \mathcal{X} \to \mathcal{U} \,|\, (A + BF)\mathcal{V} \subseteq \mathcal{V}\}.$$

Lemma 2.1.2. $\mathcal{V} \subseteq \mathcal{X}$ is (C, A)-invariant if and only if there exists a matrix G such that

$$G \in \mathcal{G}(\mathcal{V}) \equiv \{G : \mathcal{Y} \to \mathcal{X} \,|\, (A + GC)\mathcal{V} \subseteq \mathcal{V}\}.$$

Here, the disturbance decoupling problem is described as follows. The system of interest is represented, in an extended form of Eq. (2.1), as

$$\begin{aligned} \frac{dx(t)}{dt} &= Ax(t) + Bu(t) + Ed(t), \\ y(t) &= Cx(t), \quad z(t) = Hx(t), \end{aligned} \tag{2.2}$$

where $d(t)$ is the disturbance and $z(t)$ is the output to be regulated. E and H are real matrices. The other output $y(t)$ may be used for constructing a feedback controller; see Fig. 2.1. The disturbance $d(t)$ can degrade the control performance evaluated on $z(t)$. Thus it is desirable if the system structure can be modified by some means so that eventually $d(t)$ does not affect at all on $z(t)$. Note that this condition is satisfied if the transfer function from $d(s)$ to $z(s)$ is zero for all s, for the modified system. Or equivalently, the controllable subspace with respect to $d(t)$ is contained in the unobservable subspace with respect to $z(t)$, i.e., $\mathrm{Im}\,\mathcal{C}_d \subseteq \mathrm{Ker}\,\mathcal{O}_z$. This control goal is called the disturbance decoupling. Here, describe a specific feedback control method to achieve this goal. The controller configuration is illustrated in Fig. 2.1; that is, the system modification is carried out by combining an auxiliary system (controller) with the original system (plant), so that the whole closed-loop system satisfies the disturbance decoupling condition. The controller with variable $x_K \in \mathcal{X}_K \equiv \mathbb{R}^{n_k}$ is assumed to take the following form:

$$\begin{aligned} \frac{dx_K(t)}{dt} &= A_K x_K(t) + B_K y(t), \\ u(t) &= C_K x_K(t) + D_K y(t), \end{aligned} \tag{2.3}$$

where $A_K : \mathcal{X}_K \to \mathcal{X}_K$, $B_K : \mathcal{Y} \to \mathcal{X}_K$, $C_K : \mathcal{X}_K \to \mathcal{U}$, and $D_K : \mathcal{Y} \to \mathcal{U}$ are real matrices. Then, the closed-loop system defined in the augmented space $\mathcal{X}_E \equiv \mathcal{X} \oplus \mathcal{X}_K$ is given by

$$\begin{aligned} \frac{d}{dt}\begin{bmatrix} x \\ x_K \end{bmatrix} &= \begin{bmatrix} A + BD_KC & BC_K \\ B_KC & A_K \end{bmatrix}\begin{bmatrix} x \\ x_K \end{bmatrix} + \begin{bmatrix} E \\ O \end{bmatrix} d, \\ z &= \begin{bmatrix} H & O \end{bmatrix}\begin{bmatrix} x \\ x_K \end{bmatrix}. \end{aligned} \tag{2.4}$$

The control goal is to design (A_K, B_K, C_K, D_K) so that, in Eq. (2.4), the disturbance signal $d(t)$ does not appear in the output $z(t)$. Here, define

$$A_E = \begin{bmatrix} A + BD_KC & BC_K \\ B_KC & A_K \end{bmatrix}, \tag{2.5}$$

$\mathcal{B} = \mathrm{Im}\,B$, $\mathcal{C} = \mathrm{Ker}\,C$, $\mathcal{E} = \mathrm{Im}\,E$, and $\mathcal{H} = \mathrm{Ker}\,H$. Then, the following theorem gives the solvability condition for the disturbance decoupling problem.

Theorem 2.1.3. For the closed-loop system (2.4), the disturbance decoupling problem via the dynamical feedback controller (2.3) has a solution if and only if there exists a (C, A, B)-pair $(\mathcal{V}_1, \mathcal{V}_2)$ of the linear system (2.2) satisfying

$$\mathcal{E} \subseteq \mathcal{V}_1 \subseteq \mathcal{V}_2 \subseteq \mathcal{H}. \tag{2.6}$$

Note that this condition does not depend on the controller matrices to be designed. Moreover, the following corollary can be used to check if the solvability condition is satisfied.

Corollary 2.1.1. For the closed-loop system (2.4), the disturbance decoupling problem via the dynamical feedback controller (2.3) has a solution if and only if

$$\mathcal{V}_{*(\mathcal{C},\mathcal{E})} \subseteq \mathcal{V}^*_{(\mathcal{B},\mathcal{H})},$$

where $\mathcal{V}^*_{(\mathcal{B},\mathcal{H})}$ is the maximum element of (A, B)-invariant subspaces contained in $\mathcal{H}$, and $\mathcal{V}_{*(\mathcal{C},\mathcal{E})}$ is the minimum element of (C, A)-invariant subspaces containing $\mathcal{E}$. These subspaces can be computed by the algorithms given in Appendix A.

Once the solvability condition described above is satisfied, then the controller matrices (A_K, B_K, C_K, D_K) can be explicitly constructed. The following intersection and projection subspaces play a key role for this purpose; that is, for a subspace $\mathcal{V}_E \subseteq \mathcal{X}_E = \mathcal{X} \oplus \mathcal{X}_K$, define

$$\mathcal{V}_I \equiv \left\{ x \in \mathcal{X} \;\middle|\; \begin{bmatrix} x \\ O \end{bmatrix} \in \mathcal{V}_E \right\},$$
$$\mathcal{V}_P \equiv \left\{ x \in \mathcal{X} \;\middle|\; \begin{bmatrix} x \\ x_K \end{bmatrix} \in \mathcal{V}_E,\ \exists x_K \in \mathcal{X}_K \right\}.$$

Then, the following theorem is obtained:

Theorem 2.1.4. Suppose that $(\mathcal{V}_1, \mathcal{V}_2)$ is a (C, A, B)-pair of the linear system (2.2). Then, there exist $F \in \mathcal{F}(\mathcal{V}_2)$, $G \in \mathcal{G}(\mathcal{V}_1)$, and $D_K : \mathcal{Y} \to \mathcal{U}$ such that

$$\operatorname{Ker} F_0 \supseteq \mathcal{V}_1, \quad \operatorname{Im} G_0 \subseteq \mathcal{V}_2,$$

where $F_0 = F - D_K C,\ G_0 = G - BD_K$. Moreover, there exists $\mathcal{X}_K$ with

$$\dim \mathcal{X}_K = \dim \mathcal{V}_2 - \dim \mathcal{V}_1,$$

and A_E given in (2.5) has an invariant subspace $\mathcal{V}_E \subseteq \mathcal{X}_E$ such that

$$\mathcal{V}_1 = \mathcal{V}_I, \quad \mathcal{V}_2 = \mathcal{V}_P.$$

Also, the matrices (A_K, B_K, C_K) of the dynamical feedback controller (2.3) satisfies

$$\begin{aligned} A_K N &= N(A + BF_0 + GC), \\ B_K &= -NG_0, \\ C_K N &= F_0, \end{aligned} \tag{2.7}$$

where $N : \mathcal{V}_2 \to \mathcal{X}_K$ is a linear map satisfying

$$\operatorname{Ker} N = \mathcal{V}_1.$$

Here, define the following augmented subspace $\mathcal{V}_E \subseteq \mathcal{X}_E$:

$$\mathcal{V}_E \equiv \left\{ \left[\begin{array}{c} x \\ Nx \end{array} \right] \middle| \, x \in \mathcal{V}_2 \right\}.$$

Then, in fact, under the condition given in Theorem 2.1.4, $\mathcal{V}_1 = \mathcal{V}_I$ and $\mathcal{V}_2 = \mathcal{V}_P$ hold, and it follows that

$$A_E \left[\begin{array}{c} x \\ Nx \end{array} \right] = \left[\begin{array}{cc} A + BD_K C & BC_K \\ B_K C & A_K \end{array} \right] \left[\begin{array}{c} x \\ Nx \end{array} \right] = \left[\begin{array}{c} (A + BF)x \\ N(A + BF)x \end{array} \right] \in \mathcal{V}_E,$$

implying that $\mathcal{V}_E$ is actually A_E-invariant. Now, suppose that Theorem 2.1.3 holds, and take the (C, A, B)-pair $(\mathcal{V}_1, \mathcal{V}_2)$ satisfying Eq. (2.6). Then, together with the above result, $A_E \mathcal{V}_E \subseteq \mathcal{V}_E$, the following relationship holds:

$$\operatorname{Im} [E^\top \ O]^\top \subseteq \mathcal{V}_E \subseteq \operatorname{Ker} [H \ O].$$

This implies that $d(t)$ must be contained in the unobservable subspace with respect to $z(t)$, and thus the disturbance decoupling is realized.

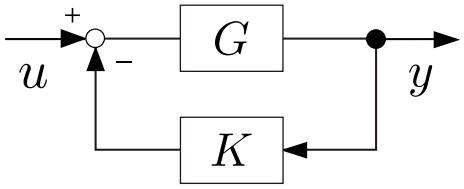

Figure 2.2: Feedback configuration for a classical system.

2.1.3 Stability of Feedback Systems

In designing feedback systems, what should be first considered is the *stability* of the system. This subsection introduces the definition of stability and some methods to determine whether the feedback system is stable or not [9, 10, 11].

First, consider the classical feedback system illustrated in Fig. 2.2. This system is composed of a plant with gain $G(s)$ and another system (controller) with gain $K(s)$. The input-output relation in the Laplace domain is given by

$$y(s) = G^{\mathrm{fb}}(s)u(s), \quad G^{\mathrm{fb}}(s) = \frac{G(s)}{1 + G(s)K(s)}, \tag{2.8}$$

where $L(s) \equiv G(s)K(s)$ is the *loop transfer function*. Note that there are two types of feedback methods. If the output signal is fed back so that it subtracts from the input signal, the controlled system is said to have a *negative feedback*, which is defined as $|1+G(s)K(s)| > 1$ ($|G^{\mathrm{fb}}(s)| < |G(s)|$). On the other hand, if the output signal is fed back so that it adds to the input signal, the controlled system is said to have a *positive feedback*, which is defined as $|1+G(s)K(s)| < 1$ ($|G^{\mathrm{fb}}(s)| > |G(s)|$).

Now the characteristic equation of the feedback system (2.8) is assumed to have the following form with constant real coefficients:

$$1 + G(s)K(s) = a_n s^n + a_{n-1}s^{n-1} + \cdots + a_1 s + a_0 = 0. \tag{2.9}$$

Here, the stability of the feedback system (2.8) is defined with the roots of the above polynomial, called *poles*, as follows:

Definition 2.1.7. The feedback system (2.8) with the characteristic equation (2.9) is stable if and only if all roots have negative real parts, that is, all poles lie in the left-half s-plane.

However, especially for high order polynomials, it is not always easy to calculate the roots of the characteristic equation. Fortunately, some useful stability criteria have been developed to test the stability of the system without actually solving for the roots. The *Routh-Hurwitz criterion* is one of the most well-known stability criteria, which is an algebraic method determining the location of roots. Note that, in the late 1800s, two different criteria were independently developed by Routh [92] and Hurwitz [93], and it is now known that these criteria are equivalent [94]. Here, the test method is summarized based on the former criterion. First, a necessary condition for stability of the system is given as follows:

Theorem 2.1.5. For the feedback system (2.8) with the characteristic equation (2.9) to be stable, it is necessary (but not sufficient) that the following two conditions hold:

(1) All the coefficients of the characteristic equation have the same sign.

(2) None of the coefficients vanish.

Without loss of generality, it is assumed that all the coefficients are positive, which is alternative to condition (1). If the above two conditions are satisfied, a necessary and sufficient condition for stability of the system is given by the following theorem:

Theorem 2.1.6. (Routh's criterion) The feedback system (2.8) with the characteristic equation (2.9) is stable if and only if all the elements in the first column of the following *Routh array* are positive:

$$
\begin{array}{c|ccccc}
s^n & a_n & a_{n-2} & a_{n-4} & \cdots & a_1 \\
s^{n-1} & a_{n-1} & a_{n-3} & a_{n-5} & \cdots & a_0 \\
s^{n-2} & b_{n-1} & b_{n-2} & b_{n-3} & \cdots & \\
s^{n-3} & c_{n-1} & c_{n-2} & c_{n-3} & \cdots & \\
\vdots & \vdots & \vdots & & & \\
s & & & & & \\
s^0 & & & & &
\end{array}
$$

where

$$b_{n-1} = \frac{a_n a_{n-3} - a_{n-1} a_{n-2}}{a_n}, \quad c_{n-1} = \frac{a_{n-1} b_{n-2} - b_{n-1} a_{n-3}}{a_{n-1}}.$$

This criterion also states that, if the elements in the first column are not all positive, the number of sign changes in the column is equal to the number of roots with positive real parts.

As mentioned above, the Routh-Hurwitz criterion provides the information on the *absolute stability*, which refers to whether the system is stable or not. However, it does not tell us the information on the *relative stability*, which refers to how stable the system is. Next, introduce the *Nyquist criterion*, which is useful not only for testing the absolute stability but also for investigating the relative stability of the system. This is a semi-graphical method that provides some information about the stability of the closed-loop system by drawing the *Nyquist plot*. This is the vector plot of the loop transfer function $L(s)$, i.e., the trajectory of $(\mathrm{Re}\,[L(i\omega)], \mathrm{Im}\,[L(i\omega)])$ with $\omega \in (-\infty, +\infty)$. Note again that, for the classical feedback system (2.8), $L(s) = G(s)K(s)$. This stability criterion is based on the *Cauchy's argument principle*, which is a well-known result in complex variable theory. For a complex function $F(s)$, let Z be the number of zeros and P be the number of poles of $F(s)$, respectively. The argument principle is stated as follows:

Theorem 2.1.7. (Argument principle) If a contour mapping of a complex function $F(s)$ in the s-plane, Γ_s, encircles Z zeros and P poles and does not path through any of them, then the contour Γ_s encircles the origin $N = Z - P$ times in the clockwise direction.

This principle is applied to the control theory as follows. Recall that the stability is defined by the poles of the characteristic equation (2.9). Now in the Nyquist criterion, consider $F(s) = 1 + L(s)$ and its contour mapping in the s-plane encircling the entire right-half plane (RHP). Then, Z and P are defined as follows: Z is the number of unstable zeros of $F(s)$, i.e., the number of unstable poles of $G^{\mathrm{fb}}(s)$, and P is the number of unstable poles of $F(s)$, i.e., the number of unstable poles of $L(s)$, respectively. Therefore, through the change of function as $F'(s) = F(s) - 1 = L(s)$, the Nyquist criterion is given as follows:

Theorem 2.1.8. (General Nyquist criterion) The feedback system (2.8) is stable if and only if, for the Nyquist plot with $\omega \in (-\infty, +\infty)$, the number of counterclockwise encirclements of the point $(-1, 0)$ is equal to the number of unstable poles of $L(s)$, that is, $N = -P(Z = 0)$ holds.

Furthermore, if the loop transfer function $L(s)$ has no unstable poles, the above criterion can be simplified as follows:

Theorem 2.1.9. (Simplified Nyquist criterion) The feedback system (2.8) is stable if and only if the Nyquist plot with $\omega \in (0, +\infty)$ does not encircle the point $(-1, 0)$, that is, $N = 0$ holds.

As mentioned before, the Nyquist plot not only tests whether or not the feedback system is stable, but also provides the information on the degree of stability, which is characterized by the concept of *stability margin*. In particular, the *gain margin* and the *phase margin* are the commonly used quantities for measuring the relative stability of the feedback system. The gain margin is the amount of open loop gain in decibels (dB) which can be increased before the feedback system becomes unstable. The definition is given as follows:

$$g_m = 20 \log_{10} \frac{1}{|L(i\omega_p)|} = -20 \log_{10} |L(i\omega_p)|,$$

where ω_p is the *phase-crossover frequency* satisfying $\angle L(i\omega_p) = -180°$; i.e., the smallest frequency where the phase of the loop transfer function is $-180°$. On the other hand, the phase margin is the amount of phase in degrees which can be added before the feedback system becomes unstable. The definition is given by

$$p_m = \angle L(i\omega_g) + 180°,$$

where ω_g is the *gain-crossover frequency* satisfying $|L(i\omega_g)| = 1$; i.e., the smallest frequency where the loop transfer function has unit magnitude. Also, it is assumed that $\angle L(i\omega)$ starts at $0°$ and decreases to $-180°$. These two quantities are evaluated from the Nyquist plot as illustrated in Fig. 2.3. The phase-crossover frequency ω_p is given as the frequency at which the Nyquist plot intersects the negative real axis, and the gain-crossover frequency ω_g is given as the frequency

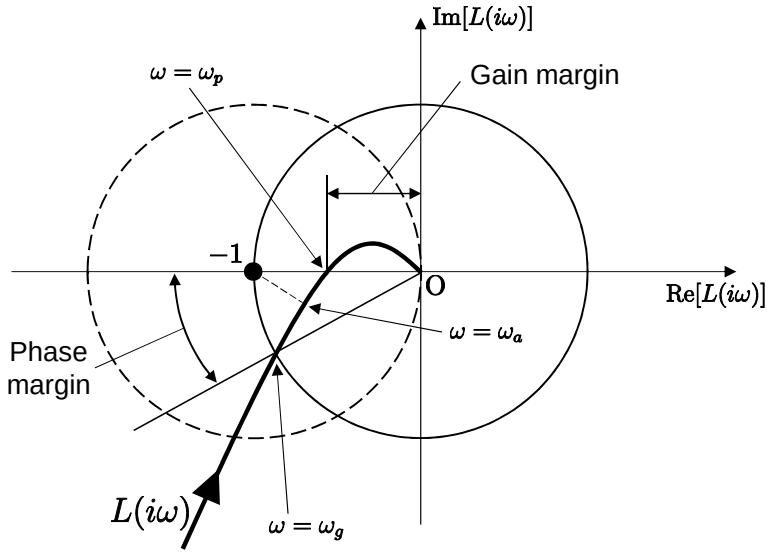

Figure 2.3: Nyquist plot and stability margins.

at which the Nyquist plot intersects the unit circle around the origin (solid line). Then, it can be seen from Fig. 2.3 that the gain margin and the phase margin together characterize how close the Nyquist plot passes from the point $(-1, 0)$, and that the feedback system with large amounts of g_m and p_m is considered to be more relatively stable. Here, note that the negative feedback and the positive feedback, introduced at the beginning of this subsection, can also be expressed in terms of the Nyquist plot. As explained before, the type of feedback is determined by the factor $1+G(s)K(s)$. Now the quantity $|1+G(s)K(s)| = |G(s)K(s)-(-1)|$ can be interpreted the distance between a point on the Nyquist plot and the point $(-1, 0)$. Then, inside the unit circle around the the point $(-1, 0)$ (dashed line) in Fig. 2.3, where $|1 + G(s)K(s)| < 1$ is satisfied, the positive feedback is applied to the system. (Outside this unit circle, the negative feedback is applied.) As a consequence, the closed-loop gain becomes greater than the open gain; $|G^{\mathrm{fb}}(s)| > |G(s)|$, and eventually $|1 + G(s)K(s)|$ reaches a minimum value at the frequency ω_a, see Fig. 2.3. This may cause a peaking to appear in the gain plot of the closed-loop system. In order to suppress the gain peaking, it is necessary to guarantee certain amount of g_m and p_m.

2.1.4 Feedback Amplification and Sensitivity Function

This subsection describes the theory of feedback amplification and the sensitivity function of the feedback system.

The idea of classical feedback amplification is described as follows. For the feedback system (2.8), if the plant has a very high gain (such a system is usually called amplifier), i.e., $|G(s)K(s)| \gg 1$ is assumed here, then, in the limit $|G(s)| \to \infty$, the closed-loop gain leads to

$$|G^{\mathrm{fb}}(s)| \approx \frac{1}{|K(s)|}.$$

This result means that the closed-loop gain becomes independent of variations in $G(s)$, i.e., the robust amplification is realized by taking a passive and attenuating controller, such as a resistor, because the characteristic change in $K(s)$ of those passive devices is generally quite small.

However, the plant gain actually has a finite value. In this case, the robustness of the feedback system is quantified in terms of the *sensitivity function* defined as follows. For the moment, (s) is omitted. Suppose that a small characteristic change ΔG occurs in the gain as $G \to G + \Delta G$, which resulting in the change of closed-loop gain as $G^{\mathrm{fb}} + \Delta G^{\mathrm{fb}}$. Then, the sensitivity function of G^{fb} with respect to G is defined as

$$S = \frac{\Delta G^{\mathrm{fb}}/G^{\mathrm{fb}}}{\Delta G/G}. \tag{2.10}$$

Now, for the closed-loop gain, the small deviation ΔG^{fb} is calculated as

$$\begin{aligned} \Delta G^{\mathrm{fb}} &= \frac{G + \Delta G}{1 + (G + \Delta G)K} - \frac{G}{1 + GK} \\ &\approx \frac{\Delta G}{(1 + GK)^2}, \end{aligned}$$

then the sensitivity function is given by

$$S = \frac{1}{1 + GK}.$$

Therefore, the open-loop gain GK should be carefully designed so that $|S| < 1$ is satisfied while retaining the stability of the closed-loop system.

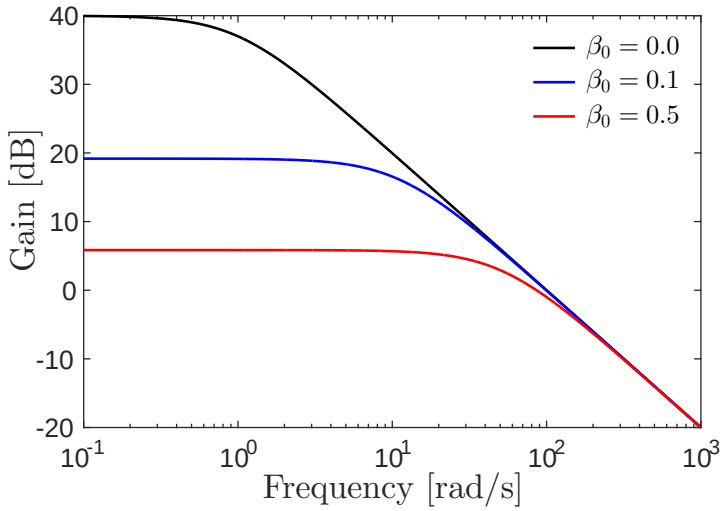

Figure 2.4: Gain plots of the closed-loop transfer function (2.11) with $A_0 = 100$.

Moreover, another important effect of negative feedback is the improvement of the frequency response of a system. Now, suppose that the plant is an amplifier with the following 1st-order low-pass transfer function:

$$G(\omega) = \frac{A_0}{1 + i\frac{\omega}{\omega_0}},$$

where A_0 is the DC gain and ω_0 the cut-off frequency of the original amplifier, and the controller is assumed to have a real feedback gain; $K(\omega) = \beta_0$. Then, the closed-loop transfer function is given by

$$G^{\mathrm{fb}}(\omega) = \frac{A_0}{1 + A_0\beta_0} \frac{1}{1 + i\frac{\omega}{(1+A_0\beta_0)\omega_0}} \equiv \frac{A^{\mathrm{fb}}}{1 + i\frac{\omega}{\omega^{\mathrm{fb}}}}. \tag{2.11}$$

This result indicates that the amplification bandwidth can be extended via negative feedback ($|1 + A_0\beta_0| > 1$) in exchange for the reduction of the amplification gain by a factor $(1 + A_0\beta_0)$. Here, the gain-bandwidth product (GBP) is calculated as

$$\mathrm{GBP} = A^{\mathrm{fb}}\omega^{\mathrm{fb}} = \frac{A_0}{1 + A_0\beta_0} \times (1 + A_0\beta_0)\omega_0 = A_0\omega_0,$$

which is the constant value dependent only on the original amplifier. Because of the above constraint, the gain and bandwidth of an amplifier cannot be freely chosen. Figure 2.4 shows the gain plots of the transfer function (2.11) with $A_0 = 100$ for the three cases $\beta_0 = 0$ (i.e., without feedback), $\beta_0 = 0.1$, and $\beta_0 = 0.5$. It can be seen that the amplification bandwidth becomes larger than that of the uncontrolled system, while the DC gain of the feedback system becomes smaller.

2.1.5 Cascaded Classical Feedback Amplifier

Next, consider the case of cascaded classical amplifier. Also, in this case, feedback stabilization is needed to suppress the amplified fluctuation of the overall gain. However, it is not obvious how to construct a feedback configuration for such a multi-component network due to a greater variety of synthesizing plant and controller. Here, as the most basic study, this subsection focus on the two types of feedback configurations depicted in Fig. 2.5 [51].

Here, it is assumed that both systems are composed of N identical amplifiers characterized by (2.8). In the type-a scheme, shown in Fig. 2.5(a), the same feedback controller with gain K_a is applied to each amplifier. The overall gain is given by the N product of the single closed-loop gain with the structure (2.8):

$$G_a^{\mathrm{fb}} = (G^{\mathrm{fb}})^N = \frac{G^N}{(1 + GK_a)^N}.$$

On the other hand, in the type-b scheme, the output of the terminal amplifier is fed back to the first one through the single controller with gain K_b. The overall gain is given by replacing G with G^N in Eq. (2.8):

$$G_b^{\mathrm{fb}} = \frac{G^N}{1 + G^N K_b}.$$

Now, suppose that the small change $G \to G + \Delta G$ occurs in one of the amplifiers, i.e., the j-th amplifier ($1 \leq j \leq N$). Then the fluctuations of G_a^{fb} and G_b^{fb}

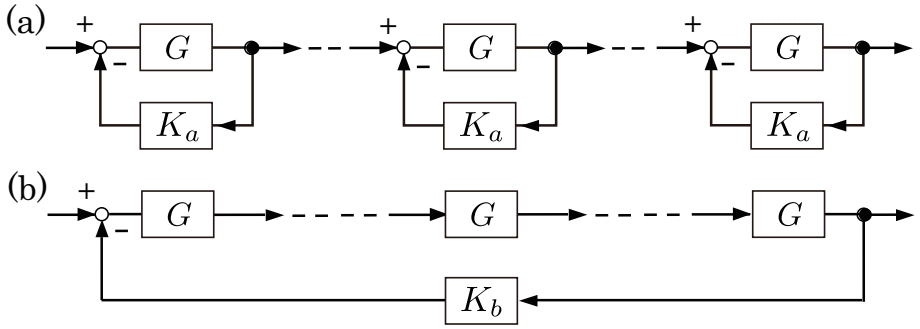

Figure 2.5: Two basic feedback configurations for cascaded classical amplifier; type-a and type-b.

are calculated as follows:

$$\begin{aligned}
\Delta G_a^{\mathrm{fb}} &= \frac{(G+\Delta G)G^{N-1}}{[1+(G+\Delta G)K_a](1+GK_a)^{N-1}} - \frac{G^N}{(1+GK_a)^N} \\
&\approx \frac{G^{N-1}\Delta G}{(1+GK_a)^{N+1}}, \\
\Delta G_b^{\mathrm{fb}} &= \frac{(G+\Delta G)G^{N-1}}{1+(G+\Delta G)G^{N-1}K_b} - \frac{G^N}{1+G^NK_b} \\
&\approx \frac{G^{N-1}\Delta G}{(1+G^NK_b)^2}.
\end{aligned}$$

From Eq. (2.10), the sensitivity functions are given by

$$S_a = \frac{1}{1+GK_a}, \quad S_b = \frac{1}{1+G^NK_b}. \tag{2.12}$$

Then, if the gains of both of the controlled systems are equal and these are smaller than the gain of the non-controlled cascaded amplifier, i.e., $|G_a^{\mathrm{fb}}| = |G_b^{\mathrm{fb}}| < |G|^N$, it follows that

$$\frac{|S_b|}{|S_a|} = \frac{1}{|1+GK_a|^{N-1}} < 1.$$

Thus, the above results shows that the type-b feedback scheme has a better performance than the type-a scheme in the sense of sensitivity.

2.2 Open Quantum Systems

2.2.1 Quantum Stochastic Calculus

This subsection provides the brief review of quantum stochastic calculus. Here, consider the open quantum system with m environmental field channels, which can be characterized by the following three parameters [95]:

$$\mathbf{G} = (\mathbf{S}, \mathbf{L}, H).$$

$\mathbf{S}$ is called the *scattering matrix* of the following form:

$$\mathbf{S} = \begin{bmatrix} S_{11} & \cdots & S_{1m} \\ \vdots & \ddots & \vdots \\ S_{m1} & \cdots & S_{mm} \end{bmatrix},$$

where $\mathbf{S}\mathbf{S}^\dagger = \mathbf{S}^\dagger\mathbf{S} = I$ holds. $\mathbf{L}$ is called the *coupling operator*, which is a column vector of the following form:

$$\mathbf{L} = \begin{bmatrix} \hat{L}_1 & \hat{L}_2 & \cdots & \hat{L}_m \end{bmatrix}^\top.$$

H is the Hamiltonian, which is a self-adjoint operator describing the energy of the system.

As for the environmental fields, let $\hat{a}_i(t)$ be the annihilation operator of the i-th quantum white noise process satisfying the following canonical commutation relation (CCR):

$$[\hat{a}_i(t), \hat{a}_j^*(t')] = \delta_{ij}\delta(t - t').$$

Note that $\hat{a}_i(t)$ is assumed to take the Markovian approximation, that is, it instantaneously interacts with the system. Also, define the quantum Wiener process $\mathbf{A}(t)$ and the gauge process $\mathbf{\Lambda}(t)$ as follows:

$$\mathbf{A}(t) = \begin{bmatrix} \hat{A}_1(t) \\ \hat{A}_2(t) \\ \vdots \\ \hat{A}_m(t) \end{bmatrix}, \quad \mathbf{\Lambda}(t) = \begin{bmatrix} \hat{\Lambda}_{11}(t) & \cdots & \hat{\Lambda}_{1m}(t) \\ \vdots & \ddots & \vdots \\ \hat{\Lambda}_{m1}(t) & \cdots & \hat{\Lambda}_{mm}(t) \end{bmatrix},$$

$$\hat{A}_i(t) = \int_0^t \hat{a}_i(s)ds, \quad \hat{\Lambda}_{ij}(t) = \int_0^t \hat{a}_i^*(s)\hat{a}_j(s)ds,$$

where $\hat{A}_i(t)$ satisfies the CCR $[\hat{A}_i(t), \hat{A}_j^*(t')] = \delta_{ij}\delta(t-t')$, and the following *quantum Itô rule*:

$$\begin{aligned} d\hat{A}_i d\hat{A}_j^* &= \delta_{ij} dt, \\ d\hat{A}_i d\hat{A}_j = d\hat{A}_i^* d\hat{A}_j &= d\hat{A}_i^* d\hat{A}_j^* = 0. \end{aligned}$$

Now, in the Heisenberg picture, the time evolution a system observable $\hat{X}(0)$ is given by

$$j_t(\hat{X}) \equiv \hat{X}(t) = \hat{U}^*(t)\hat{X}(0)\hat{U}(t), \tag{2.13}$$

where $\hat{U}(t)$ is the unitary operator which obeys the following Hudson-Parthasarathy equation [96]:

$$d\hat{U}(t) = \Big(\mathrm{tr}\left[(\mathbf{S}-\mathbf{I})d\mathbf{\Lambda}^\top(t)\right] + d\mathbf{A}^\dagger(t)\mathbf{L} - \mathbf{L}^\dagger\mathbf{S}d\mathbf{A}(t) - \frac{1}{2}\mathbf{L}^\dagger\mathbf{L}dt - i\hat{H}dt\Big)\hat{U}(t), \tag{2.14}$$

with $\hat{U}(0) = I$. From (2.13), (2.14), and the following *Itô product rule* for the product process $X(t)Y(t)$:

$$d[X(t)Y(t)] = dX(t)Y(t) + X(t)dY(t) + dX(t)dY(t),$$

the system observable $\hat{X}(t)$ obeys the following quantum stochastic differential equation (QSDE):

$$\begin{aligned} d\hat{X}(t) = &\Big(i[\hat{H}(t), \hat{X}(t)] + \mathcal{L}_{\mathbf{L}(t)}[\hat{X}(t)]\Big)dt \\ &+ [\mathbf{L}^\dagger(t), \hat{X}(t)]\mathbf{S}(t)d\mathbf{A}(t) + d\mathbf{A}^\dagger(t)\mathbf{S}^\dagger(t)[\hat{X}(t), \mathbf{L}(t)] \\ &+ \mathrm{tr}\Big([\mathbf{S}^\dagger(t)\hat{X}(t)\mathbf{S}(t) - \hat{X}(t)]d\mathbf{\Lambda}^\top(t)\Big), \end{aligned} \tag{2.15}$$

where $\mathcal{L}_{\mathbf{L}}[\bullet]$ is the *Lindblad superoperator* of the following form:

$$\begin{aligned} \mathcal{L}_{\mathbf{L}}[\bullet] &= \mathbf{L}^\dagger \bullet \mathbf{L} - \frac{1}{2}\mathbf{L}^\dagger\mathbf{L}\bullet - \frac{1}{2}\bullet\mathbf{L}^\dagger\mathbf{L} \\ &= \frac{1}{2}\mathbf{L}^\dagger[\bullet, \mathbf{L}] + \frac{1}{2}[\mathbf{L}^\dagger, \bullet]\mathbf{L}. \end{aligned}$$

The output fields $\mathbf{A}(t)^{\text{out}}$ and $\mathbf{\Lambda}(t)^{\text{out}}$ are defined as

$$\mathbf{A}^{\text{out}}(t) = \hat{U}^*(t)\mathbf{A}(t)\hat{U}(t), \quad \mathbf{\Lambda}^{\text{out}}(t) = \hat{U}^*(t)\mathbf{\Lambda}(t)\hat{U}(t).$$

Therefore, the following output relations are obtained:

$$\begin{aligned} d\mathbf{A}^{\text{out}}(t) &= \mathbf{L}(t)dt + \mathbf{S}(t)d\mathbf{A}(t), \\ d\mathbf{\Lambda}^{\text{out}}(t) &= \mathbf{S}^\sharp(t)d\mathbf{\Lambda}(t)\mathbf{S}^\top(t) + \mathbf{S}^\sharp(t)d\mathbf{A}^\sharp(t)\mathbf{L}^\top(t) \\ &\quad + \mathbf{L}^\sharp(t)d\mathbf{A}^\top(t)\mathbf{S}^\top(t) + \mathbf{L}^\sharp(t)\mathbf{L}^\top(t)dt. \end{aligned} \tag{2.16}$$

2.2.2 Linear Quantum Systems

This subsection introduces the special class of quantum stochastic systems. Suppose that a quantum system is composed of n bosonic subsystems, and that the j-th mode can be modeled as a harmonic oscillator with the canonical conjugate pairs (or quadratures) $\hat{q}_j$ and $\hat{p}_j$ satisfying the following CCR:

$$[\hat{q}_j, \hat{p}_k] = \hat{q}_j\hat{p}_k - \hat{p}_k\hat{q}_j = i\delta_{jk}.$$

Now, define the vector of quadratures as

$$\hat{x} = \begin{bmatrix} \hat{q}_1 & \hat{p}_1 & \cdots & \hat{q}_n & \hat{p}_n \end{bmatrix}^\top,$$

then the CCRs are summarized as

$$\hat{x}\hat{x}^\top - (\hat{x}\hat{x}^\top)^\top = i\Sigma_n, \quad \Sigma_n = \operatorname{diag}\{\Sigma, \ldots, \Sigma\}, \quad \Sigma = \begin{bmatrix} 0 & 1 \\ -1 & 0 \end{bmatrix},$$

where Σ is called the *symplectic matrix* and Σ_n is a $2n \times 2n$ block diagonal matrix.

Here, consider a *linear quantum system* which is characterized by the Hamiltonian and the coupling operator of the following forms:

$$\hat{H} = \frac{1}{2}\hat{x}^\top R\hat{x}, \quad \hat{L}_j = c_j^\top \hat{x}, \tag{2.17}$$

where $R = R^\top \in \mathbb{R}^{2n\times 2n}$ and $c_j \in \mathbb{C}^{2n}$. Also, the coupling between the system and m environment fields is described by the following interaction Hamiltonian:

$$\hat{H}_{\text{int}} = i\sum_{j=1}^{m}(\hat{L}_j\hat{A}_j^* - \hat{L}_j^*\hat{A}_j),$$

where $\hat{A}_j(t)$ is the field annihilation operator satisfying $[\hat{A}_j(t), \hat{A}_k^*(t')] = \delta_{jk}\delta(t-t')$. The quadrature pairs of $\hat{A}_j(t)$ are given by

$$\hat{Q}_j = \frac{\hat{A}_j + \hat{A}_j^*}{\sqrt{2}}, \quad \hat{P}_j = \frac{\hat{A}_j - \hat{A}_j^*}{\sqrt{2}i},$$

and define the vector of these quadratures as

$$\hat{W}_j = \begin{bmatrix} \hat{Q}_j & \hat{P}_j \end{bmatrix}^\top.$$

Then, from the QSDE (2.15), the Heisenberg equation of $\hat{x}$ is given by

$$\frac{d\hat{x}(t)}{dt} = A\hat{x}(t) + \sum_{j=1}^{m} B_j \hat{W}_j(t), \tag{2.18}$$

where

$$\begin{aligned} A &= \Sigma_n(R + \sum_{j=1}^{m} C_j^\top \Sigma C_j/2) \in \mathbb{R}^{2n\times 2n}, \\ B_j &= \Sigma_n C_j^\top \Sigma, \\ C_j &= \sqrt{2}[\Re(c_j), \Im(c_j)]^\top \in \mathbb{R}^{2\times 2n}. \end{aligned}$$

Also, from (2.16), the instantaneous change of $\hat{W}_j(t)$ via the system-field coupling is given by

$$\hat{W}_j^{\rm out}(t) = C_j\hat{x}(t) + \hat{W}_j(t). \tag{2.19}$$

Summarizing, as shown above, the linear quantum system is characterized by the dynamics (2.18) and the output (2.19), which are exactly of the same form as those in Eq. (2.1) ($l = m$ in this case). However, note that the system matrices have to satisfy the above-described special structure, which is equivalently converted to the following *physical realizability condition* [80, 81]:

$$A\Sigma_n + \Sigma_n A^\top + \sum_{j=1}^{m} B_j \Sigma B_j^\top = O, \quad B_j = \Sigma_n C_j^\top \Sigma. \tag{2.20}$$

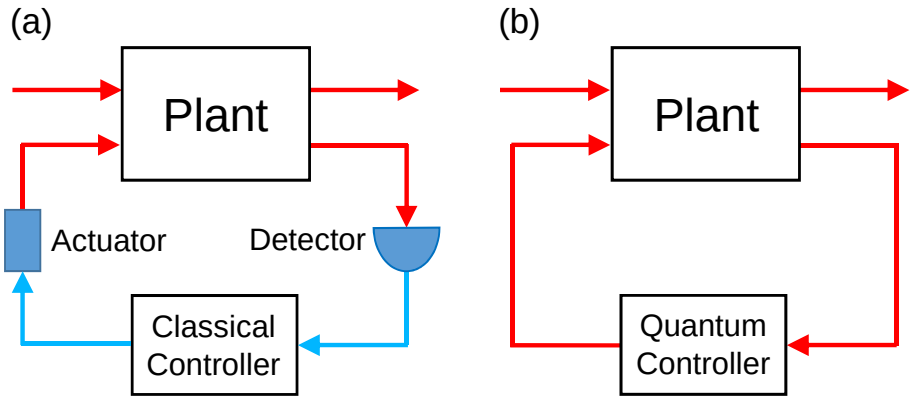

Figure 2.6: General configurations of feedback control for a given plant quantum system: (a) measurement-based feedback and (b) coherent feedback.

2.2.3 Measurement-Based Feedback and Coherent Feedback

This subsection describes two types of feedback control schemes for a quantum system. Recall that it is a critical question whether or not the measurement should be performed on a quantum system. The first one is the measurement-based feedback illustrated in Fig. 2.6 (a). In this scheme, the output fields are measured and a classical controller generates and feeds back the control signal to the plant system based on the measurement results. The measurement process can be formulated as follows. Now, define the output vector $\hat{W}^{\rm out}$ as

$$\begin{aligned}\hat{W}^{\rm out} &= \left[(\hat{W}_1^{\rm out})^\top\ (\hat{W}_2^{\rm out})^\top\ \cdots\ (\hat{W}_m^{\rm out})^\top\right]^\top \\ &= \left[\hat{Q}_1^{\rm out}\ \hat{P}_1^{\rm out}\ \hat{Q}_2^{\rm out}\ \hat{P}_2^{\rm out}\ \cdots\ \hat{Q}_m^{\rm out}\ \hat{P}_m^{\rm out}\right]^\top.\end{aligned}$$

Also, the input vector $\hat{W}$ is defined in the same way. Importantly, note that all the elements of $\hat{W}^{\rm out}$ cannot be simultaneously measured (only half of them can be measured at most), because they do not commute with each other; $[\hat{Q}_i^{\rm out}(t), \hat{P}_j^{\rm out}(t')] = i\delta_{ij}\delta(t-t')$. Therefore, the measurement result given by a homodyne detection can be represented as

$$\hat{y}_1(t) = M_1\hat{W}^{\rm out}(t) = M_1C\hat{x}(t) + M_1\hat{W}(t), \tag{2.21}$$

where $M_1 \in \mathbb{R}^{m\times 2m}$ satisfies

$$M_1 M_1^\top = I_m,\ M_1 \Sigma_m M_1^\top = O_m$$

and all the elements of $\hat{y}_1(t)$ commute with each other. The classical controller produces the control signal based on $\hat{y}_1(t)$ and the actuator generates the quantum control input. Moreover, the canonical conjugate elements to $\hat{y}_1(t)$ is measured by another matrix M_2 as $\hat{y}_2(t) = M_2 \hat{W}^{\rm out}(t)$, where M_1, M_2 satisfy the following relations:

$$M_1 M_2^\top = O_m,\ M_1 \Sigma_m M_2^\top = I_m,\ M_1^\top M_1 + M_2^\top M_2 = I_{2m}.$$

On the other hand, in the coherent feedback scheme shown in Fig. 2.6 (b), the feedback loop does not contain any measurement component and the plant system is controlled by another fully quantum system. In this case, the system matrices of the designed quantum controller are under some constraint. As shown in the previous subsection, first they have to satisfy the physical realizability condition given in (2.20).

2.2.4 Quantum Optical Devises

The general descriptions of the open quantum systems are given in the above subsections. Then, using these backgrounds, this subsection introduces some examples of physical quantum systems and provides their mathematical models. In particular, focus on the typical class of bosonic quantum systems, quantum optics, where the Markov approximation holds. First, consider the static (without dynamics) and passive systems illustrated in Fig. 2.7; a *phase-shifter* and a *beam-splitter*. The phase-shifter (PS) is a single input-output device that generates the phase-shifted field for the input $\hat{A}$. The (S, L, H) parameters are given by

$$S = e^{i\theta},\ \hat{L} = 0,\ \hat{H} = 0,$$

where $\theta \in \mathbb{R}$ is the phase shift. The input-output relation is written as $\hat{A}^{\rm out} = e^{i\theta}\hat{A}$, or equivalently, in the quadrature form, represented as

$$\begin{bmatrix} \hat{Q}^{\rm out} \\ \hat{P}^{\rm out} \end{bmatrix} = S(\theta) \begin{bmatrix} \hat{Q} \\ \hat{P} \end{bmatrix} = \begin{bmatrix} \cos\theta & -\sin\theta \\ \sin\theta & \cos\theta \end{bmatrix} \begin{bmatrix} \hat{Q} \\ \hat{P} \end{bmatrix}.$$

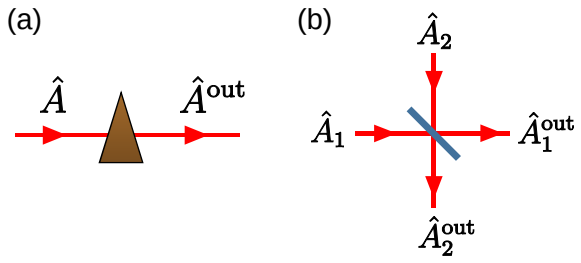

Figure 2.7: Static optical devices: (a) phase-shifter and (b) optical empty cavity.

Next, the beam-splitter (BS) is a 2 input-output device that produces the combination of two input fields $\hat{A}_1$ and $\hat{A}_2$. The (S, L, H) parameters of a phase-free BS are given by

$$S = \begin{bmatrix} \alpha & -\beta \\ \beta & \alpha \end{bmatrix}, \ \hat{L} = 0, \ \hat{H} = 0,$$

where $\alpha, \beta \in \mathbb{R}, \alpha^2 + \beta^2 = 1$ represent the transmissivity and reflectivity of the mirror, respectively. Then, the input-output relation is written by the following transformation:

$$\begin{bmatrix} \hat{A}_1^{\text{out}} \\ \hat{A}_2^{\text{out}} \end{bmatrix} = \begin{bmatrix} \alpha & -\beta \\ \beta & \alpha \end{bmatrix} \begin{bmatrix} \hat{A}_1 \\ \hat{A}_2 \end{bmatrix}.$$

Moreover, here introduce some "dynamical" optical devices. An empty optical cavity is one of the most typical examples. Suppose that an internal cavity mode, characterized by an annihilation operator $\hat{a}$, couples to two external fields $\hat{A}_1$ and $\hat{A}_2$, as illustrated in Fig. 2.8. The (S, L, H) parameters are given by

$$S = I, \ \hat{L} = \sqrt{\kappa_j}\hat{a}, \ \hat{H} = \omega_c \hat{a}^* \hat{a},$$

where $\sqrt{\kappa_j} = cT_j/l$ is the coupling strength between the cavity and j-th external field with c the speed of light, T_j the transmittance of the j-th mirror, and l the cavity length. ω_c represents the resonance frequency of $\hat{a}$. Now, write the system operators in the rotating frame at the resonance frequency of the probe beam ω_0, i.e., an operator $\hat{\mathcal{O}}$ is transformed to a new rotating frame operator as $\hat{\mathcal{O}}_{\text{rot}} = e^{i\omega_0 t}\hat{\mathcal{O}}$. (In what follows, the new rotating frame operators are denoted

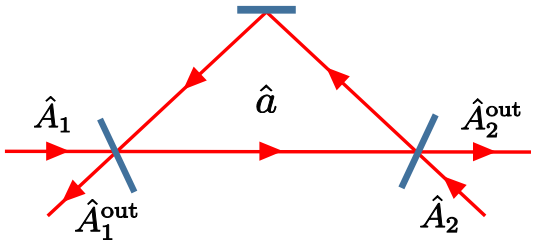

Figure 2.8: Empty optical cavity with two input fields.

again by $\hat{\mathcal{O}}$.) Then, from Eqs. (2.15) and (2.16), the following equations are obtained:

$$\frac{d\hat{a}}{dt} = -(i\Delta + \frac{\kappa_1 + \kappa_2}{2})\hat{a} - \sqrt{\kappa_1}\hat{A}_1 - \sqrt{\kappa_2}\hat{A}_2,$$
$$\hat{A}_j^{\text{out}} = \sqrt{\kappa_j}\hat{a} + \hat{A}_j,$$

where $\Delta = \omega_c - \omega_0$ is the detuning of the cavity.

Moreover, the opto-mechanical oscillator illustrated in Fig. 2.9 serves as a sensor for a very weak force. This system is composed of an optical cavity with a moving mirror. Let $\hat{q}_1$ and $\hat{p}_1$ be the oscillator's position and momentum operators, and $\hat{a}_2 = (\hat{q}_2 + i\hat{p}_2)/\sqrt{2}$ represents the annihilation operator of the cavity mode. The (S, L, H) parameters are given by

$$S = I,\ \hat{L}_1 = \sqrt{\kappa}\hat{a}_2,\ \hat{H} = \frac{\omega_m}{2}(\hat{q}_1^2 + \hat{p}_1^2) - g\hat{q}_1\hat{q}_2 + \omega_c\hat{a}_2^*\hat{a}_2,$$

where the system Hamiltonian is composed of the oscillator's free evolution with resonant frequency ω_m plus the linearized radiation pressure interaction between the oscillator and the cavity field with coupling strength g. The system couples to an external probe field (thus $m = 1$) via the coupling operator $\hat{L}_1$, with κ the coupling constant between the cavity and the probe field. The matrix R and vector c_1 corresponding to Eq. (2.17) are given by

$$R = \begin{bmatrix} \omega_m & 0 & -g & 0 \\ 0 & \omega_m & 0 & 0 \\ -g & 0 & 0 & 0 \\ 0 & 0 & 0 & 0 \end{bmatrix}, \quad c_1 = \sqrt{\frac{\kappa}{2}} \begin{bmatrix} 0 \\ 0 \\ 1 \\ i \end{bmatrix}.$$

In addition, suppose that the moving mirror is driven by an unknown force $\hat{f}(t)$ with coupling constant γ. Then, the system equations are summarized in the quadrature form as follows:

$$\frac{d}{dt}\begin{bmatrix}\hat{q}_1\\ \hat{p}_1\\ \hat{q}_2\\ \hat{p}_2\end{bmatrix} = \begin{bmatrix}0 & \omega_m & 0 & 0\\ -\omega_m & 0 & g & 0\\ 0 & 0 & -\kappa/2 & 0\\ g & 0 & 0 & -\kappa/2\end{bmatrix}\begin{bmatrix}\hat{q}_1\\ \hat{p}_1\\ \hat{q}_2\\ \hat{p}_2\end{bmatrix} - \begin{bmatrix}0 & 0\\ 0 & 0\\ \sqrt{\kappa} & 0\\ 0 & \sqrt{\kappa}\end{bmatrix}\begin{bmatrix}\hat{Q}_1\\ \hat{P}_1\end{bmatrix} + \begin{bmatrix}0\\ \sqrt{\gamma}\\ 0\\ 0\end{bmatrix}\hat{f},$$

$$\begin{bmatrix}\hat{Q}_1^{\mathrm{out}}\\ \hat{P}_1^{\mathrm{out}}\end{bmatrix} = \begin{bmatrix}0 & 0 & \sqrt{\kappa} & 0\\ 0 & 0 & 0 & \sqrt{\kappa}\end{bmatrix}\begin{bmatrix}\hat{q}_1\\ \hat{p}_1\\ \hat{q}_2\\ \hat{p}_2\end{bmatrix} + \begin{bmatrix}\hat{Q}_1\\ \hat{P}_1\end{bmatrix}.$$

The above equations are written in the rotating frame at the frequency of the probe field, and that $\Delta = \omega_c - \omega_0$ is set to be zero. Note that the equations for $\hat{q}_1$ and $\hat{p}_1$ can also be derived from the oscillator's classical equations of motion, see Appendix B, where the definition of $\hat{f}(t)$ is also given.

Finally, introduce the *phase-preserving linear quantum amplifier* [53, 54, 55, 56, 57, 58, 59, 60, 61]. Now, the symbol $\hat{}$ is omitted. First, review the mechanics of quantum amplification. Let $b(t)$ be a field annihilation operator called the *signal*, which satisfies the canonical commutation relation (CCR), $b(t)b^*(t') - b^*(t')b(t) = \delta(t - t')$. The amplifier transforms $b(t)$ to

$$\tilde{b}(t) = gb(t) + \sqrt{g^2 - 1}\, d^*(t),$$

where $d(t)$ is an additional field annihilation operator called the *idler*, which is necessary to preserve the CCR of the output $\tilde{b}(t)$. Also, $g > 1$ is the amplification gain.

In quantum optics, the non-degenerate parametric amplifier (NDPA) [12] shown in Fig. 2.10 is often used. This is an optical cavity with two inputs b_1 (signal) and

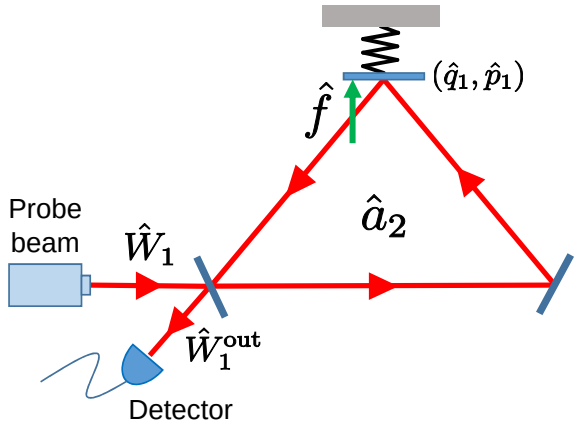

Figure 2.9: Opto-mechanical system for weak force sensing.

b_2 (idler), which are orthogonally polarized. The corresponding internal cavity modes a_1 and a_2 couple with each other at the pumped nonlinear crystal. The mirror M_i is partially transmissive for a_i but perfectly reflective for the other cavity mode. The (S, L, H) parameters are given by

$$S = I, \;\; L_j = \sqrt{\kappa_j}\hat{a}_j, \;\; H = \omega_1 a_1^* a_1 + \omega_2 a_2^* a_2 + i\varepsilon(a_1^* a_2^* e^{-2i\omega_p t} - a_1 a_2 e^{2i\omega_p t}),$$

where κ_j represents the coupling constant a_j and b_j, ω_j the resonant frequencies of a_j $(j = 1, 2)$, ε the parametric coupling strength, $2\omega_p$ the pumping laser frequency satisfying $\omega_1 + \omega_2 = 2\omega_p$. Then, under the ideal setup, i.e., detuning $\Delta_1 = \omega_1 - \omega_p$ and $\Delta_2 = \omega_2 - \omega_p$ are set to be zero, $\kappa_1 = \kappa_2 = \kappa$, and there are no losses, the dynamical equations of the NDPA are given by

$$\frac{da_1}{dt} = -\frac{\kappa}{2}a_1 + \varepsilon a_2^* - \sqrt{\kappa}b_1, \;\; \frac{da_2^*}{dt} = -\frac{\kappa}{2}a_2^* + \varepsilon a_1 - \sqrt{\kappa}b_2^*,$$
$$\tilde{b}_1 = \sqrt{\kappa}a_1 + b_1, \;\; \tilde{b}_2^* = \sqrt{\kappa}a_2^\dagger + b_2^*.$$

The above equations are written in the rotating frame at the half of input laser frequency ω_p. In the Laplace domain, the amplified output signal $\tilde{b}_1(s)$ is, together with the amplified idler $\tilde{b}_2(s)$, represented as

$$\begin{bmatrix} \tilde{b}_1(s) \\ \tilde{b}_2^*(s) \end{bmatrix} = \begin{bmatrix} g_1(s) & g_2(s) \\ g_2(s) & g_1(s) \end{bmatrix} \begin{bmatrix} b_1(s) \\ b_2^*(s) \end{bmatrix}, \tag{2.22}$$

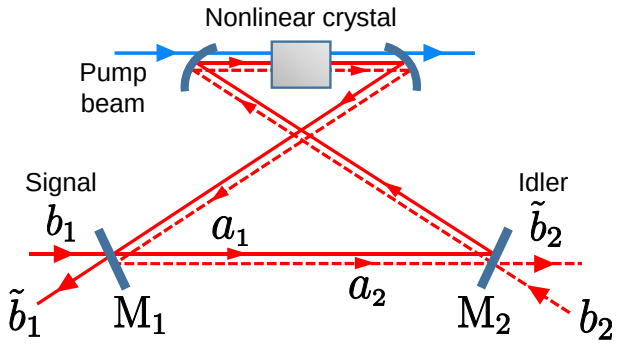

Figure 2.10: Non-degenerate parametric amplifier.

where $g_1(s) = (s^2 - \kappa^2/4 - \varepsilon^2)/D(s)$ and $g_2(s) = -\kappa\varepsilon/D(s)$ are the transfer functions with $D(s) = s^2 + \kappa s + \kappa^2/4 - \varepsilon^2$. Note that $|g_1(i\omega)|^2 - |g_2(i\omega)|^2 = 1$, $\forall\omega$ holds to satisfy the CCR of the output, represented by $\tilde{b}(i\omega)\tilde{b}^*(i\omega') - \tilde{b}^*(i\omega')\tilde{b}(i\omega) = \delta(\omega - \omega')$ in the Fourier domain. Also the characteristic equation $D(s) = 0$ yields the stability condition $0 < x = 2\varepsilon/\kappa < 1$. The gain at the center frequency satisfies $|g_1(0)| = (1 + x^2)/|1 - x^2| \to \infty$ as $x \to 1 - 0$. Therefore, the NDPA actually works as an amplifier.

2.3 Summary

This chapter has been devoted to the preliminaries including classical control theory and open quantum systems. In particular, Section 2.1 has reviewed two important tools; geometric control for the disturbance decoupling and sensitivity analysis for the cascaded amplifier. First, the geometric control theory characterizes the properties of the system in terms of linear subspaces, and the power of the theory is that, given a structure of the plant system, the solvability condition can be easily checked and the dynamical feedback controller realizing disturbance decoupling can be fully parameterized. Second, the sensitivity function quantifies the robustness of the feedback system, and it can also be defined for the simple cascaded feedback systems. In the main parts of this thesis, these well-established results will be extended to the quantum regime. Moreover, in Section 2.2, the mathe-

matical description of open quantum systems has been shown. The point is that the above quantum systems can be characterized by three parameters $(\mathbf{S}, \mathbf{L}, H)$, and they determine the dynamics and input-output relation of the system. Then, by specifying the above parameters, the concrete examples of physical quantum devices have been given.

Chapter 3

Geometric Control Theory for Back-Action Evasion

Abstract This chapter discusses a general method for engineering a linear quantum sensor achieving back-action evasion (BAE). The control problem of BAE is formulated in terms of the transfer functions, or equivalently of the controllable/observable subspaces. The perfect BAE can be considered as the quantum version of the disturbance decoupling problem, then it can be solved within the framework of geometric control theory, introduced in Subsection 2.1.2. The system configurations for the coherent feedback control and the direct interaction control are shown such that the classical geometric control theory can be directly applied. Also, for an opto-mechanical system, the general theory is used to provide a full parameterization of BAE controller. Finally, a simple approach based on the geometric control theory is demonstrated for engineering approximate BAE controller under realistic imperfections.

3.1 Weak Force Sensing

3.1.1 Linear Quantum Sensor

This subsection formulates the problem of weak force sensing within the framework of systems and control theory. Here, again focus on the opto-mechanical oscillator introduced in Subsection 2.2.4, which serves as a quantum sensor for a very weak force. Recall that $\hat{q}_1$ and $\hat{p}_1$ represent the oscillator's position and momentum operators, and $\hat{a}_2 = (\hat{q}_2 + i\hat{p}_2)/\sqrt{2}$ is the annihilation operator of the cavity mode. The vector of input and output quadratures are written by $\hat{W}_1 = [\hat{Q}_1 \ \hat{P}_1]^\top$ and $\hat{W}_1^{\rm out} = [\hat{Q}_1^{\rm out} \ \hat{P}_1^{\rm out}]^\top$, respectively. Also, the oscillator is driven by a weak force $\hat{f}(t)$ with coupling constant γ. Then, the vector of system variables $\hat{x} = [\hat{q}_1 \ \hat{p}_1 \ \hat{q}_2 \ \hat{p}_2]^\top$ satisfies

$$\begin{aligned} \frac{d\hat{x}}{dt} &= A\hat{x} + B_1\hat{W}_1 + b\hat{f}, \\ \hat{W}_1^{\rm out} &= C_1\hat{x} + \hat{W}_1, \end{aligned} \tag{3.1}$$

where

$$\begin{aligned} A &= \begin{bmatrix} 0 & \omega_m & 0 & 0 \\ -\omega_m & 0 & g & 0 \\ 0 & 0 & -\kappa/2 & 0 \\ g & 0 & 0 & -\kappa/2 \end{bmatrix}, \ B_1 = -C_1^\top = -\begin{bmatrix} 0 & 0 \\ 0 & 0 \\ \sqrt{\kappa} & 0 \\ 0 & \sqrt{\kappa} \end{bmatrix}, \\ b &= \sqrt{\gamma}\begin{bmatrix} 0 & 1 & 0 & 0 \end{bmatrix}^\top, \end{aligned} \tag{3.2}$$

ω_m is the resonant frequency of the oscillator, g the coupling strength between the oscillator and the cavity field, and κ the coupling constant between the cavity and the probe field. In the Laplace domain, the input-output relation of the linear quantum sensor (3.1) is given by

$$\begin{bmatrix} \hat{Q}_1^{\rm out}(s) \\ \hat{P}_1^{\rm out}(s) \end{bmatrix} = \begin{bmatrix} 0 & \Xi_P(s) & 0 \\ \Xi_f(s) & \Xi_Q(s) & \Xi_P(s) \end{bmatrix} \begin{bmatrix} \hat{Q}_1(s) \\ \hat{P}_1(s) \end{bmatrix}, \tag{3.3}$$

where $\Xi_f(s)$, $\Xi_Q(s)$, and $\Xi_P(s)$ are the transfer functions given as follows:

$$\Xi_f(s) = \frac{g\omega_m\sqrt{\gamma\kappa}}{(s^2+\omega_m^2)(s+\kappa/2)},$$
$$\Xi_Q(s) = -\frac{g^2\omega_m\kappa}{(s^2+\omega_m^2)(s+\kappa/2)^2},$$
$$\Xi_P(s) = \frac{s-\kappa/2}{s+\kappa/2}.$$

The above input-output relation means that the information about $\hat{f}$ can be extracted by a homodyne detection of $\hat{P}_1^{\rm out}$. Hence, the measurement output of interest is given by

$$\hat{P}_1^{\rm out}(s) = \Xi_f(s)\hat{f}(s) + \Xi_Q(s)\hat{Q}_1(s) + \Xi_P(s)\hat{P}_1(s). \tag{3.4}$$

However, note that the measurement output (3.4) is subjected to two types of fundamental quantum noises. The second term is called the back-action noise or the *radiation-pressure noise*, which arises from the uncertainty of the oscillator's position due to the radiation pressure force fluctuation. On the other hand, the third term is called the shot noise, which arises from the photon number fluctuation at the photodetector. Now, from Eq. (3.4), the normalized output is given by

$$y_1(s) = \frac{\hat{P}_1^{\rm out}(s)}{\Xi_f(s)} = \hat{f}(s) + \frac{\Xi_Q(s)}{\Xi_f(s)}\hat{Q}_1(s) + \frac{\Xi_P(s)}{\Xi_f(s)}\hat{P}_1(s),$$

and the normalized noise power spectral density of y_1 in the Fourier domain ($s = i\omega$) is calculated as follows:

$$\begin{aligned} S(\omega) = \langle|y_1-\hat{f}|^2\rangle &= \left|\frac{\Xi_Q}{\Xi_f}\right|^2\langle|\hat{Q}_1|^2\rangle + \left|\frac{\Xi_P}{\Xi_f}\right|^2\langle|\hat{P}_1|^2\rangle \\ &\geq 2\sqrt{\frac{|\Xi_Q|^2|\Xi_P|^2}{|\Xi_f|^4}\langle|\hat{Q}_1|^2\rangle\langle|\hat{P}_1|^2\rangle} \\ &\geq \frac{|\omega^2-\omega_m^2|}{\gamma\omega_m} \equiv S_{\rm SQL}(\omega). \end{aligned}$$

Then, the noise power has a lower bound called the standard quantum limit (SQL). The last inequality is due to the Heisenberg uncertainty relation, $\langle|\hat{Q}_1|^2\rangle\langle|\hat{P}_1|^2\rangle \geq 1/4$. The essential reason why the SQL appears is that the measurement output (3.4) contains both the back-action noise $\hat{Q}_1$ and the shot noise $\hat{P}_1$.

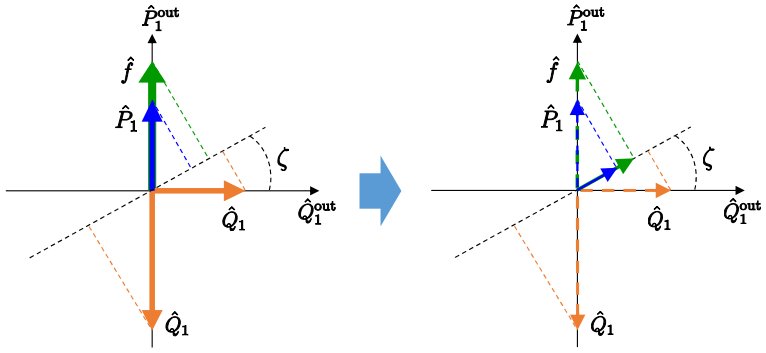

Figure 3.1: Variational measurement for back-action noise cancellation.

3.1.2 Back-Action Evasion

Toward the high-precision detection of $\hat{f}$, beating the SQL is the most important task for engineers. Note that the shot noise is unavoidable and always present in an optical system. Therefore, the sensor system should be carefully modified by some means so that the back-action noise is completely evaded in the measurement output. This control goal is called the back-action evasion (BAE). Many methods for realizing BAE have been proposed. Here, review the variational measurement [37, 38, 39]. For the input-output relation (3.3), consider the combination of $\hat{Q}_1^{\rm out}$ and $\hat{P}_1^{\rm out}$ such that

$$y_\zeta(s) = \hat{Q}_1^{\rm out}(s)\cos\zeta + \hat{P}_1^{\rm out}(s)\sin\zeta,$$

where ζ is the homodyne phase, as illustrated in Fig. 3.1. The transfer function from $\hat{Q}_1$ to the output is given by $\Xi_P\cos\zeta + \Xi_Q\sin\zeta$. Then, the back-action noise can be completely evaded by choosing

$$\zeta = \operatorname{arccot}\left[-\frac{\Xi_Q(s)}{\Xi_P(s)}\right].$$

However, the above optimal homodyne phase is frequency-dependent, which means that the BAE is possible only in a narrow frequency band. To realize a broad-band BAE, some systematic methods have been studied recently [44, 45]. In this approach, the back-action noise is canceled out by designing an auxiliary system and connecting it to a sensor system. As a result, the back-action noise does not

appear in the the measurement output. The condition for BAE can be expressed in terms of the transfer function as follows; i.e., for the modified (controlled) sensor, the transfer function from the back-action noise to the measurement output must satisfy

$$\Xi_Q(s) = 0, \quad \forall s. \tag{3.5}$$

In addition, the equivalent condition to Eq. (3.5) in terms of geometric subspaces can be expressed as

$$\operatorname{Im} \mathcal{C}_{\hat{Q}_1} \subseteq \operatorname{Ker} \mathcal{O}_{\hat{P}_1^{\mathrm{out}}}.$$

If BAE is realized, then $\hat{P}_1^{\mathrm{out}}$ contains only the shot noise $\hat{P}_1$. Hence, in this case the signal to noise ratio can be further improved by injecting a $\hat{P}_1$-squeezed (meaning $\langle |\hat{P}_1|^2 \rangle < 1/2$) probe field into the system.

3.2 Coherent Feedback Control for BAE

3.2.1 Feedback Control Configuration

This subsection discusses the general theory for designing a coherent feedback controller achieving BAE. The key idea is the geometric control theory introduced in Subsection 2.1.2. Note that, the classical geometric control theory for disturbance decoupling problem is formulated for the controlled system with the special structure (2.4); in particular, the coefficient matrix of the disturbance $d(t)$ is of the form $[E^\top \ O]^\top$ and that of the state vector in the output $z(t)$ is $[H \ O]$. Here, consider a class of coherent feedback configuration such that the whole closed-loop system dynamics has this structure, in order for the geometric control theory to be directly applicable.

The point for realizing the above special structure is to connect an MIMO controller to the plant, which is also an MIMO system. It is also necessary for the quantum system to couple to all the probe fields in the same way. That is, in general, the plant system is formulated as the following linear quantum system

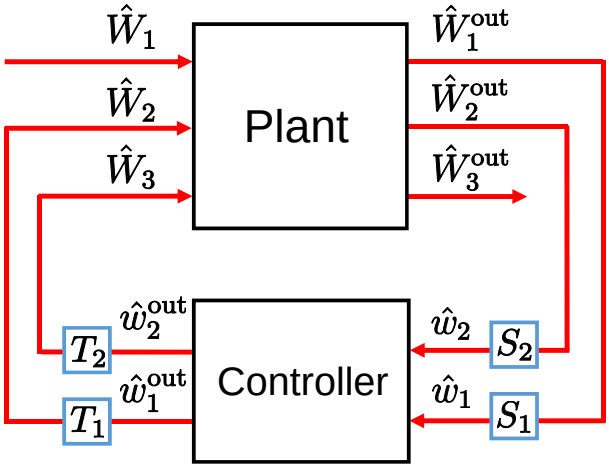

Figure 3.2: Coherent feedback control of the 3 input-output plant system via the 2 input-output controller.

with m input-output fields:

$$\frac{d\hat{x}}{dt} = A\hat{x} + \sum_{j=1}^{m} B_j \hat{W}_j + b\hat{f},$$
$$\hat{W}_j^{\text{out}} = C_j\hat{x} + \hat{W}_j \quad (j = 1, 2, \ldots, m),$$

where it is assumed that $B_j = B, \;\; C_j = C, \; \forall j$. Also, the controller is formulated as the following special linear quantum system with $(m-1)$ input-output fields:

$$\frac{d\hat{x}_K}{dt} = A_K\hat{x}_K + \sum_{j=1}^{m-1} B_K\hat{w}_j,$$
$$\hat{w}_j^{\text{out}} = C_K\hat{x}_K + \hat{w}_j \quad (j = 1, 2, \ldots, m-1), \tag{3.6}$$

where the matrices (A_K, B_K, C_K) satisfy the physical realizability condition (2.20). Note that, corresponding to the plant structure, the controller is also assumed to couple to all the fields in the same way, specified by B_K and C_K. What is important here is that, for the controller, the number of channels, $m-1$, should be even and as small as possible from a viewpoint of implementation. Hence, in this subsection, consider the case of $m = 3$.

Figure 3.2 shows the coherent feedback configuration for the 3 input-output plant system with the 2 input-output controller. The plant-controller connections are given by

$$\hat{w}_1 = S_1\hat{W}_1^{\rm out}, \quad \hat{w}_2 = S_2\hat{W}_2^{\rm out},$$
$$\hat{W}_2 = T_1\hat{w}_1^{\rm out}, \quad \hat{W}_3 = T_2\hat{w}_2^{\rm out},$$

where S_j and T_j $(j = 1, 2)$ are 2×2 unitary matrices representing the scattering process of the fields realized by the phase-shifter; see Subsection 2.2.4. Then, for the whole closed-loop system, the augmented system variable $\hat{x}_{\scriptscriptstyle E} = [\hat{x}^\top \ \hat{x}_{\scriptscriptstyle K}^\top]^\top$ is given by

$$\begin{aligned} \frac{d\hat{x}_{\scriptscriptstyle E}}{dt} &= A_{\scriptscriptstyle E}\hat{x}_{\scriptscriptstyle E} + B_{\scriptscriptstyle E}\hat{W}_1 + b_{\scriptscriptstyle E}\hat{f}, \\ \hat{W}_3^{\rm out} &= C_{\scriptscriptstyle E}\hat{x}_{\scriptscriptstyle E} + D_{\scriptscriptstyle E}\hat{W}_1, \end{aligned} \tag{3.7}$$

where

$$A_{\scriptscriptstyle E} = \left[\begin{array}{c|c} A + B\left[T_1S_1 + T_2S_2(T_1S_1 + I_2)\right]C & B\left[T_1 + T_2(I_2 + S_2T_1)\right]C_{\scriptscriptstyle K} \\ \hline B_{\scriptscriptstyle K}\left[(I_2 + S_2T_1)S_1 + S_2\right]C & A_{\scriptscriptstyle K} + B_{\scriptscriptstyle K}S_2T_1C_{\scriptscriptstyle K} \end{array}\right],$$
$$B_{\scriptscriptstyle E} = \left[\begin{array}{c} B(I_2 + T_1S_1 + T_2S_2T_1S_1) \\ \hline B_{\scriptscriptstyle K}(I_2 + S_2T_1)S_1 \end{array}\right],$$
$$C_{\scriptscriptstyle E} = \left[\begin{array}{c|c} (T_2S_2T_1S_1 + T_2S_2 + I_2)C & T_2(S_2T_1 + I_2)C_{\scriptscriptstyle K} \end{array}\right],$$
$$D_{\scriptscriptstyle E} = T_2S_2T_1S_1, \quad b_{\scriptscriptstyle E} = \left[\begin{array}{c|c} b^\top & O \end{array}\right]^\top.$$

Therefore, the desired system structure of the form (2.4) is realized if the scattering processes satisfy

$$S_2T_1 = -I_2. \tag{3.8}$$

In addition, it is also required that the back-action noise $\hat{Q}_1$ does not appear directly in $\hat{P}_3^{\rm out}$, which can be realized by taking

$$D_{\scriptscriptstyle E} = -T_2S_1 = \pm I_2. \tag{3.9}$$

Here, to satisfy the above conditions (3.8) and (3.9), set S_j and T_j to be the $\pi/2$-phase shifter as follows:

$$S_j = T_j \equiv S = \begin{bmatrix} 0 & -1 \\ 1 & 0 \end{bmatrix} \quad (j = 1, 2). \tag{3.10}$$

As a consequence, the matrices of the whole closed-loop system are written as follows:

$$A_{\scriptscriptstyle E} = \begin{bmatrix} A - BC & BSC_{\scriptscriptstyle K} \\ B_{\scriptscriptstyle K}SC & A_{\scriptscriptstyle K} - B_{\scriptscriptstyle K}C_{\scriptscriptstyle K} \end{bmatrix}, \quad b_{\scriptscriptstyle E} = \begin{bmatrix} b \\ O \end{bmatrix}, \quad B_{\scriptscriptstyle E} = \begin{bmatrix} B \\ O \end{bmatrix},$$
$$C_{\scriptscriptstyle E} = \begin{bmatrix} C & O \end{bmatrix}, \quad D_{\scriptscriptstyle E} = I_2. \tag{3.11}$$

This is certainly of the form (2.4) with $D_{\scriptscriptstyle K} = -I_2$. Hence, now the geometric control theory can be directly applied to design a coherent feedback controller achieving BAE; that is, the aim is to find $(A_{\scriptscriptstyle K}, B_{\scriptscriptstyle K}, C_{\scriptscriptstyle K})$ such that, for the closed-loop system (3.7), the back-action noise $\hat{Q}_1$ (the first element of $\hat{W}_1$) does not appear in the measurement output $\hat{P}_3^{\rm out}$ (the second element of $\hat{W}_3^{\rm out}$). Note that those matrices must satisfy the physical realizability condition (2.20), and thus they cannot be freely chosen. This additional constraint is needed to taken into account when applying the geometric control theory to determine the controller matrices.

3.2.2 Coherent Feedback Realization in Opto-Mechanical System

Here, apply the coherent feedback scheme elaborated in the previous subsection to the opto-mechanical system studied in Subsection 2.2.4 and 3.1.1. The goal is, as mentioned before, to determine the controller matrices $(A_{\scriptscriptstyle K}, B_{\scriptscriptstyle K}, C_{\scriptscriptstyle K})$ such that the closed-loop system achieves BAE. Here, to solve this problem, a step-by-step procedure is provided; the relationships of the class of controllers determined in each step is depicted in Fig. 3.3.

(i) First, to apply the geometric control theory developed above, the plant system needs to be modified so that it is a 3 input-output linear quantum system;

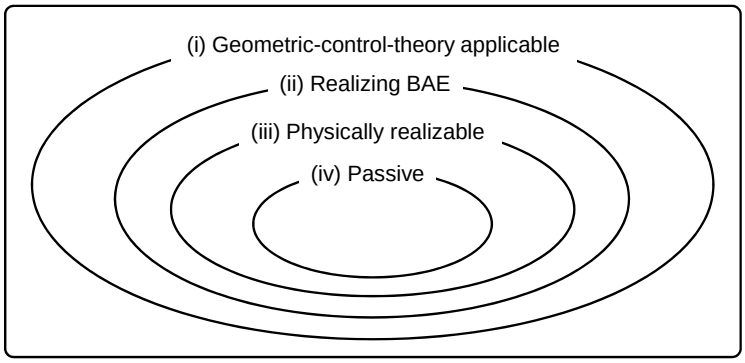

Figure 3.3: The set of controllers satisfying the condition in each step. For the controller to be a quantum system, it must be included in the set (iii). In the set (iv), all the controllers are equivalent up to the phase shift.

then, consider the plant composed of a mechanical oscillator and a 3-ports optical cavity, shown in Fig. 3.4. As assumed before, those ports have the same coupling constant κ. In this case, the matrix A given in Eq. (3.2) is replaced by

$$A = \begin{bmatrix} 0 & \omega_m & 0 & 0 \\ -\omega_m & 0 & g & 0 \\ 0 & 0 & -3\kappa/2 & 0 \\ g & 0 & 0 & -3\kappa/2 \end{bmatrix}.$$

Now, focus only on the back-action noise $\hat{Q}_1$ and the measurement output $\hat{P}_3^{\text{out}}$; hence, the closed-loop system (3.7) and (3.11), which ignores the shot noise term in the dynamical equation, is given by

$$\begin{aligned} \frac{d\hat{x}_{_E}}{dt} &= \begin{bmatrix} A - BC & BSC_{_K} \\ B_{_K}SC & A_{_K} - B_{_K}C_{_K} \end{bmatrix} \hat{x}_{_E} + \begin{bmatrix} E \\ O \end{bmatrix} \hat{Q}_1 + \begin{bmatrix} b \\ O \end{bmatrix} \hat{f}, \\ \hat{P}_3^{\text{out}} &= \begin{bmatrix} H & O \end{bmatrix} \hat{x}_{_E} + \hat{P}_1, \end{aligned}$$

where $B = B_1$, $C = C_1$, and b are given in Eq. (3.2), and

$$E = -\sqrt{\kappa} \begin{bmatrix} 0 & 0 & 1 & 0 \end{bmatrix}^\top, \quad H = \sqrt{\kappa} \begin{bmatrix} 0 & 0 & 0 & 1 \end{bmatrix}.$$

This system is certainly of the form (2.4), where now $D_{_K} = -I_2$.

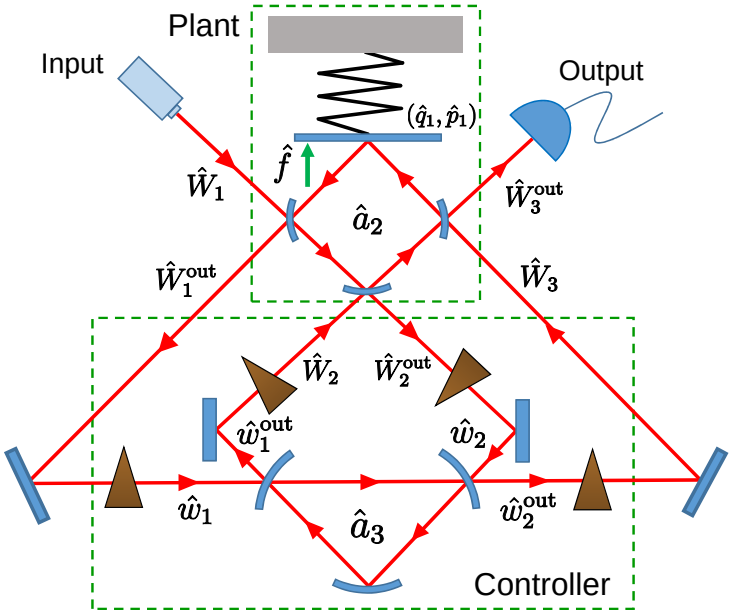

Figure 3.4: Coherent feedback controlled system composed of the opto-mechanical oscillator, for realizing BAE. The triangle represents the $\pi/2$-phase shifter corresponding to Eq. (3.10).

(ii) In the next step, Theorem 2.1.3 is applied to check if there exists a feedback controller such that the above closed-loop system achieves BAE. Recall that the necessary and sufficient condition is Eq. (2.6), i.e., $\mathcal{E} \subseteq \mathcal{V}_1 \subseteq \mathcal{V}_2 \subseteq \mathcal{H}$, where now

$$\mathcal{E} = \mathrm{Im}\, E = \mathrm{span}\left\{ \begin{bmatrix} 0 \\ 0 \\ 1 \\ 0 \end{bmatrix} \right\}, \quad \mathcal{H} = \mathrm{Ker}\, H = \mathrm{span}\left\{ \begin{bmatrix} 1 \\ 0 \\ 0 \\ 0 \end{bmatrix}, \begin{bmatrix} 0 \\ 1 \\ 0 \\ 0 \end{bmatrix}, \begin{bmatrix} 0 \\ 0 \\ 1 \\ 0 \end{bmatrix} \right\}.$$

To check if this solvability condition is satisfied, Corollary 2.1.1 is used; from $\mathcal{E} \cap \mathcal{C} = \mathrm{Im}\, E \cap \mathrm{Ker}\, C = \phi$ and $\mathcal{H} \oplus \mathcal{B} = \mathrm{Ker}\, H \oplus \mathrm{Im}\, B = \mathbb{R}^4$, the algorithms given in Appendix A yield

$$\mathcal{V}_{*(\mathcal{C},\mathcal{E})} = \mathcal{E}, \quad \mathcal{V}^*{}_{(\mathcal{B},\mathcal{H})} = \mathcal{H},$$

implying that the condition in Corollary 2.1.1, i.e., $\mathcal{V}_{*(\mathcal{C},\mathcal{E})} \subseteq \mathcal{V}^{*}_{(\mathcal{B},\mathcal{H})}$, is satisfied. Thus, it can be seen that the BAE problem is solvable, as long as there is no constraint on the controller parameters.

The next goal is to determine the controller matrices (A_K, B_K, C_K), using Theorem 2.1.4. First, set $\mathcal{V}_1 = \mathcal{V}_{*(\mathcal{C},\mathcal{E})} = \mathcal{E}$ and $\mathcal{V}_2 = \mathcal{V}^{*}_{(\mathcal{B},\mathcal{H})} = \mathcal{H}$; note that $(\mathcal{V}_1, \mathcal{V}_2)$ is a (C, A, B)-pair. Then, from Theorem 2.1.4, there exists a feedback controller with dimension $\dim \mathcal{X}_K = \dim \mathcal{V}_2 - \dim \mathcal{V}_1 = 2$. Moreover, noting again that $D_K = -I_2$, there exist matrices $F \in \mathcal{F}(\mathcal{V}_2)$, $G \in \mathcal{G}(\mathcal{V}_1)$, and N such that

$$\mathrm{Ker}\, F_0 = \mathrm{Ker}\,(F + C) \supseteq \mathcal{V}_1, \quad \mathrm{Im}\, G_0 = \mathrm{Im}\,(G + B) \subseteq \mathcal{V}_2, \quad \mathrm{Ker}\, N = \mathcal{V}_1.$$

These conditions lead to

$$F = \begin{bmatrix} f_{11} & f_{12} & -\sqrt{\kappa} & f_{14} \\ \frac{g}{\sqrt{\kappa}} & 0 & 0 & f_{24} \end{bmatrix}, G = \begin{bmatrix} 0 & g_{12} \\ -\frac{g}{\sqrt{\kappa}} & g_{22} \\ g_{31} & g_{32} \\ 0 & \sqrt{\kappa} \end{bmatrix}, N = \begin{bmatrix} n_{11} & n_{12} & 0 & n_{14} \\ n_{21} & n_{22} & 0 & n_{24} \end{bmatrix}, \tag{3.12}$$

where f_{ij}, g_{ij}, and n_{ij} are free parameters. Then, the controller matrices (A_K, B_K, C_K) can be identified by Eq. (2.7) with the above matrices (F, G, N); specifically, by substituting $C_K \to SC_K$, $B_K \to B_K S$, and $A_K \to A_K - B_K C_K$ in Eq. (2.7), A_K, B_K and C_K satisfy

$$\begin{aligned} &SC_K N = F + C, \\ &B_K S = -N(G + B), \\ &(A_K - B_K C_K)N = N(A + BF_0 + GC), \end{aligned}$$

which yield

$$\begin{aligned} A_K &= N(A + BF_0 + GC + G_0 F_0)N^{+}, \\ B_K &= -NG_0\Sigma, \\ C_K &= \Sigma F_0 N^{+}, \end{aligned} \tag{3.13}$$

where N^{+} is the right inverse to N, i.e., $NN^{+} = I_2$.

(iii) Note again that the controller (3.6) has to satisfy the physical realizability condition (2.20), which is now $A_K\Sigma + \Sigma A_K^\top + 2B_K\Sigma B_K^\top = O$ and $B_K = \Sigma C_K^\top \Sigma$. These constraints are represented in terms of the parameters as follows:

$$\begin{aligned}
&f_{12} = -g_{12},\ f_{11} = g_{22},\ n_{11}n_{22} - n_{12}n_{21} = -1,\\
&f_{12}n_1 = f_{11}n_2 - f_{14},\ f_{24} + \sqrt{\kappa} = \frac{g}{\sqrt{\kappa}}n_2,\\
&\left(\frac{3}{2}\kappa + \sqrt{\kappa}f_{24}\right)n_1 + \omega_m n_2 = -\sqrt{\kappa}f_{11},\\
&\omega_m n_1 - \left(\frac{3}{2}\kappa + \sqrt{\kappa}f_{24}\right)n_2 = \sqrt{\kappa}f_{12},
\end{aligned} \tag{3.14}$$

where

$$n_1 = n_{11}n_{24} - n_{14}n_{21}, \quad n_2 = n_{12}n_{24} - n_{14}n_{22}.$$

This is one of the main results; the coherent feedback controller (3.6) achieving BAE for the opto-mechanical oscillator can be fully parametrized by Eq. (3.13) satisfying the conditions given in (3.14). It should be emphasized that this full parametrization of the controller can be obtained thanks to the general problem formulation based on the geometric control theory.

(iv) In practice, of course, a concrete set of parameters need to be determined to construct the controller. Especially, here consider a passive system; this is a static quantum system such as an empty optical cavity. The main reason for choosing a passive system rather than a non-passive (or active) one such as an optical parametric amplifier is that, due to the external pumping energy, the latter could become fragile and also its physical implementation must be more involved compared to a passive system [97]. Now the condition for the system (A_K, B_K, C_K) to be passive is given by

$$\Sigma A_K \Sigma = -A_K, \quad \Sigma B_K \Sigma = -B_K.$$

The general result of this fact is given by Theorem C.1 in Appendix C. From these conditions, the system parameters are imposed to satisfy, in addition to Eq. (3.14), the following equalities:

$$f_{12} = \frac{g}{\sqrt{\kappa}}, \quad f_{11} = 0, \quad n_{11} = -n_{22}, \quad n_{12} = n_{21}. \tag{3.15}$$

There is still some freedom in determining n_{ij}, which however corresponds to simply the phase shift at the input-output ports of the controller, as indicated from Eq. (3.13). Thus, the passive controller achieving BAE in this example is unique up to the phase shift. Here particularly, choose $n_{11} = 1$ and $n_{12} = 0$. Then, the controller matrices (3.13) satisfying Eqs. (3.14) and (3.15) are determined as

$$A_K = \begin{bmatrix} -\frac{g^2}{\kappa} & -\omega_m \\ \omega_m & -\frac{g^2}{\kappa} \end{bmatrix}, \quad C_K = -B_K^\top = \begin{bmatrix} \frac{g}{\sqrt{\kappa}} & 0 \\ 0 & \frac{g}{\sqrt{\kappa}} \end{bmatrix}.$$

As illustrated in Fig. 3.4, the controller specified by these matrices can be realized as a single-mode, 2 input-output optical cavity with decay rate g^2/κ and detuning $-\omega_m$. In other words, the above controller is realized by taking the cavity with the following Hamiltonian and the coupling operator:

$$\hat{H}_K = \Delta \hat{a}_3^* \hat{a}_3 = \frac{\Delta}{2}(\hat{q}_3^2 + \hat{p}_3^2), \quad \hat{L}_K = \sqrt{\kappa_K}\hat{a}_3 = \sqrt{\frac{\kappa_K}{2}}(\hat{q}_3 + i\hat{p}_3), \tag{3.16}$$

where $\hat{a}_3 = (\hat{q}_3 + i\hat{p}_3)/\sqrt{2}$ is the cavity mode of the controller, and then, to satisfy the BAE condition, the controller parameters (Δ, κ_K) must satisfy

$$\Delta = -\omega_m, \quad \kappa_K = \frac{g^2}{\kappa}. \tag{3.17}$$

Summarizing, the above-designed sensing system composed of the opto-mechanical oscillator (plant) and the optical cavity (controller), which are combined via coherent feedback, satisfies the BAE condition. Hence, it can work as a high-precision sensor of the force $\hat{f}$ below the SQL, particularly when the $\hat{P}_1$-squeezed probe field is used; this fact will be demonstrated in Section 3.4.

3.3 Direct Interaction Control for BAE

This section studies another control scheme for achieving BAE. As illustrated in Fig. 3.5, in this case, the controller is directly connected to the plant, not through a coherent feedback; hence, this scheme is called the direct interaction. The controller is characterized by the following two Hamiltonians:

$$\hat{H}_K = \frac{1}{2}\hat{x}_K^\top R_K \hat{x}_K, \quad \hat{H}_{\rm int} = \frac{1}{2}(\hat{x}^\top R_1 \hat{x}_K + \hat{x}_K^\top R_2 \hat{x}), \tag{3.18}$$

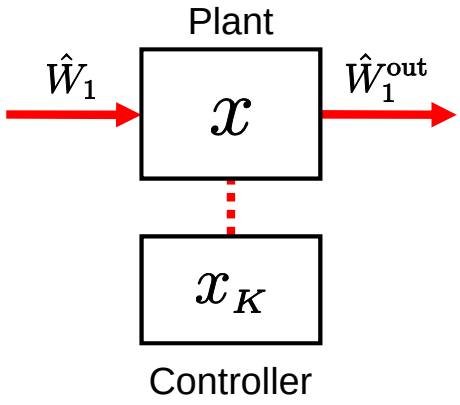

Figure 3.5: General configuration of direct interaction control.

where $\hat{x}_K = [\hat{q}_1' \ \hat{p}_1' \ \cdots \ \hat{q}_{n_k}' \ \hat{p}_{n_k}']^\top$ is the vector of controller variables with n_k the number of modes of the controller. $\hat{H}_K$ is the controller's self Hamiltonian with $R_K \in \mathbb{R}^{2n_k \times 2n_k}$. Also $\hat{H}_{\text{int}}$ with $R_1 \in \mathbb{R}^{2n \times 2n_k}$, $R_2 \in \mathbb{R}^{2n_k \times 2n}$ represents the coupling between the plant and the controller. Note that, for the Hamiltonians $\hat{H}_K$ and $\hat{H}_{\text{int}}$ to be Hermitian, the matrices must satisfy

$$R_K = R_K^\top, \quad R_1^\top = R_2.$$

These are the physical realizability conditions in the scenario of direct interaction. In particular, here consider a plant system interacting with a single probe field $\hat{W}_1$, with coupling matrices $B_1 = B$ and $C_1 = C$. As for the coupling operator, $\hat{L}_K = 0$ because $\hat{x}_K$ is not directly affected by $\hat{W}_1$. Then, the whole dynamics of the augmented system with variable $\hat{x}_E = [\hat{x}^\top \ \hat{x}_K^\top]^\top$ is given by

$$\begin{aligned} \frac{d\hat{x}_E}{dt} &= A_E \hat{x}_E + B_E \hat{W}_1 + b_E \hat{f}, \\ \hat{W}_1^{\text{out}} &= C_E \hat{x}_E + \hat{W}_1, \end{aligned} \tag{3.19}$$

where

$$A_E = \begin{bmatrix} A & \Sigma_n R_1 \\ \Sigma_{n_k} R_2 & \Sigma_{n_k} R_K \end{bmatrix}, \ B_E = \begin{bmatrix} B \\ O \end{bmatrix}, \ C_E = \begin{bmatrix} C^\top \\ O \end{bmatrix}^\top, \ b_E = \begin{bmatrix} b \\ O \end{bmatrix}. \tag{3.20}$$

Note that B_E, C_E, and b_E are the same matrices as those in Eq. (3.11). Also, comparing the matrices (2.5) and (3.20), it follows that $D_K = O$, which thus leads

to $F = F_0$ and $G = G_0$ in Theorem 2.1.4. Now, again for the opto-mechanical system illustrated in Fig. 2.9, the aim is to design the direct interaction controller, so that the whole system (3.19) achieves BAE; that is, the problem is to determine the matrices (R_K, R_1, R_2) so that the back-action noise $\hat{Q}_1$ does not appear in the measurement output $\hat{P}_1^{\rm out}$. For this purpose, go through the same procedure as that taken in Subsection 3.2.2.

(i) Because of the structure of the matrices B_E and C_E, the system is already of the form (2.4), where the geometric control theory is directly applicable.

(ii) Because this subsection now focuses on the same plant system as that in Subsection 3.2.2, the same conclusion is obtained; that is, the BAE problem is solvable as long as there is no constraint on the controller matrices (R_K, R_1, R_2). The controller matrices can be determined in a similar way to Subsection 3.2.2 as follows. First, because the (C, A, B)-pair $(\mathcal{V}_1, \mathcal{V}_2)$ is the same as before, it follows that $\dim \mathcal{X}_K = 2$, i.e., $n_k = 1$. Then, from Theorem 2.1.4 with the fact that $F = F_0$ and $G = G_0$, the direct interaction controller can be parameterized as follows:

$$R_K = -\Sigma N(A + BF + GC)N^+, \quad R_1 = -\Sigma_2 BFN^+, \quad R_2 = \Sigma NGC. \tag{3.21}$$

The matrices F, G, and N satisfy $\mathrm{Ker}\, F \supseteq \mathcal{V}_1$, $\mathrm{Im}\, G \subseteq \mathcal{V}_2$, and $\mathrm{Ker}\, N = \mathcal{V}_1$, which lead to

$$F = \begin{bmatrix} f_{11} & f_{12} & 0 & f_{14} \\ \frac{g}{\sqrt{\kappa}} & 0 & 0 & f_{24} \end{bmatrix}, \; G = \begin{bmatrix} 0 & g_{12} \\ -\frac{g}{\sqrt{\kappa}} & g_{22} \\ g_{31} & g_{32} \\ 0 & 0 \end{bmatrix}, \; N = \begin{bmatrix} n_{11} & n_{12} & 0 & n_{14} \\ n_{21} & n_{22} & 0 & n_{24} \end{bmatrix}, \tag{3.22}$$

where f_{ij}, g_{ij}, and n_{ij} are free parameters.

(iii) Next, the controller matrices have to satisfy the physical realizability conditions $R_K = R_K^\top$ and $R_1^\top = R_2$; these constraints impose the parameters to

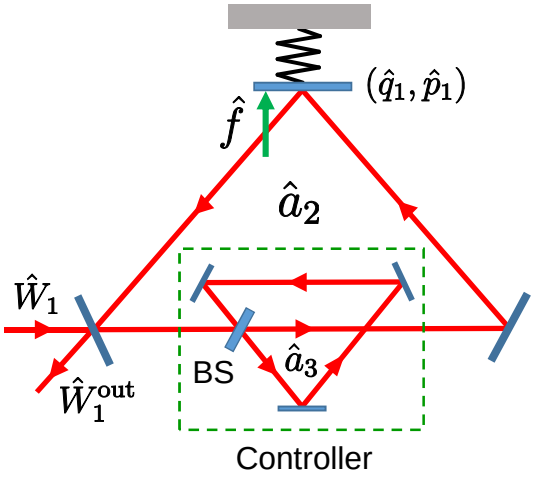

Figure 3.6: Physical implementation of the passive direct interaction controller for the opto-mechanical oscillator.

satisfy

$$\begin{aligned}
&f_{12} = -g_{12}, \quad f_{11} = g_{22}, \quad n_{11}n_{22} - n_{12}n_{21} = -1, \\
&f_{12}n_1 = f_{11}n_2 - f_{14}, \quad f_{24} = \frac{g}{\sqrt{\kappa}}n_2, \\
&\left(\frac{\kappa}{2} + \sqrt{\kappa}f_{24}\right) n_1 + \omega_m n_2 = -\sqrt{\kappa}f_{11}, \\
&\omega_m n_1 - \left(\frac{\kappa}{2} + \sqrt{\kappa}f_{24}\right) n_2 = \sqrt{\kappa}f_{12},
\end{aligned} \tag{3.23}$$

where $n_1 = n_{11}n_{24} - n_{14}n_{21}$ and $n_2 = n_{12}n_{24} - n_{14}n_{22}$. Eqs (3.21), (3.22), and (3.23) provide the full parametrization of the direct interaction controller.

(iv) To specify a set of parameters, as in the case of Subsection 3.2.2, aim to design a passive controller. From Theorem C.2 in Appendix C, R_K and $R_2 = R_1^\top$ satisfy following the conditions:

$$\Sigma R_K \Sigma = -R_K, \quad \Sigma R_2 \Sigma_2 = -R_2,$$

which lead to the same equalities given in Eq. (3.15). Then, setting the parameters to be $n_{11} = 1$ and $n_{12} = 0$, the matrices R_K and R_2 can be determined as follows:

$$R_K = \begin{bmatrix} -\omega_m & 0 \\ 0 & -\omega_m \end{bmatrix}, \quad R_2 = R_1^\top = \begin{bmatrix} 0 & 0 & g & 0 \\ 0 & 0 & 0 & g \end{bmatrix}.$$

The controller specified by these matrices can be physically implemented as illustrated in Fig. 3.6; that is, it is a single-mode detuned cavity with Hamiltonian $\hat{H}_K = -\omega_m \hat{a}_3^* \hat{a}_3$, which couples to the plant through a beam-splitter (BS) represented by $\hat{H}_{\rm int} = g(\hat{a}_3 \hat{a}_2^* + \hat{a}_3^* \hat{a}_2)$.

Remark 3.3.1. As proposed in [44], an active controller can be employed to achieve BAE. In this case, the interaction Hamiltonian is given by

$$\hat{H}_{\rm int} = g_{\rm B}(\hat{a}_3 \hat{a}_2^* + \hat{a}_3^* \hat{a}_2) + g_{\rm D}(\hat{a}_3 \hat{a}_2 + \hat{a}_3^* \hat{a}_2^*),$$

while the system's self-Hamiltonian is the same as above; $\hat{H}_K = -\omega_m \hat{a}_3^* \hat{a}_3$. That is, the controller couples to the plant through a non-degenerate optical parametric amplification process in addition to the BS interaction. To satisfy the BAE condition, the parameters must satisfy $g_{\rm B} + g_{\rm D} = g$. Note that this direct interaction controller can be specified, in the full-parameterization (3.21), (3.22), and (3.23), by

$$f_{11} = f_{12} = f_{14} = 0, \quad n_{11} = -n_{22} = 1, \quad n_{12} = n_{21} = 0.$$

3.4 Approximate BAE

Sections 3.2 and 3.3 have demonstrated that the BAE condition can be achieved by engineering an appropriate auxiliary system and connecting it to the plant. However, in a practical situation, it cannot be expected to realize such perfect BAE due to several experimental imperfections. Hence, in a realistic setup, the control strategy should be modified for engineering a sensor so that it would accomplish *approximate BAE*. Then, looking back into Subsection 3.1.2 where the BAE condition, $\Xi_Q(s) = 0 \ \forall s$, was obtained, the control goal is naturally reformulated as the following optimization problem to design an auxiliary system achieving the approximate BAE:

$$\min \left\| \frac{\Xi_Q(s)}{\Xi_f(s)} \right\|, \tag{3.24}$$

where $\| \bullet \|$ denotes a valid norm of a complex function. In particular, in the field of robust control theory, the following H_2 norm and the H_∞ norm are often used:

$$\|\Xi\|_2 = \sqrt{\frac{1}{2\pi}\int_{-\infty}^{\infty} |\Xi(i\omega)|^2 d\omega}, \quad \|\Xi\|_\infty = \max_\omega |\Xi(i\omega)|.$$

That is, the H_2 or H_∞ control theory provides a general procedure for synthesizing a feedback controller that minimizes the above norm [98]. This section takes the H_2 norm, mainly owing to the broadband noise-reduction nature of the H_2 controller. Then, rather than pursuing an optimal quantum H_2 controller based on the quantum H_2 control theory [81, 84], here take the following geometric-control-theoretical approach to solve the problem (3.24). That is, first apply the method developed in Section 3.2 or 3.3 to the idealized system and obtain the controller achieving perfect BAE; then, in the practical setup containing some unwanted noise, make a local modification of the controller parameters obtained in the first step, to minimize the cost $\|\Xi_Q(s)/\Xi_f(s)\|_2$.

As a demonstration, here consider the coherent feedback control for the opto-mechanical system studied in Section 3.1, which is now subjected to the thermal noise $\hat{f}_{\rm th}$ and the damping effect $-\gamma\hat{p}_1$. Following the above-described policy, employ the coherent feedback controller constructed for the idealized system that ignores $\hat{f}_{\rm th}$ and $-\gamma\hat{p}_1$, leading to the controller given by Eqs. (3.16) and (3.17), illustrated in Fig. 3.4. The closed-loop system with variable $\hat{x}_{\!E} = [\hat{x}^\top \ \hat{x}_{\!K}^\top]^\top$, obeys the following dynamics:

$$\begin{aligned} \frac{d\hat{x}_{\!E}}{dt} &= \widetilde{A}_{\!E}\hat{x}_{\!E} + B_{\!E}\hat{W}_1 + b_{\!E}(\hat{f} + \hat{f}_{\rm th}), \\ \hat{W}_3^{\rm out} &= C_{\!E}\hat{x}_{\!E} + \hat{W}_1, \end{aligned}$$

where

$$\widetilde{A}_{\!E} = \left[\begin{array}{cccc|cc} 0 & \omega_m & 0 & 0 & 0 & 0 \\ -\omega_m & -\gamma & g & 0 & 0 & 0 \\ 0 & 0 & -\kappa/2 & 0 & 0 & \sqrt{\kappa\kappa_{\!K}} \\ g & 0 & 0 & -\kappa/2 & -\sqrt{\kappa\kappa_{\!K}} & 0 \\ \hline 0 & 0 & 0 & \sqrt{\kappa\kappa_{\!K}} & 0 & \Delta \\ 0 & 0 & -\sqrt{\kappa\kappa_{\!K}} & 0 & -\Delta & 0 \end{array}\right].$$

B_E, C_E, and b_E are the same matrices given in Eq. (3.11). $\hat{f}_{\rm th}$ is the thermal noise satisfying $\langle \hat{f}_{\rm th}(t)\hat{f}_{\rm th}(t')\rangle \simeq \bar{n}\delta(t-t')$, where $\bar{n}$ is the mean phonon number at thermal equilibrium [99, 100]. Note that the damping effect appears in the $(2,2)$ component of $\widetilde{A}_E$ due to the stochastic nature of $\hat{f}_{\rm th}$. Also, again, κ_K and Δ are the decay rate and the detuning of the controller cavity, respectively. In the idealized setting where $\hat{f}_{\rm th}$ and $-\gamma\hat{p}_1$ are negligible, the perfect BAE is achieved by choosing the parameters satisfying Eq. (3.17). The measurement output of this closed-loop system is, in the Laplace domain, represented by

$$\hat{P}_3^{\rm out}(s) = \widetilde{\Xi}_f(\hat{f}(s) + \hat{f}_{\rm th}(s)) + \widetilde{\Xi}_Q\hat{Q}_1(s) + \widetilde{\Xi}_P\hat{P}_1(s).$$

The normalized noise power spectral density of $y_3(s) = \hat{P}_3^{\rm out}(s)/\widetilde{\Xi}_f(s)$ is calculated as

$$\begin{aligned}\widetilde{S}(\omega) &= \langle |y_3(i\omega) - \hat{f}(i\omega)|^2\rangle \\ &= \langle |\hat{f}_{\rm th}|^2\rangle + \left|\frac{\widetilde{\Xi}_Q}{\widetilde{\Xi}_f}\right|^2 \langle |\hat{Q}_1|^2\rangle + \left|\frac{\widetilde{\Xi}_P}{\widetilde{\Xi}_f}\right|^2 \langle |\hat{P}_1|^2\rangle, \end{aligned} \tag{3.25}$$

and the coefficient of the back-action noise is given by

$$\frac{\widetilde{\Xi}_Q(s)}{\widetilde{\Xi}_f(s)} = -\frac{\sqrt{\kappa}\{\kappa\kappa_K\Delta(s^2+\gamma s+\omega_m^2) + g^2\omega_m(s^2+\Delta^2)\}}{g\omega_m\sqrt{\gamma}\{(s+\kappa/2)(s^2+\Delta^2)+\kappa\kappa_K s\}}.$$

The goal is to find the optimal parameters (κ_K, Δ) that minimize the H_2 norm of the transfer function, $\widetilde{\Xi}_Q(s)/\widetilde{\Xi}_f(s)$.

The system parameters are taken as follows [100]: $\omega_m/2\pi = 0.5$ MHz, $\kappa/2\pi = 1.0$ MHz, $\gamma/2\pi = 5.0$ kHz, $g/2\pi = 0.3$ MHz, and $\bar{n} \simeq 8.33\times 10^2$. Figure 3.7 shows $\|\widetilde{\Xi}_Q(s)/\widetilde{\Xi}_f(s)\|_2$ as a function of κ_K and Δ. It is indicated that there exists a unique pair of $(\kappa_K^{\rm opt}, \Delta^{\rm opt})$ that minimizes the norm, and they are given by $\kappa_K^{\rm opt}/2\pi = 0.093$ MHz and $\Delta^{\rm opt}/2\pi = -0.5$ MHz, which are actually close to the ideal values (3.17). Figure 3.8 shows the value of Eq. (3.25) with these optimal parameters $(\kappa_K^{\rm opt}, \Delta^{\rm opt})$, where the noise floor $\langle |\hat{f}_{\rm th}|^2\rangle$ is subtracted. The solid black line represents the SQL, which is now given by

$$\widetilde{S}_{\rm SQL}(\omega) = \frac{|(\omega^2-\omega_m^2) - i\gamma\omega|}{\gamma\omega_m}. \tag{3.26}$$

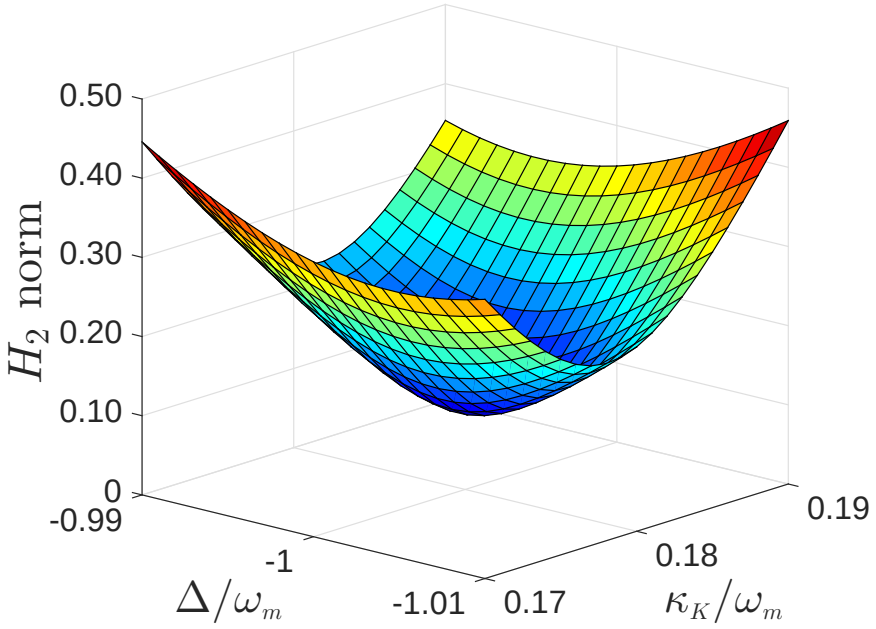

Figure 3.7: H_2 norm $\|\widetilde{\Xi}_Q/\widetilde{\Xi}_f\|_2$ versus coupling constant κ_K and detuning Δ.

Then the dot-dashed blue and dotted green lines indicate that, in the low frequency range, the coherent feedback controller can suppress the noise below the SQL, while, by definition, the noise power of the autonomous (i.e., uncontrolled) plant system is above the SQL. Moreover, this effect can be enhanced by injecting a $\hat{P}_1$-squeezed probe field (meaning $\langle|\hat{Q}_1|^2\rangle = e^r/2$ and $\langle|\hat{P}_1|^2\rangle = e^{-r}/2$) into the system. In fact, the dashed red line in Fig. 3.8 illustrates the case $r = 2$ (about 9 dB squeezing), showing the significant reduction of the noise power.

3.5 Summary

This chapter has been discussed a general method for engineering a BAE controller for linear quantum sensors, based on the geometric control theory. What should be noted is that the geometric control is such a powerful tool that the coherent feedback control and the direct interaction control can be formulated within this

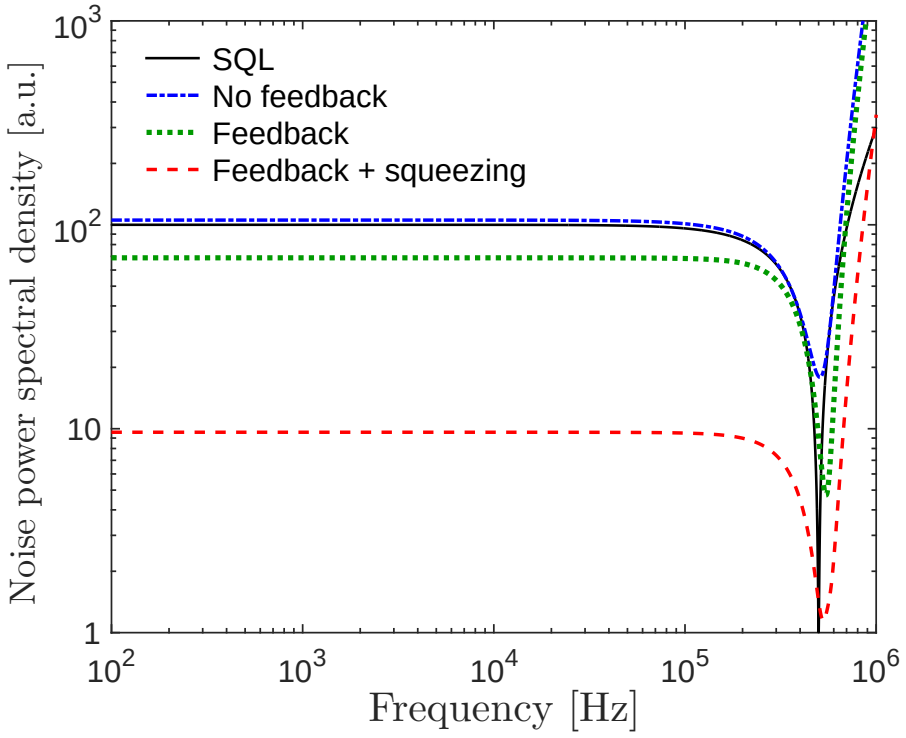

Figure 3.8: Normalized power spectral densities of the noise. The black solid line represents the SQL (3.26), and the dot-dashed blue line does the case without feedback. The dotted green and dashed red lines show the cases for the feedback controlled system, with coherent and squeezed probe field, respectively.

framework. In the former case, coherent feedback controller is modified to be a multi-input and multi-output system so that the coefficient matrices of the whole closed-loop system have special structures as explained in Subsection 3.2.1. For both control methods, the full parametrization of the BAE controller is obtained once a plant sensor system is given. Moreover, the design of coherent feedback controller has been demonstrated for achieving approximate BAE. The optimal parameters minimizing the H_2 norm can be found through the numerical simulation.

Chapter 4

Feedback Stabilization of Cascaded Quantum Amplifier

Abstract This chapter studies a feedback control method for a cascaded quantum amplifier. This control problem becomes further non-trivial compared to the classical case, because the quantum amplifier is essentially modeled as a multi-input and multi-output (MIMO) system. As an important first step to develop a general control theory for cascaded quantum amplifier, this chapter particularly considers the quantum versions of the two types of feedback structures introduced in Subsection 2.1.5. To quantify the robustness of the above two feedback schemes, the sensitivity functions are defined under some reasonable assumptions. It is shown that a single feedback control for cascaded amplifier is better than a cascade connection of feedback-controlled amplifiers in the sense of sensitivity. Finally, actual performance of the cascade feedback systems is numerically investigated.

4.1 Single Quantum Feedback Amplifier

This section reviews the general feedback method for a single quantum amplifier [65]. In what follows, the Hermitian conjugate of $b(t)$ is represented as $b^\dagger(t)$. As shown in Subsection 2.2.4, the phase-preserving linear quantum amplifier is modeled as an open quantum system with two input fields; the signal mode b_1 and

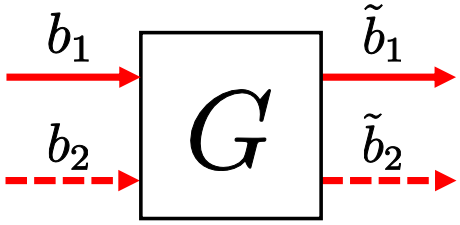

Figure 4.1: 1-signal 1-idler quantum amplifier.

the idler mode b_2 (see Fig. 4.1). Then, in the Laplace domain, the input-output relation is represented as follows:

$$\begin{bmatrix} \tilde{b}_1(s) \\ \tilde{b}_2^\dagger(s) \end{bmatrix} = G(s) \begin{bmatrix} b_1(s) \\ b_2^\dagger(s) \end{bmatrix}, \; G(s) = \begin{bmatrix} G_{11}(s) & G_{12}(s) \\ G_{21}(s) & G_{22}(s) \end{bmatrix}. \tag{4.1}$$

Note here that there are some constraints on the elements of the transfer function matrix $G(s)$. First, the amplified output fields satisfy the CCR, $[\tilde{b}_1(s), \tilde{b}_1^\dagger(s)] = [\tilde{b}_2(s), \tilde{b}_2^\dagger(s)] = 1$, then the following relation holds:

$$|G_{11}(i\omega)|^2 - |G_{12}(i\omega)|^2 = |G_{22}(i\omega)|^2 - |G_{21}(i\omega)|^2 = 1, \; \forall \omega$$

Also, two amplified output fields are uncorrelated, i.e., $[\tilde{b}_1(s), \tilde{b}_2(s)] = 0$, which leads to

$$G_{21}(i\omega)G_{11}^*(i\omega) - G_{22}(i\omega)G_{12}^*(i\omega) = 0, \; \forall \omega$$

Next, to stabilize the above quantum amplifier, the controller is designed based on the coherent feedback scheme. Recall that, as discussed in Subsection 2.1.3, the robust amplification is realized by taking a passive and attenuating controller. The quantum controller satisfying these requirements can be represented as a system with 2 input fields b_3 and b_4. The input-output relation is given as follows:

$$\begin{bmatrix} \tilde{b}_3^\dagger(s) \\ \tilde{b}_4^\dagger(s) \end{bmatrix} = K(s) \begin{bmatrix} b_3^\dagger(s) \\ b_4^\dagger(s) \end{bmatrix}, \quad K(s) = \begin{bmatrix} K_{11}(s) & K_{12}(s) \\ K_{21}(s) & K_{22}(s) \end{bmatrix}. \tag{4.2}$$

$K^\dagger(i\omega)K(i\omega) = I, \; \forall \omega$ holds for the controller to be passive.

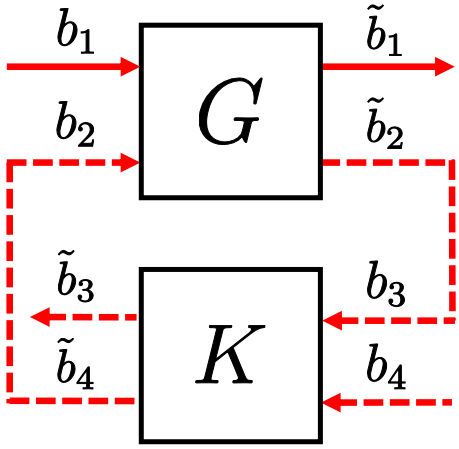

Figure 4.2: Feedback configuration for a single quantum amplifier.

Now, the amplifier (4.1) and the controller (4.2) are connected through the coherent feedback $b_2 = \tilde{b}_4$ and $b_3 = \tilde{b}_2$, as shown in Fig. 4.2. The input-output relation of the closed-loop system is given by

$$\begin{bmatrix} \tilde{b}_1(s) \\ \tilde{b}_3^\dagger(s) \end{bmatrix} = \begin{bmatrix} G_{11}^{\rm fb}(s) & G_{12}^{\rm fb}(s) \\ G_{21}^{\rm fb}(s) & G_{22}^{\rm fb}(s) \end{bmatrix} \begin{bmatrix} b_1(s) \\ b_4^\dagger(s) \end{bmatrix}, \tag{4.3}$$

where

$$\begin{aligned} G_{11}^{\rm fb}(s) &= \frac{G_{11}(s) - K_{21}(s)\big[G_{11}(s)G_{22}(s) - G_{12}(s)G_{21}(s)\big]}{1 - G_{22}(s)K_{21}(s)}, \\ G_{12}^{\rm fb}(s) &= \frac{G_{12}(s)K_{22}(s)}{1 - G_{22}(s)K_{21}(s)}, \quad G_{21}^{\rm fb}(s) = \frac{G_{21}(s)K_{11}(s)}{1 - G_{22}(s)K_{21}(s)}, \\ G_{22}^{\rm fb}(s) &= \frac{K_{12}(s) + G_{22}(s)\big[K_{11}(s)K_{22}(s) - K_{12}(s)K_{21}(s)\big]}{1 - G_{22}(s)K_{21}(s)}. \end{aligned}$$

Then, in the high-gain limit $|G_{11}(s)| \to \infty$, the following result can be obtained:

$$|G_{11}^{\rm fb}(s)| \to \frac{1}{|K_{21}(s)|}.$$

This result means that the quantum amplification process can be made robust by feedback control as in the classical case.

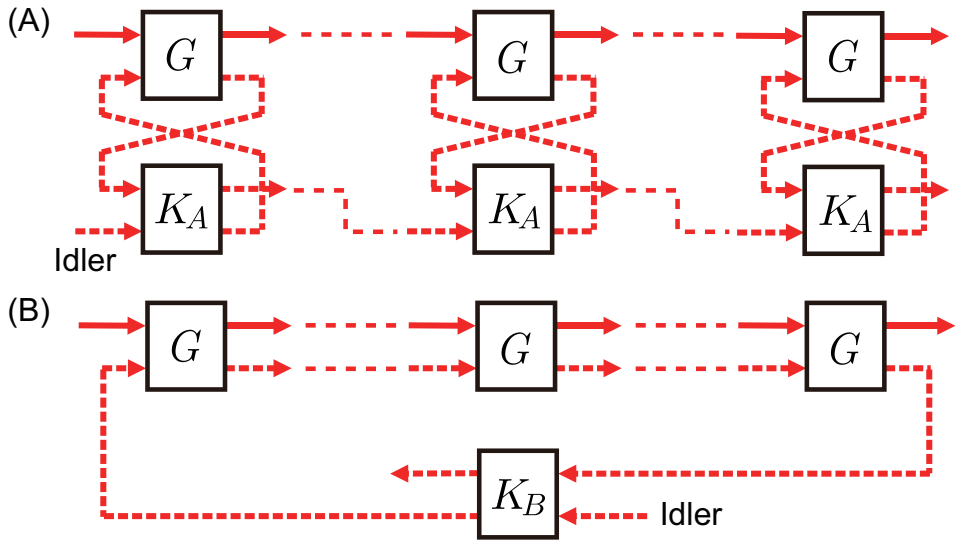

Figure 4.3: Two basic feedback configurations for cascaded quantum amplifier; type-A and type-B.

4.2 Cascaded Quantum Feedback Amplifier

This section provides the quantum version of the classical cascade amplification theory given in Subsection 2.1.5. First note that, because the quantum amplifier is an MIMO system and hence it essentially differs from the classical one, specifying the feedback network composed of amplifiers and controllers, which corresponds to the classical one shown in Fig. 2.5, is a non-trivial problem. Here particularly consider the case where the idler mode of the amplifier can be used, in addition to the signal mode, to construct the feedback network; actually in the standard experiments of quantum optics [12, 13] and superconductivity [14, 15, 16, 17], the idler mode is artificially implemented and is thus accessible. In this formulation, reasonable quantum versions of the classical feedback networks are illustrated in Fig. 4.3; the type-A and type-B schemes correspond to the classical type-a and type-b schemes, respectively. In both cases, the signal-out and the idler-out are connected to the signal-in and the idler-in, respectively, and eventually the whole system has only one idler input from outside. Note that, if the idler modes are not accessible and only the signal modes can be connected, then in both configurations

the whole closed-loop system has multiple idler inputs and eventually it is subjected to a large noise coming from those idler input channels.

4.3 Sensitivity Analysis

This section theoretically studies the performance of the two feedback schemes proposed in the previous section. To tackle this problem, define the sensitivity functions in the case of cascaded quantum feedback amplifier. For simplicity, the following setting is assumed. First, focus on the gain at the center frequency, $\omega = 0$. Then, the quantum amplifier has the following transfer function matrix:

$$G(0) \equiv \begin{bmatrix} G_1 & G_2 \\ G_2 & G_1 \end{bmatrix}, \quad G_1^2 - G_2^2 = 1, \quad G_i \in \mathbb{R}. \tag{4.4}$$

Note that the ideal NDPA with transfer functions (2.22) certainly satisfies this condition. Suppose that both feedback networks are composed of N identical quantum amplifiers characterized by Eq. (4.4), and that the gain of only the j-th amplifier changes as $G_1 \to G_1 + \Delta G_1$ and $G_2 \to G_2 + \Delta G_2$. From Eq. (4.4), it is shown that the characteristic changes ΔG_1 and ΔG_2 satisfy the following equality:

$$G_2 \Delta G_2 = G_1 \Delta G_1. \tag{4.5}$$

Moreover, without loss of generality, the transfer function matrix of the controller at $\omega = 0$ can be set to the following form:

$$K_\bullet(0) \equiv \begin{bmatrix} K_{1\bullet} & K_{2\bullet} \\ -K_{2\bullet} & K_{1\bullet} \end{bmatrix}, \; K_{1\bullet}^2 + K_{2\bullet}^2 = 1, \quad K_{i\bullet} \in \mathbb{R},$$

where $\bullet = A, B$; i.e., $K_A(0)$ and $K_B(0)$ represent the coherent feedback controllers applied to the type-A and the type-B schemes, respectively.

First, consider the overall gain for the type-A feedback scheme, where the feedback-controlled quantum amplifiers are connected in series. From Eq. (4.3), each feedback-controlled amplifier has the following transfer function matrix:

$$G^{\mathrm{fb}}(0) \equiv \begin{bmatrix} G_1^{\mathrm{fb}} & G_2^{\mathrm{fb}} \\ G_2^{\mathrm{fb}} & G_1^{\mathrm{fb}} \end{bmatrix} = \frac{1}{1 + G_1 K_{2A}} \begin{bmatrix} G_1 + K_{2A} & G_2 K_{1A} \\ G_2 K_{1A} & G_1 + K_{2A} \end{bmatrix}. \tag{4.6}$$

This matrix can be diagonalized by the orthogonal matrix as follows;

$$P^{-1}G^{\rm fb}(0)P = {\rm diag}\{\lambda_+^{\rm fb},\ \lambda_-^{\rm fb}\} = \begin{bmatrix} \lambda_+^{\rm fb} & 0 \\ 0 & \lambda_-^{\rm fb} \end{bmatrix},$$

where $\lambda_\pm^{\rm fb} = (G_1 + K_{2A} \pm G_2K_{1A})/(1 + G_1K_{2A})$ are the eigenvalues of $G^{\rm fb}(0)$ and

$$P = \frac{1}{\sqrt{2}} \begin{bmatrix} 1 & 1 \\ 1 & -1 \end{bmatrix}.$$

Then, the overall transfer function matrix is given by the N product of $G^{\rm fb}(0)$ as follows:

$$\begin{aligned} G_A^{\rm fb} &\equiv \begin{bmatrix} G_{1A}^{\rm fb} & G_{2A}^{\rm fb} \\ G_{2A}^{\rm fb} & G_{1A}^{\rm fb} \end{bmatrix} = \left[G^{\rm fb}(0)\right]^N \\ &= \frac{1}{2} \begin{bmatrix} (\lambda_+^{\rm fb})^N + (\lambda_-^{\rm fb})^N & (\lambda_+^{\rm fb})^N - (\lambda_-^{\rm fb})^N \\ (\lambda_+^{\rm fb})^N - (\lambda_-^{\rm fb})^N & (\lambda_+^{\rm fb})^N + (\lambda_-^{\rm fb})^N \end{bmatrix}. \end{aligned}$$

The gain of interest is the (1,1) element of $G_A^{\rm fb}$, i.e., $G_{1A}^{\rm fb}$. Using Eq. (4.5), the fluctuation of $G_{1A}^{\rm fb}$ is calculated as

$$\begin{aligned} \Delta G_{1A}^{\rm fb} =& \frac{1}{2}\left[\frac{G_1 + \Delta G_1 + K_{2A} + (G_2 + \Delta G_2)K_{1A}}{1 + (G_1 + \Delta G_1)K_{2A}} - \frac{G_1 + K_{2A} + G_2K_{1A}}{1 + G_1K_{2A}}\right]\left(\lambda_+^{\rm fb}\right)^{N-1} \\ &+ \frac{1}{2}\left[\frac{G_1 + \Delta G_1 + K_{2A} - (G_2 + \Delta G_2)K_{1A}}{1 + (G_1 + \Delta G_1)K_{2A}} - \frac{G_1 + K_{2A} - G_2K_{1A}}{1 + G_1K_{2A}}\right]\left(\lambda_-^{\rm fb}\right)^{N-1} \\ \approx& \frac{K_{1A}\Delta G_1}{2G_2(1 + G_1K_{2A})}\left[\left(\lambda_+^{\rm fb}\right)^N - \left(\lambda_-^{\rm fb}\right)^N\right]. \end{aligned}$$

As a result, the sensitivity function for the type-A scheme is represented as

$$S_A = \frac{\Delta G_{1A}^{\rm fb}/G_{1A}^{\rm fb}}{\Delta G_1/G_1} = \frac{K_{1A}G_1}{G_2(1 + G_1K_{2A})}\frac{G_{2A}^{\rm fb}}{G_{1A}^{\rm fb}}. \tag{4.7}$$

Next, consider the type-B feedback scheme, where the single feedback control is applied to the series of quantum amplifiers with transfer function matrix (4.4). Note that $G(0)$ can also be diagonalized by the orthogonal matrix P as

$$P^{-1}G(0)P = {\rm diag}\{\lambda_+,\ \lambda_-\} = \begin{bmatrix} \lambda_+ & 0 \\ 0 & \lambda_- \end{bmatrix},$$

where $\lambda_\pm = G_1 \pm G_2$ are the eigenvalues of $G(0)$. Then, the N product of $G(0)$ is given as follows:

$$[G(0)]^N \equiv \begin{bmatrix} M_1 & M_2 \\ M_2 & M_1 \end{bmatrix} = \frac{1}{2}\begin{bmatrix} \lambda_+^N + \lambda_-^N & \lambda_+^N - \lambda_-^N \\ \lambda_+^N - \lambda_-^N & \lambda_+^N + \lambda_-^N \end{bmatrix}.$$

From Eq. (4.6), the whole closed-loop system has the following transfer function matrix

$$G_B^{\rm fb} \equiv \begin{bmatrix} G_{1B}^{\rm fb} & G_{2B}^{\rm fb} \\ G_{2B}^{\rm fb} & G_{1B}^{\rm fb} \end{bmatrix} = \frac{1}{1+M_1K_{2B}}\begin{bmatrix} M_1+K_{2B} & M_2K_{1B} \\ M_2K_{1B} & M_1+K_{2B} \end{bmatrix}.$$

The characteristic change in G_1 and G_2 induces a small fluctuation in the overall gain, $G_{1B}^{\rm fb}$, as follows:

$$\begin{aligned}
\Delta G_{1B}^{\rm fb} &= \frac{M_1+\Delta M_1+K_{2B}}{1+(M_1+\Delta M_1)K_{2B}} - \frac{M_1+K_{2B}}{1+M_1K_{2B}} \\
&= \frac{K_{1B}^2\Delta M_1}{(1+M_1K_{2B})[1+(M_1+\Delta M_1)K_{2B}]} \\
&= \frac{K_{1B}^2M_2\Delta G_1}{(1+M_1K_{2B})[G_2+(M_1G_2+M_2\Delta G_1)K_{2B}]} \\
&\approx \frac{K_{1B}G_{2B}^{\rm fb}\Delta G_1}{G_2(1+M_1K_{2B})},
\end{aligned}$$

where $G_2\Delta M_1 = M_2\Delta G_1$ is used. The proof of this equation is shown as follows. If the gain of the j-th amplifier changes as $G_1 \to G_1+\Delta G_1$ and $G_2 \to G_2+\Delta G_2$, then $M_1 = (\lambda_+^N+\lambda_-^N)/2$ changes as follows:

$$\begin{aligned}
\Delta M_1 &= \frac{1}{2}\Big[(G_1+\Delta G_1+G_2+\Delta G_2)\lambda_+^{N-1} \\
&\qquad +(G_1+\Delta G_1-G_2-\Delta G_2)\lambda_-^{N-1}\Big] - M_1 \\
&= \frac{1}{2}\Big[(\Delta G_1+\Delta G_2)\lambda_+^{N-1}+(\Delta G_1-\Delta G_2)\lambda_-^{N-1}\Big] \\
&= \frac{\Delta G_1}{2}\left[\left(1+\frac{G_1}{G_2}\right)\lambda_+^{N-1}+\left(1-\frac{G_1}{G_2}\right)\lambda_-^{N-1}\right] \\
&= \frac{\Delta G_1}{2G_2}\Big[\lambda_+^N-\lambda_-^N\Big] = \frac{M_2}{G_2}\,\Delta G_1.
\end{aligned}$$

Therefore, the sensitivity function for the type-B scheme is given by

$$S_B = \frac{\Delta G_{1B}^{\rm fb}/G_{1B}^{\rm fb}}{\Delta G_1/G_1} = \frac{K_{1B}G_1}{G_2(1+M_1K_{2B})}\frac{G_{2B}^{\rm fb}}{G_{1B}^{\rm fb}}. \tag{4.8}$$

Now if the gains of both of the controlled systems are equal and these are smaller than the gain of the non-controlled cascaded amplifier, i.e., $|G_{1A}^{\rm fb}| = |G_{1B}^{\rm fb}| < |M_1|$, it is shown that

$$|S_B| < |S_A|. \tag{4.9}$$

Therefore, the type-B feedback scheme is better than the type-A scheme in terms of the sensitivity to the characteristic uncertainty ΔG_1. The proof of Eq. (4.9) is given as follows. To make a fair comparison, assume that both the controlled systems have the same amplification gain at $\omega = 0$, i.e., $|G_{1A}^{\rm fb}| = |G_{1B}^{\rm fb}|$, which leads to $|G_{2A}^{\rm fb}| = |G_{2B}^{\rm fb}|$. Then,

$$\frac{|S_B|}{|S_A|} = \left|\frac{K_{1B}}{K_{1A}}\frac{1+G_1K_{2A}}{1+M_1K_{2B}}\right| = \left|\frac{1+G_1K_{2A}}{K_{1A}}\right|\left|\frac{\left(\lambda_+^{\rm fb}\right)^N - \left(\lambda_-^{\rm fb}\right)^N}{\lambda_+^N - \lambda_-^N}\right|. \tag{4.10}$$

Here, from the relations $a^n - b^n = (a-b)\sum_{k=1}^n a^{n-k}b^{k-1}$ and $\lambda_+\lambda_- = \lambda_+^{\rm fb}\lambda_-^{\rm fb} = 1$, it follows that

$$\begin{aligned}
&\left(\lambda_+^{\rm fb}\right)^N - \left(\lambda_-^{\rm fb}\right)^N \\
&= \left(\lambda_+^{\rm fb} - \lambda_-^{\rm fb}\right)\left[\left(\lambda_+^{\rm fb}\right)^{N-1} + \left(\lambda_+^{\rm fb}\right)^{N-3} + \cdots + \left(\lambda_+^{\rm fb}\right)^{-(N-1)}\right] \\
&= \frac{2G_2K_{1A}}{1+G_1K_{2A}}\sum_{k=1}^{N}\left(\lambda_+^{\rm fb}\right)^{N-2k+1},
\end{aligned}$$

and likewise $\lambda_+^N - \lambda_-^N = 2G_2\sum_{k=1}^N \lambda_+^{N-2k+1}$. Hence, $|S_B|/|S_A|$ is now expressed as

$$\frac{|S_B|}{|S_A|} = \left|\frac{\sum_{k=1}^N\left(\lambda_+^{\rm fb}\right)^{N-2k+1}}{\sum_{k=1}^N\lambda_+^{N-2k+1}}\right|. \tag{4.11}$$

In addition to the condition $|G_{1A}^{\rm fb}| = |G_{1B}^{\rm fb}|$, assume that the gains of both of the type-A and type-B controlled systems are smaller than the gain of the non-controlled cascaded amplifier; $|G_{1A}^{\rm fb}| = |G_{1B}^{\rm fb}| < |M_1|$, which is represented as

$$\frac{|G_{1A}^{\rm fb}|}{|M_1|} = \left|\frac{\left(\lambda_+^{\rm fb}\right)^k + \left(\lambda_+^{\rm fb}\right)^{-k}}{\lambda_+^k + \lambda_+^{-k}}\right| < 1, \quad \forall k = 1, \cdots, N.$$

Then, if N is odd, Eq. (4.11) leads to

$$\frac{|S_B|}{|S_A|} = \left| \frac{1 + \sum_{k=1}^{(N-1)/2} \left[\left(\lambda_+^{\mathrm{fb}}\right)^{2k} + \left(\lambda_+^{\mathrm{fb}}\right)^{-2k} \right]}{1 + \sum_{k=1}^{(N-1)/2} \left(\lambda_+^{2k} + \lambda_+^{-2k}\right)} \right| = \frac{1 + \sum_{k=1}^{(N-1)/2} \left[\left(\lambda_+^{\mathrm{fb}}\right)^{2k} + \left(\lambda_+^{\mathrm{fb}}\right)^{-2k} \right]}{1 + \sum_{k=1}^{(N-1)/2} \left(\lambda_+^{2k} + \lambda_+^{-2k}\right)} < 1.$$

Also, if N is even, particularly $N = 4l - 2$ $(l = 1, 2, \cdots)$,

$$\frac{|S_B|}{|S_A|} = \left| \frac{\lambda_+^{\mathrm{fb}} + \left(\lambda_+^{\mathrm{fb}}\right)^{-1}}{\lambda_+ + \lambda_+^{-1}} \right| \frac{1 + \sum_{k=1}^{l-1} \left[\left(\lambda_+^{\mathrm{fb}}\right)^{4k} + \left(\lambda_+^{\mathrm{fb}}\right)^{-4k} \right]}{1 + \sum_{k=1}^{l-1} \left(\lambda_+^{4k} + \lambda_+^{-4k}\right)},$$

and if $N = 4l$ $(l = 1, 2, \cdots)$,

$$\frac{|S_B|}{|S_A|} = \left| \frac{\lambda_+^{\mathrm{fb}} + \left(\lambda_+^{\mathrm{fb}}\right)^{-1}}{\lambda_+ + \lambda_+^{-1}} \right| \frac{\sum_{k=1}^{l} \left[\left(\lambda_+^{\mathrm{fb}}\right)^{4k-2} + \left(\lambda_+^{\mathrm{fb}}\right)^{-(4k-2)} \right]}{\sum_{k=1}^{l} \left[\lambda_+^{4k-2} + \lambda_+^{-(4k-2)} \right]},$$

which are both less than 1. This completes the proof.

Remark 4.3.1. This remark discusses a difference between the quantum and classical sensitivity functions. Because the aim is to construct a high-gain feedback controlled amplifier, it can be assumed that $|G_{1\bullet}^{\mathrm{fb}}| \gg 1$ $(\bullet = A, B)$. Then, due to the constraint $|G_{1\bullet}^{\mathrm{fb}}|^2 - |G_{2\bullet}^{\mathrm{fb}}|^2 = 1$, the quantum sensitivity functions given in Eqs. (4.7) and (4.8) are then approximated as

$$S_A \approx \frac{K_{1A} G_1}{G_2(1 + G_1 K_{2A})}, \quad S_B \approx \frac{K_{1B} G_1}{G_2(1 + M_1 K_{2B})}.$$

Now further take $|G_1| \gg 1$; then, from $G_1^2 - G_2^2 = 1$, the quantum sensitivity function $S_\bullet$ is identical to the classical one (2.12) except for $K_{1\bullet}$. However, the idea of cascade amplification is to connect many low-gain amplifiers in series to realize $|G_{1\bullet}^{\mathrm{fb}}| \gg 1$ (e.g., Case 4 in Section 4.4); in this case G_1/G_2 takes a large value, and eventually $S_\bullet$ can become bigger than the classical one or even 1. In the classical case, this type of performance degradation does not occur, which is due to the increase of G_1/G_2. Note that this term stems from the CCR constraint on quantum mechanical systems.

Table 4.1: Nominal parameters and the resulting sensitivity.

	Case 1	Case 2	Case 3	Case 4
N	2		5	
M_1 [dB]	45	30	45	30
x	0.90	0.78	0.53	0.393
β_A	0.2	0.1	0.07	0.03
β_B	-0.0412	-0.0291	0.0034	0.0046
S_A	0.3388	0.7259	1.0718	1.4094
S_B	0.1190	0.5271	0.7428	1.2802
g_m [dB]	8.1310	18.4593	8.5699	19.9847

4.4 Simulation Results

As shown in the previous section, the superiority of the type-B scheme over the type-A is guaranteed to hold only at the center frequency $\omega = 0$. Thus, this section focuses on a specific system and numerically investigates the frequency dependence of the amplification gain in those two schemes, with particular attention to the robustness and stability properties. Here, the ideal NDPA, introduced in Subsection 2.2.4, is taken as the quantum amplifier. Moreover, as for the controller, consider the beam-splitter (BS), also introduced in Subsection 2.2.4, which is a 2 input-output passive static system with the following transfer function matrix:

$$K_\bullet(s) = \begin{bmatrix} \alpha_\bullet & -\beta_\bullet \\ \beta_\bullet & \alpha_\bullet \end{bmatrix}, \quad \alpha_\bullet^2 + \beta_\bullet^2 = 1,$$

where $\bullet = A, B$. The real parameters $\alpha_\bullet, \beta_\bullet \in \mathbb{R}$ represent the transmissivity and reflectivity of the mirror, respectively. Note that, from Eq. (4.3), the single NDPA with this controller has the amplification gain $1/|\beta_\bullet|$ in the limit $x \to 1 - 0$.

Now, consider the four cases summarized in Table 4.1; the number of amplifiers is $N = 2$ (Cases 1 and 2) or $N = 5$ (Cases 3 and 4); the gain of the (1,1) element of

$[G(0)]^N$, i.e., the non-controlled cascaded NDPA at $\omega = 0$, is $M_1 = 45$ dB (Cases 1 and 3) or $M_1 = 30$ dB (Cases 2 and 4). In each case, the cavity decay rate of the NDPA is fixed to $\kappa = 1.8 \times 10^7$ Hz [83, 101], while $x = 2\varepsilon/\kappa$ is chosen so that M_1 equals to 45 dB or 30 dB. The reflectivity β_B was determined as follows; first the parameters of the type-A system is fix, x and β_A, and then β_B is determined so that the gains at $\omega = 0$ of both of the schemes are the same, i.e., $|G_{1A}^{\mathrm{fb}}| = |G_{1B}^{\mathrm{fb}}|$.

First, see the stability of the feedback-controlled systems. For the type-A system, it is enough to analyze the stability of the single feedback-controlled NDPA; its characteristic equation is given by

$$s^2 + \frac{\kappa}{1-\beta_A}s + \frac{1+\beta_A}{1-\beta_A}\frac{\kappa^2}{4} - \varepsilon^2 = 0.$$

Using Routh's stability criterion introduced in Subsection 2.1.3, the type-A system is stable if and only if

$$x = \frac{2\varepsilon}{\kappa} < \sqrt{\frac{1+\beta_A}{1-\beta_A}}.$$

This condition is always satisfied if the NDPA is stable ($x < 1$) and $0 \le \beta_A < 1$.

On the other hand, to analyze the stability property of the type-B system, the Nyquist plot is used, which is now directly applicable because all the parameters $(\kappa, \varepsilon, \alpha_B, \beta_B)$ are real. Now, from Eq. (4.3), the type-B system has the open-loop transfer function $L(s) = -[G^N]_{22}(s)\beta_B$, where $[G^N]_{22}(s)$ is the (2,2) element of $G(s)^N$. The Nyquist plots are shown in Fig. 4.4; hence, from the Nyquist stability criterion, the type-B system is stable in all Cases.

Next, discuss the sensitivity of the controlled systems. To see this explicitly, suppose that the characteristic change of the amplifier, ΔG_1, stems from the fluctuation of the parameter ε. This uncertainty is modeled as $\varepsilon' = (1+0.05r)\varepsilon$, where r is the random number generated from the uniform distribution over $[-1, 1]$; that is, the nominal parameter $x = 2\varepsilon/\kappa$ given in Table 4.1 experiences up to 5% deviation. The gain plots are shown in Fig. 4.5, where the red and blue lines represent the gains of the type-A and the type-B systems, respectively. Also, the black lines are the gain plots of the cascaded amplifier without feedback. In each scheme

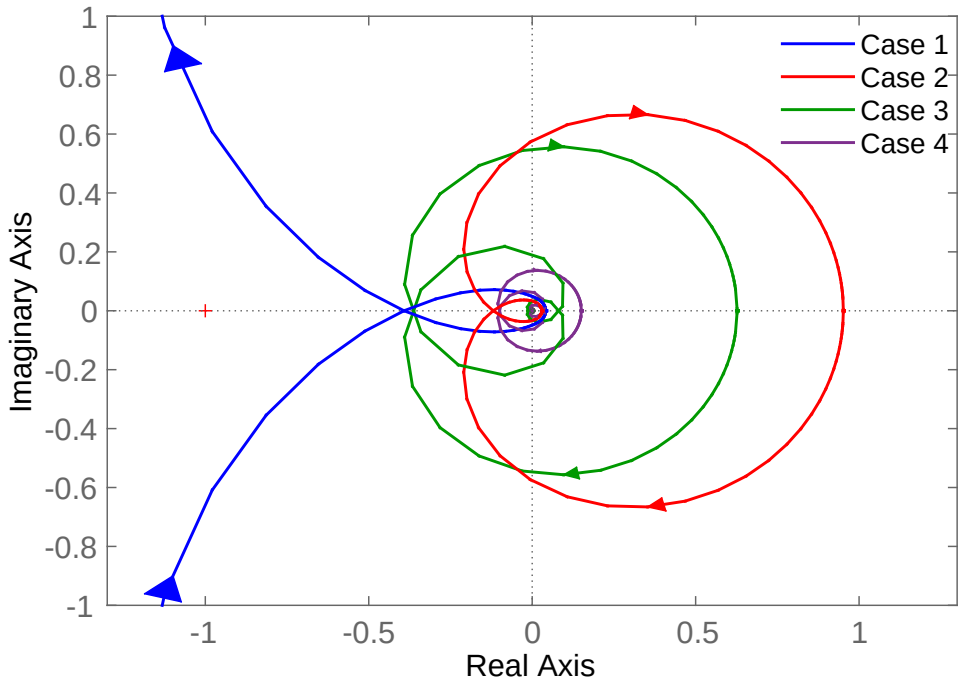

Figure 4.4: Nyquist plots of the type-B controlled system.

(color), 100 sample paths are produced from the above-mentioned probability distribution. To make the feature of each Case visible, the gain plots are drawn with the different scale of the vertical axis. Figure 4.5 shows that, in all Cases, the fluctuation of the gain at $\omega = 0$ of the type-B controlled system is always smaller than that of the type-A, i.e., $|S_B| < |S_A|$, as proven in the previous section. Moreover, in Case 1, 2, and 3, the gain fluctuation of the controlled systems at $\omega = 0$ can be smaller than that of the uncontrolled system; that is, the feedback control works well to suppress the gain fluctuation of the amplifier, at the price of decreasing the gain. However, importantly, this fact does not hold over all frequencies; particularly in Cases 1 and 3, the type-A scheme is better than the type-B, at the frequency $\omega \sim \kappa/10$ where there is a peaking in the gain.

Finally, discuss the control performance, with the focus on both stability and sensitivity. Now, as shown in Table 4.1, the gain margin g_m in Cases 1 and 3 are smaller than that in Cases 2 and 4. Hence, the feedback systems in Cases 1

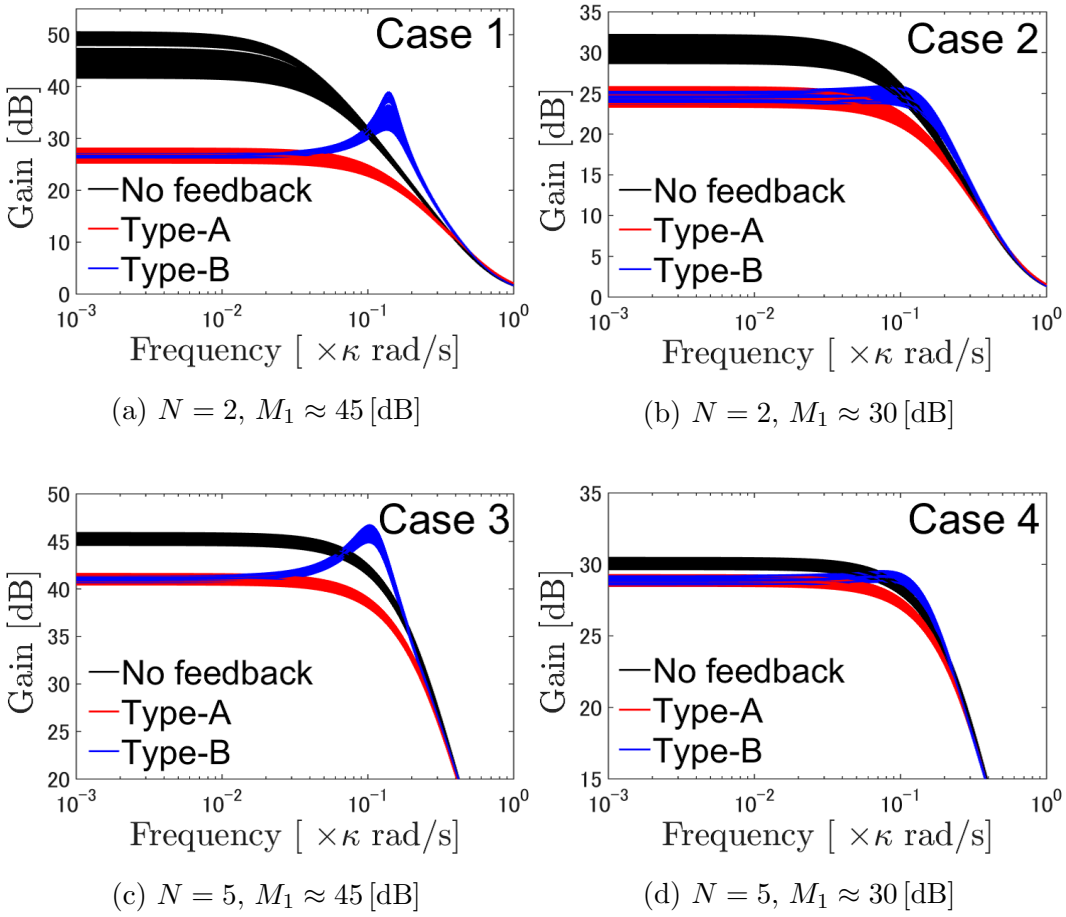

(a) $N = 2$, $M_1 \approx 45$ [dB]

(b) $N = 2$, $M_1 \approx 30$ [dB]

(c) $N = 5$, $M_1 \approx 45$ [dB]

(d) $N = 5$, $M_1 \approx 30$ [dB]

Figure 4.5: Gain plots of the feedback-controlled system.

and 3 are less stable than those in Cases 2 and 4; actually a peaking appears in Figs. 4.5(a) and (c), but not in (b) and (d). However, as implied by Fig. 4.5, it is harder to reduce the sensitivity in Cases 2 and 4, compared to Cases 1 and 3. That is, there is a trade-off between the stability and robustness. Note also that the controlled system with less number of amplifiers has the better sensitivity; that is, if the controlled system composed of $N = 5$ amplifiers has the same level of sensitivity as that of the system with $N = 2$, it will become unstable.

4.5 Summary

This chapter has studied two types of feedback control schemes for the cascaded quantum amplifier. The sensitivity analysis has shown the following theorem, which is useful in constructing a robust high-gain quantum amplifier by connecting some low-gain amplifiers: it is always better to construct a single feedback loop for the cascaded amplifier, than to connect feedback-controlled amplifiers. Moreover, importantly note that the quantum sensitivity functions have different characteristic from the classical ones. This fact indicates that the robustness of whole closed-loop system may be degraded by connecting some quantum amplifiers with very low-gain (the amplification is realized at quantum-level). In the numerical simulation shown in Section 4.4, the performance in robustness and stability has been investigated, and especially in Case 4, the quantumness of sensitivity function becomes prominent.

Chapter 5

Conclusions and Future Works

5.1 Conclusions

This thesis has provided the design methods for engineering quantum signal detectors within the framework of coherent feedback control. These methods will work as the key techniques for the quantum sensor and the quantum amplifier, and will become the first step for developing more advanced control theory. The main results have been shown in Chapter 3 and 4.

Chapter 3 has provided the general theory for constructing a back-action evading sensor for linear quantum systems, based on the well-developed classical geometric control theory. The main contribution of Chapter 3 is to show the class of linear quantum systems with special structure (3.11), which can be realized by using the multi-input and multi-output controller and some scattering processes. This system modification enables the geometric control theory to be directly applicable. The power of the theory has been shown by demonstrating the controller design for the typical opto-mechanical oscillator. First, given a plant sensor system, then whether the BAE controller exists or not can be checked by the solvability conditions given in Theorem 2.1.3 or Corollary 2.1.1. Note that this condition depends only on the given plant matrices. If the solvability condition is satisfied, then the BAE controller can be fully parametrized by the matrices (A_K, B_K, C_K) given in (3.13) with (3.12). A notable fact is that not only the coherent feedback control

scheme but also the direct interaction control scheme can be formulated within the framework of geometric control theory. Then, the design theory developed in Chapter 3 contains the result of Ref. [44].

Moreover, another contribution of Chapter 3 is to provide a general procedure for designing an approximate BAE controller under realistic imperfections. That is, an optimal approximate BAE system can be obtained by solving the minimization problem of the transfer function from the back-action noise to the measurement output.

Chapter 4 has discussed the sensitivity of cascaded quantum feedback amplifier. The long-term goal of this work is to develop the design theory for feedback-controlled quantum networks containing amplifiers, corresponding to the established classical one [46, 47, 48, 49, 50, 51, 52]. Toward this goal, as an important first step, Chapter 4 considers the quantum versions of the two types of cascaded feedback structures discussed in Ref. [51]. The sensitivity functions of the cascaded quantum systems are defined under some reasonable assumptions, and by analyzing them, the following theorem is obtained: to construct a robust high-gain quantum amplifier from some low-gain amplifiers, it is always better to stabilize the cascaded amplifier via constructing a single feedback loop, than to take a cascade connection of feedback-controlled amplifiers. Recall that, although this is the same conclusion as the classical one, the proof of this fact is highly non-trivial. Also, as stated in Remark 4.3.1 and shown in Section 4.4, the sensitivity functions of the quantum feedback amplifiers have different characteristic from the classical counterparts. As a consequence, a more careful sensitivity analysis will be required in general for designing a practical quantum network device, e.g., a robust quantum communication channel over a specific bandwidth [62, 63, 64].

5.2 Future Works

The Final goal is to realize a high-precision detection of weak signals in the quantum regime by using some feedback-controlled detectors. Toward this goal, the systematic approach shown in this thesis will become the first step for giving an

answer to the question of how each quantum signal detector should be designed. Also, two works shown in this thesis will lead to the following future works.

As for engineering a quantum sensor for a weak signal, there are mainly two research directions. From the view of experiment, it is important to physically implement the BAE controller based on the control theory and to study how much the noise power can be suppressed. Moreover, although the opto-mechanical system has been studied as a simple example for the purpose of demonstration, the theory developed in this thesis can be applied to various types of linear quantum sensor because of its generality. Then, the real advantage of the theory will appear when dealing with more complicated multi-mode systems such as the interferometer [3] shown in Chapter 1, or an opto-mechanical system containing a membrane [102, 103, 104]. Another important work is to develop the design theory for engineering an approximate BAE controller. In such a practical case, whether or not the measurement should be performed becomes an open problem again. That is, it is important to compare the measurement-based feedback and the coherent feedback, and to select the better control scheme. There are some possible control methods in classical control theory, e.g., observer-based control [9], linear quadratic Gaussian (LQG) control, and H_∞ control theory [98]. If the controller is designed within the framework of coherent feedback control, the quantum version of these well-developed methods has been recently studied [80, 81, 84, 105, 106].

On the other hand, as for the cascaded quantum feedback amplifier, this thesis has focused only on the $(1,1)$ elements of the closed-loop transfer functions. Then, the next important task is to study the sensitivity of an idler mode, whose existence is a clear difference between the quantum and classical amplifier. Furthermore, the sensitivity analysis shown in this thesis will be extended to another type of quantum amplifier such as 2-signal microwave amplifier based on the dc-superconducting quantum interference detector (SQUID) [107].

Appendix A

Algorithms for Computing $\mathcal{V}^*$ and $\mathcal{V}_*$

The set of (A, B)-invariant subspaces has a unique maximum element contained in a given subspace $\mathcal{H} \subseteq \mathcal{X}$. This space, denoted by $\mathcal{V}^*{}_{(\mathcal{B},\mathcal{H})}$, can be computed by the following algorithm:

$\mathcal{V}^*$ - **algorithm** :

(Step 1) $\mathcal{V}_0 \equiv \mathcal{H}$,

(Step 2) $\mathcal{V}_i \equiv \mathcal{H} \cap A^{-1}(\mathcal{V}_{i-1} \oplus \mathcal{B})$ $(i = 1, 2, \ldots)$,

(Step 3) $\mathcal{V}^*{}_{(\mathcal{B},\mathcal{H})} = \mathcal{V}_i$ (if $\mathcal{V}_i = \mathcal{V}_{i-1}$ in Step 2).

Similarly, the set of (C, A)-invariant subspaces has a unique minimum element containing a given subspace $\mathcal{E} \subseteq \mathcal{X}$. This space, denoted by $\mathcal{V}_{*(\mathcal{C},\mathcal{E})}$, can be computed by the following algorithm:

$\mathcal{V}_*$ - **algorithm** :

(Step 1) $\mathcal{V}_0 \equiv \mathcal{E}$,

(Step 2) $\mathcal{V}_i \equiv \mathcal{E} \oplus A(\mathcal{V}_{i-1} \cap \mathcal{C})$ $(i = 1, 2, \ldots)$,

(Step 3) $\mathcal{V}_{*(\mathcal{C},\mathcal{E})} = \mathcal{V}_i$ (if $\mathcal{V}_i = \mathcal{V}_{i-1}$ in Step 2).

Appendix B

Classical Description of Opto-mechanics

Consider the following equations of classical harmonic oscillator [100]:

$$\frac{dq}{dt} = \frac{p}{m},$$
$$\frac{dp}{dt} = -m\omega_m^2 q - \gamma p + F + F_{\rm th},$$

where q and p are the position and momentum of the oscillator, m the mass, ω_m the resonant frequency, γ the damping rate, F the unknown force, and $F_{\rm th}$ the thermal force. The above q and p do not satisfy the canonical commutation relation, $[q, p] \neq i$, then introduce the dimensionless position and momentum operators such that

$$\hat{q}_1 = \frac{q}{x_{\rm zpf}} = q\sqrt{\frac{m\omega_m}{\hbar}}, \quad \hat{p}_1 = \frac{p x_{\rm zpf}}{\hbar} = \frac{p}{\sqrt{m\hbar\omega_m}},$$

where $x_{\rm zpf} = \sqrt{\hbar/m\omega_m}$ is the zero point fluctuation, and $\hbar = h/2\pi$ the (reduced) Planck constant. These new operators obey the following equations:

$$\frac{d\hat{q}_1}{dt} = \omega_m \hat{p}_1,$$
$$\frac{d\hat{p}_1}{dt} = -\omega_m \hat{q}_1 - \gamma \hat{p}_1 + \sqrt{\gamma}(\hat{f} + \hat{f}_{\rm th}),$$

where $\hat{f} = F/\sqrt{\hbar m\gamma\omega_m}$ and $\hat{f}_{\rm th} = F_{\rm th}/\sqrt{\hbar m\gamma\omega_m}$. Finally, the additional terms, $i[H_{\rm rad}, \hat{q}_1]$ and $i[H_{\rm rad}, \hat{p}_1]$, which are due to the radiation-pressure interaction, are

added to the above equations, $\hat{H}_{\rm rad} = -g\hat{q}_1\hat{q}_2$. As a result, the following equations are obtained:

$$\begin{aligned}\frac{d\hat{q}_1}{dt} &= \omega_m \hat{p}_1, \\ \frac{d\hat{p}_1}{dt} &= -\omega_m \hat{q}_1 - \gamma\hat{p}_1 + g\hat{q}_2 + \sqrt{\gamma}(\hat{f} + \hat{f}_{\rm th}).\end{aligned}$$

In Section 3.1, 3.2, and 3.3, the thermal noise $\hat{f}_{\rm th}$ and the damping effect $-\gamma\hat{p}_1$ are ignored.

Appendix C

Passivity Condition of Linear Quantum Systems

This appendix provides the passivity condition of a general linear quantum system. First note that the system dynamics (2.18) and (2.19), which can be represented as

$$\frac{d\hat{x}}{dt} = A\hat{x} + B\hat{W}, \quad \hat{W}^{\rm out} = C\hat{x} + D\hat{W}, \tag{C.1}$$

with $\hat{W} = [(\hat{W}_1)^\top \ \cdots \ (\hat{W}_m)^\top]^\top$ and $\hat{W}^{\rm out} = [(\hat{W}_1^{\rm out})^\top \ \cdots \ (\hat{W}_m^{\rm out})^\top]^\top$, has the following equivalent expression:

$$\begin{aligned} \frac{d}{dt}\begin{bmatrix} \hat{a} \\ \hat{a}^\sharp \end{bmatrix} &= \mathscr{A}\begin{bmatrix} \hat{a} \\ \hat{a}^\sharp \end{bmatrix} + \mathscr{B}\begin{bmatrix} \hat{A} \\ \hat{A}^\sharp \end{bmatrix}, \\ \begin{bmatrix} \hat{A}^{\rm out} \\ \hat{A}^{{\rm out}\sharp} \end{bmatrix} &= \mathscr{C}\begin{bmatrix} \hat{a} \\ \hat{a}^\sharp \end{bmatrix} + \mathscr{D}\begin{bmatrix} \hat{A} \\ \hat{A}^\sharp \end{bmatrix}, \end{aligned} \tag{C.2}$$

where $\hat{a} = [\hat{a}_1 \ \cdots \ \hat{a}_n]^\top$ and $\hat{A} = [\hat{A}_1 \ \cdots \ \hat{A}_m]^\top$ are vectors of annihilation operators. By definition, $\hat{a}^\sharp = [\hat{a}_1^* \ \cdots \ \hat{a}_n^*]^\top$. The coefficient matrices are of the form

$$\begin{aligned} \mathscr{A} &= \begin{bmatrix} \mathscr{A}_- & \mathscr{A}_+ \\ \mathscr{A}_+^\sharp & \mathscr{A}_-^\sharp \end{bmatrix}, \quad \mathscr{B} = \begin{bmatrix} \mathscr{B}_- & \mathscr{B}_+ \\ \mathscr{B}_+^\sharp & \mathscr{B}_-^\sharp \end{bmatrix}, \\ \mathscr{C} &= \begin{bmatrix} \mathscr{C}_- & \mathscr{C}_+ \\ \mathscr{C}_+^\sharp & \mathscr{C}_-^\sharp \end{bmatrix}, \quad \mathscr{D} = \begin{bmatrix} \mathscr{D}_- & \mathscr{D}_+ \\ \mathscr{D}_+^\sharp & \mathscr{D}_-^\sharp \end{bmatrix}. \end{aligned} \tag{C.3}$$

As in the case of (C.1), these matrices have to satisfy the physical realizability condition; e.g., see [108, 109]. The passivity condition of this system is defined as follows:

Definition C.1. The system (C.2) is said to be passive if the matrices satisfy $\mathscr{A}_+ = O$ and $\mathscr{B}_+ = O$, in addition to the physical realizability condition.

Note that a passive system is constituted only with annihilation operator variables; a typical optical realization of the passive system is an empty optical cavity. Moreover, $\mathscr{D}_+ = O$ is already satisfied and $\mathscr{B}_+ = O$ leads to $\mathscr{C}_+ = O$. This is the reason why it is sufficient to consider the constraints only on $\mathscr{A}_+$ and $\mathscr{B}_+$. Then the goal here is to represent the conditions $\mathscr{A}_+ = O$ and $\mathscr{B}_+ = O$ in terms of the coefficient matrices of Eq. (C.1). For this purpose, introduce the permutation matrix P_n as follows; for a column vector $z = [z_1 \ z_2 \ \cdots \ z_{2n}]^\top$, P_n is defined through $P_n z = [z_1 \ z_3 \ \ldots \ z_{2n-1} \ z_2 \ z_4 \ \cdots \ z_{2n}]^\top$. Note that P_n satisfies $P_n P_n^\top = P_n^\top P_n = I_{2n}$. Then, the coefficient matrices of the above two system representations are connected by

$$A = P_n^\top \tilde{\mathscr{A}} P_n, \quad B = P_n^\top \tilde{\mathscr{B}} P_m, \quad C = P_m^\top \tilde{\mathscr{C}} P_n, \quad D = P_m^\top \tilde{\mathscr{D}} P_m,$$

where

$$\tilde{\mathscr{A}} = \frac{1}{2} \begin{bmatrix} \mathscr{A}_- + \mathscr{A}_-^\sharp + \mathscr{A}_+ + \mathscr{A}_+^\sharp & i(\mathscr{A}_- - \mathscr{A}_-^\sharp - \mathscr{A}_+ + \mathscr{A}_+^\sharp) \\ -i(\mathscr{A}_- - \mathscr{A}_-^\sharp + \mathscr{A}_+ - \mathscr{A}_+^\sharp) & \mathscr{A}_- + \mathscr{A}_-^\sharp - (\mathscr{A}_+ + \mathscr{A}_+^\sharp) \end{bmatrix}.$$

$\tilde{\mathscr{B}}$, $\tilde{\mathscr{C}}$, and $\tilde{\mathscr{D}}$ have the same forms as above. Then, the following theorem, providing the passivity condition in the quadrature form, is obtained:

Theorem C.1. The system (C.1) is passive if and only if, in addition to the physical realizability condition (2.20), the following equalities hold:

$$\Sigma_n A \Sigma_n = -A, \quad \Sigma_n B \Sigma_m = -B.$$

Proof: First define $\Psi_n = \Sigma \otimes I_n = [O, I_n; -I_n, O]$, which leads to $P_n^\top \Psi_n P_n = \Sigma_n$. Then, it can be shown that

$$\Sigma_n A \Sigma_n = -A \iff \Psi_n \tilde{\mathscr{A}} \Psi_n = -\tilde{\mathscr{A}}.$$

The condition in the right hand side is equivalent to $\mathscr{A}_+ + \mathscr{A}_+^\sharp = O$ and $\mathscr{A}_+ - \mathscr{A}_+^\sharp = O$, which thus leads to $\mathscr{A}_+ = O$. Also, from a similar calculation, $\Sigma_n B \Sigma_m = -B \Leftrightarrow \mathscr{B}_+ = O$. ■

Next consider the passivity condition of the direct interaction controller discussed in Section 3.3. The setup is that, for a given linear quantum system, an auxiliary component with variable $\hat{x}_K$is added, which is characterized by the Hamiltonians (3.18). The point is that these Hamiltonians have the following equivalent representations in terms of the vector of annihilation operators $\hat{a}$ and $\hat{a}_K$:

$$\begin{aligned}
\hat{H}_K &= \frac{1}{2} \begin{bmatrix} \hat{a}_K^\dagger & \hat{a}_K^\top \end{bmatrix} \mathscr{R}_K \begin{bmatrix} \hat{a}_K \\ \hat{a}_K^\sharp \end{bmatrix}, \\
\hat{H}_{\rm int} &= \frac{1}{2} \left(\begin{bmatrix} \hat{a}^\dagger & \hat{a}^\top \end{bmatrix} \mathscr{R}_1 \begin{bmatrix} \hat{a}_K \\ \hat{a}_K^\sharp \end{bmatrix} + \begin{bmatrix} \hat{a}_K^\dagger & \hat{a}_K^\top \end{bmatrix} \mathscr{R}_2 \begin{bmatrix} \hat{a} \\ \hat{a}^\sharp \end{bmatrix} \right).
\end{aligned} \tag{C.4}$$

The matrices $\mathscr{R}_K, \mathscr{R}_1$, and $\mathscr{R}_2$ are of the same forms as those in Eq. (C.3). Note that they have to satisfy the physical realizability conditions $\mathscr{R}_K = \mathscr{R}_K^\dagger$ and $\mathscr{R}_1^\dagger = \mathscr{R}_2$. Now, the passivity property of the direct interaction controller can be defined; that is, if the Hamiltonians (C.4) does not contain any quadratic term such as $\hat{a}_{K,1}^{*2}$ and $\hat{a}_1^* \hat{a}_{K,1}^*$, then the direct interaction controller is passive. The formal definition is given as follows:

Definition C.2. The direct interaction controller constructed by Hamiltonians (C.4) is said to be passive if, in addition to the physical realizability conditions $\mathscr{R}_K = \mathscr{R}_K^\dagger$ and $\mathscr{R}_1^\dagger = \mathscr{R}_2$, the matrices satisfy $\mathscr{R}_{K+} = O$ and $\mathscr{R}_{2+} = O$.

Through almost the same way shown above, the following result is obtained:

Theorem C.2. The direct interaction controller constructed by Hamiltonians (3.18) is passive if and only if, in addition to the physical realizability conditions $R_K = R_K^\top$ and $R_1^\top = R_2$, the following equalities hold:

$$\Sigma_{n_k} R_K \Sigma_{n_k} = -R_K, \quad \Sigma_{n_k} R_2 \Sigma_n = -R_2.$$

Bibliography

[1] C. L. Degen, F. Reinhard, and P. Cappellaro, "Quantum sensing," *Rev. Mod. Phys.*, vol. 89, no. 3, 2017, Art. no. 035002.

[2] C. M. Caves, K. S. Thorne, R. W. P. Drever, V. D. Sandberg, and M. Zimmermann, "On the measurement of a weak classical force coupled to a quantum-mechanical oscillator. I. Issues of principle," *Rev. Mod. Phys.*, vol. 52, no. 2, pp. 341–392, 1980.

[3] H. Miao, *Exploring Macroscopic Quantum Mechanics in Optomechanical Devices*, Springer Berlin, 2012.

[4] Y. Chen, "Macroscopic quantum mechanics: theory and experimental concepts of optomechanics," *J. Phys. B: At. Mol. Opt. Phys.*, vol. 46, no 10, 2013, Art. no. 104001.

[5] J. M. Taylor *et al.*, "High-sensitivity diamond magnetometer with nanoscale resolution," *Nat. Phys.*, vol. 4, pp. 810–816, 2008.

[6] K. Fang *et al.*, "High-sensitivity magnetometry based on quantum beats in diamond nitrogen-vacancy centers," *Phys. Rev. Lett.*, vol. 110, no. 13, 2013, Art. no. 130802.

[7] Y. Matsuzaki *et al.*, "Optically detected magnetic resonance of high-density ensemble of NV^- centers in diamond," *J. Phys. Condensed Matter*, vol. 28, no. 27, 2016, Art. no. 275302.

[8] W. Nawrocki, *Measurement Systems and Sensors*, London, UK: Artech House, 2005.

[9] R. C. Dorf and R. H. Bishop, *Modern Control Systems*, 11th ed. Upper Saddle River, NJ, USA: Pearson Prentice Hall, 2008.

[10] G. F. Franklin, J. D. Powell, and A. Emani-Naeini, *Feedback Control of Dynamic Systems*, 6th ed. Upper Saddle River, NJ, USA: Pearson Prentice Hall, 2010.

[11] F. Golnaraghi and B. C. Kuo, *Automatic Control Systems*, 9th ed. Hoboken, NJ, USA: Wiley, 2010.

[12] Z. Y. Ou, S. F. Pereira, and H. J. Kimble, "Realization of the Einstein-Podolsky-Rosen paradox for continuous variables in nondegenerate parametric amplification," *Appl. Phys. B*, vol. 55, no. 3, pp. 265–278, 1992.

[13] Y. Wang *et al.*, "Experimental generation of 6 dB continuous variable entanglement from a nondegenerate optical parametric amplifier," *Opt. Express*, vol. 18, no. 6, pp. 6149–6155, 2010.

[14] B. Yurke *et al.*, "Observation of 4.2-K equilibrium-noise squeezing via a Josephson-parametric amplifier," *Phys. Rev. Lett.*, vol. 60, no. 9, pp. 764–767, 1988.

[15] B. Yurke *et al.*, "Observation of parametric amplification and deamplification in a Josephson parametric amplifier," *Phys. Rev. A*, vol. 39, no. 5, pp. 2519–2533, 1989.

[16] B. Abdo, F. Schackert, M. Hatridge, C. Rigetti, and M. Devoret, "Josephson amplifier for qubit readout," *Appl. Phys. Lett.*, vol. 99, no. 16, 2011, Art. no. 162506.

[17] B. Abdo *et al.*, "Josephson directional amplifier for quantum measurement of superconducting circuits," *Phys. Rev. Lett.*, vol. 112, no. 16, 2014, Art. no. 167701.

[18] H. A. Bachor and T. C. Ralph, *A Guide to Experiments in Quantum Optics,* 2nd ed. Weinheim, Germany: Wiley-VCH, 2004.

[19] A. Furusawa and P. van Loock, *Quantum Teleportation and Entanglement: A Hybrid Approach to Optical Quantum Information Processing,* Berlin, Germany: Wiley-VCH, 2011.

[20] V. B. Braginsky and F. Y. Khalili, *Quantum Measurement*, Cambridge, UK: Cambridge Univ. Press, 1992.

[21] V. B. Braginsky, "Detection of gravitational waves from astrophysical sources," *Astronomy Lett.* vol. 34, no. 8, pp. 558–562, 2008.

[22] A. Einstein, "Approximative integration of the field equations of gravitation," *Proceedings of the Royal Prussian Academy of Sciences*, vol. 1, pp. 688–696, 1916.

[23] A. Einstein, "About gravity waves," *Proceedings of the Royal Prussian Academy of Sciences*, vol. 1, pp. 154–167, 1918.

[24] B. P. Abbott *et al.*, "Observation of gravitational waves from a binary black hole merger," *Phys. Rev. Lett.*, vol. 116, no. 6, 2016, Art. no. 061102.

[25] G. J. Milburn and M. J. Woolley, "An introduction to quantum optomechanics," *Acta Physica Slovaca*, vol. 61, no. 5, pp. 483–601, 2011.

[26] C. L. Latune, B. M. Escher, R. L. de Matos Filho, and L. Davidovich, "Quantum limit for the measurement of a classical force coupled to a noisy quantum-mechanical oscillator," *Phys. Rev. A*, vol. 88, no. 4, 2013, Art. no. 042112.

[27] M. Aspelmeyer, T. J. Kippenberg, and F. Marquardt, "Cavity optomechanics," *Rev. Mod. Phys.*, vol. 86, no. 4, pp. 1391–1452, 2014.

[28] T. Corbitt, Y. Chen, E. Innerhofer, H. Müller-Ebhardt, D. Ottaway, H. Rehbein, D. Sigg, S. Whitcomb, C. Wipf, and N. Mavalvala, "An all-optical trap for a gram-scale mirror," *Phys. Rev. Lett.*, vol. 98, no. 15, 2007, Art. no. 150802.

[29] J. D. Thompson, B. M. Zwickl, A. M. Jayich, F. Marquardt, S. M. Girvin, and J. G. E. Harris, "Strong dispersive coupling of a high-finesse cavity to a micromechanical membrane," *Nature*, vol. 452, pp. 72–75, 2008.

[30] E. Verhagen, S. Deléglise, S. Weis, A. Schliesser, and T. J. Kippenberg, "Quantum-coherent coupling of a mechanical oscillator to an optical cavity mode," *Nature*, vol. 482, pp. 63–67, 2012.

[31] N. Matsumoto, K. Komori, Y. Michimura, G. Hayase, Y. Aso, and K. Tsubono, "5-mg suspended mirror driven by measurement-induced backaction," *Phys. Rev. A*, vol. 92, no. 3, 2015, Art. no. 033825.

[32] M. Underwood, D. Mason, D. Lee, H. Xu, L. Jiang, A. B. Shkarin, K. Børkje, S. M. Girvin, and J. G. E. Harris, "Measurement of the motional sidebands of a nanogram-scale oscillator in the quantum regime," *Phys. Rev. A*, vol. 92, no. 6, 2015, Art. no. 061801.

[33] H. P. Yuen, "Contractive states and the standard quantum limit for monitoring free-mass positions," *Phys. Rev. Lett.*, vol. 51, no. 9, pp. 719–722, 1983.

[34] C. M. Caves, "Defense of the standard quantum limit for free-mass position," *Phys. Rev. Lett.*, vol. 54, no. 23, pp. 2465–2468, 1985.

[35] M. Ozawa, "Measurement breaking the standard quantum limit for free-mass position," *Phys. Rev. Lett.*, vol. 60, no. 5, pp. 385–388, 1988.

[36] J. Maddox, "Beating the quantum limits," *Nature*, vol. 331, p. 559, 1988.

[37] S. P. Vyatchanin and E. A. Zubova, "Quantum variation measurement of a force," *Phys. Lett. A*, vol. 201, no. 4, pp. 269–274, 1995.

[38] H. J. Kimble, Y. Levin, A. B. Matsko, K. S. Thorne, and S. P. Vyatchanin, "Conversion of conventional gravitational-wave interferometers into quantum nondemolition interferometers by modifying their input and/or output optics," *Phys. Rev. D*, vol. 65, no. 2, 2001, Art. no. 022002.

[39] F. Y. Khalili, "Quantum variational measurement in the next generation gravitational-wave detectors," *Phys. Rev. D*, vol. 76, no. 10, 2007, Art. no. 102002.

[40] J. M. Courty, A. Heidmann, and M. Pinard, "Back-action cancellation in interferometers by quantum locking," *Europhys. Lett.*, vol. 63, no. 2, pp. 226–232, 2003.

[41] J. M. Courty, A. Heidmann, and M. Pinard, "Quantum locking of mirrors in interferometers," *Phys. Rev. Lett.*, vol. 90, no. 8, 2003, Art. no. 083601.

[42] D. Vitali, M. Punturo, S. Mancini, P. Amico, and P. Tombesi, "Noise reduction in gravitational wave interferometers using feedback," *J. Opt. B: Quantum Semiclass. Opt.*, vol. 6, no. 8, pp. S691–S697, 2004.

[43] H. Miao, H. Yang, R. X. Adhikari, and Y. Chen, "Quantum limits of interferometer topologies for gravitational radiation detection," *Class. Quantum Grav.* vol. 31, no. 16, 2014, Art. no. 165010.

[44] M. Tsang and C. M. Caves, "Coherent quantum-noise cancellation for optomechanical sensors," *Phys. Rev. Lett.*, vol. 105, no. 12, 2010, Art. no. 123601.

[45] N. Yamamoto, "Coherent versus measurement feedback: Linear systems theory for quantum information," *Phys. Rev. X*, vol. 4, no. 4, 2014, Art. no. 041029.

[46] J. G. Graeme, G. E. Tobey, and L. P. Huelsman, *Operational Amplifiers: Design and Applications*, New York, NY, USA: McGraw-Hill, 1971.

[47] H. S. Black, "Stabilized feedback amplifiers," *Bell Syst. Tech. J.*, vol. 13, no. 1, pp. 1–18, 1934.

[48] R. B. Blackman, "Effect of feedback on impedance," *Bell Syst. Tech. J.*, vol. 22, no. 3, pp. 269–277, 1943.

[49] H. W. Bode, *Network Analysis and Feedback Amplifier Design*. Princeton, NJ, USA: D. Van Nostrand, 1945.

[50] H. Nyquist, "Regeneration Theory," *Bell Syst. Tech. J.*, vol. 11, no. 3, pp. 126–147, 1932.

[51] D. H. Horrocks, *Feedback Circuits and Op. Amps*, 2nd ed. London, UK: Chapman and Hall, 1990.

[52] M. R. Samadi, A. I. Karsilayan and J. Silva-Martinez, "Bandwidth enhancement of multi-stage amplifiers using active feedback," *IEEE International Symposium on Circuits and Systems*, Vancouver, BC, pp. I-609–612, 2004.

[53] W. H. Louisell, A. Yariv, and A. E. Siegman, "Quantum fluctuations and noise in parametric processes. I," *Phys. Rev.*, vol. 124, no. 6, pp. 1646–1654, 1961.

[54] H. A. Haus and J. A. Mullen, "Quantum noise in linear amplifiers," *Phys. Rev.*, vol. 128, no. 5, pp. 2407–2413, 1962.

[55] J. P. Gordon, W. H. Louisell, and L. R. Walker, "Quantum fluctuations and noise in parametric processes. II," *Phys. Rev.*, vol. 129, no. 1, pp. 481–485, 1963.

[56] B. R. Mollow and R. J. Glauber, "Quantum theory of parametric amplification. I," *Phys. Rev.*, vol. 160, no. 5, pp. 1076–1096, 1967.

[57] B. R. Mollow and R. J. Glauber, "Quantum theory of parametric amplification. II," *Phys. Rev.*, vol. 160, no. 5, pp. 1097–1108, 1967.

[58] C. M. Caves, "Quantum limits on noise in linear amplifiers," *Phys. Rev. D*, vol. 26, no. 8, pp. 1817–1839, 1982.

[59] S. Stenholm, "The theory of quantum amplifiers," *Physica Scripta*, vol. 12, pp. 56–66. 1986

[60] A. A. Clerk, M. H. Devoret, S. M. Girvin, F. Marquardt, and R. J. Schoelkopf, "Introduction to quantum noise, measurement, and amplification," *Rev. Mod. Phys.*, vol. 82, no. 2, pp. 1155–1208, 2010.

[61] C. M. Caves, J. Combes, Z. Jiang, and S. Pandey, "Quantum limits on phase-preserving linear amplifiers," *Phys. Rev. A*, vol. 86, no. 6, 2012, Art. no. 063802.

[62] S. Pirandola, R. Laurenza, C. Ottaviani, and L. Banchi, "Fundamental limits of repeaterless quantum communications," *Nat. Commun.*, vol. 8, 2017, Art. no. 15043.

[63] H. Qi and M. M. Wilde, "Capacities of quantum amplifier channels," *Phys. Rev. A*, vol. 95, no. 1, 2017, Art. no. 012339.

[64] H. Elemy, "A one-way quantum amplifier for long-distance quantum communication," *Quantum Inf. Process.*, vol. 16, no. 5, 2017, Art. no. 134.

[65] N. Yamamoto, "Quantum feedback amplification," *Phys. Rev. Applied*, vol. 5, no. 4, 2016, Art. no. 044012.

[66] Z. Yan, X. Jia, X. Su, Z. Duan, C. Xie, and K. Peng, "Cascaded entanglement enhancement," *Phys. Rev. A*, vol. 85, no. 4, 2012, Art. no. 040305.

[67] W. P. He and F. L. Li, "Generation of broadband entangled light through cascading nondegenerate optical parametric amplifiers," *Phys. Rev. A*, vol. 76, no. 1, 2007, Art. no. 012328.

[68] D. Wang, Y. Zhang, and M. Xiao, "Quantum limits for cascaded optical parametric amplifiers," *Phys. Rev. A*, vol. 87, no. 2, 2013, Art. no. 023834.

[69] H. M. Wiseman and G. J. Milburn, *Quantum Measurement and Control*, Cambridge, UK: Cambridge Univ. Press, 2010.

[70] K. Jacobs, *Quantum Measurement Theory and its Applications*, Cambridge, UK: Cambridge Univ. Press, 2014.

[71] V. P. Belavkin, "Measurement, filtering and control in quantum open dynamical systems," *Rep. on Math. Phys.*, vol. 43, no. 3, pp. 405–425, 1999.

[72] L. Bouten, R. van Handel, and M. R. James, "An introduction to quantum filtering," *SIAM J. Control Optim.* vol. 46, no. 6, pp. 2199–2241, 2007.

[73] L. Bouten, R. van Handel, and M. R. James, "A discrete invitation to quantum filtering and feedback control," *SIAM Review*, vol. 51, no. 2, pp. 239–316, 2009.

[74] C. Sayrin *et al.*, "Real-time quantum feedback prepares and stabilizes photon number states," *Nature*, vol. 477, pp. 73–77, 2011.

[75] R. Inoue, S. Tanaka, R. Namiki, T. Sagawa, and Y. Takahashi, "Unconditional quantum-noise suppression via measurement-based quantum feedback," *Phys. Rev. Lett.*, vol. 110, no. 16, 2013, Art. no. 163602.

[76] H. M. Wiseman and G. J. Milburn, "All-optical versus electro-optical quantum-limited feedback," *Phys. Rev. A*, vol. 49, no. 5, pp. 4110–4125, 1994.

[77] S. Lloyd, "Coherent quantum feedback," *Phys. Rev. A*, vol. 62, no. 2, 2000, Art. no. 022108.

[78] M. Yanagisawa and H. Kimura, "Transfer function approach to quantum control– Part I: Dynamics of quantum feedback systems," *IEEE Trans. Autom. Control*, vol. 48, no. 12, pp. 2107–2120, 2003.

[79] M. Yanagisawa and H. Kimura, "Transfer function approach to quantum control– Part II: Control concepts and applications," *IEEE Trans. Autom. Control*, vol. 48, no. 12, pp. 2121–2132, 2003.

[80] M. R. James, H. I. Nurdin, and I. R. Petersen, "H^∞ control of linear quantum stochastic systems," *IEEE Trans. Autom. Control*, vol. 53, no. 8, pp. 1787–1803, 2008.

[81] H. I. Nurdin, M. R. James, and I. R. Petersen, "Coherent quantum LQG control," *Automatica*, vol. 45, no. 8, pp. 1837–1846, 2009.

[82] H. Mabuchi, "Coherent-feedback quantum control with a dynamic compensator," *Phys. Rev. A*, vol. 78, no. 3, 2008, Art. no. 032323.

[83] S. Iida, M. Yukawa, H. Yonezawa, N. Yamamoto, and A. Furusawa, "Experimental demonstration of coherent feedback control on optical field squeezing," *IEEE Trans. Autom. Control*, vol. 57, no. 8, pp. 2045–2050, 2012.

[84] R. Hamerly and H. Mabuchi, "Advantages of coherent feedback for cooling quantum oscillators," *Phys. Rev. Lett.*, vol. 109, no. 17, 2012, Art. no. 173602.

[85] K. Jacobs, X. Wang, and H. M. Wiseman, "Coherent feedback that beats all measurement-based feedback protocols," *New J. Phys.*, vol. 16, no. 7, 2014, Art. no. 073036.

[86] Y. Liu, S. Shankar, N. Ofek, M. Hatridge, A. Narla, K. M. Sliwa, L. Frunzio, R. J. Schoelkopf, and M. H. Devoret, "Comparing and combining measurement-based and driven-dissipative entanglement stabilization," *Phys. Rev. X*, vol. 6, no. 1, 2016, Art. no. 011022.

[87] J. M. Schumacher, "Compensator synthesis using (C, A, B)-pairs," *IEEE Trans. Autom. Control*, vol. 25, no. 6, pp. 1133–1138, 1980.

[88] J. M. Schumacher, "Regulator synthesis using (C, A, B)-pairs," *IEEE Trans. Autom. Control*, vol. 27, no. 6, pp. 1211–1221, 1982.

[89] W. M. Wonham, *Linear Multivariable Control: A Geometric Approach*, 3rd ed. Springer-Verlag, Berlin, 1985.

[90] G. Marro, F. Morbidi, L. Ntogramatzidis, and D. Prattichizzo, "Geometric control theory for linear systems: a tutorial," *Proceedings of the 19th MTNS*, pp. 1579–1590, 2010.

[91] N. Otsuka, "Disturbance decoupling via measurement feedback for switched linear systems," *Systems Control Lett.*, vol. 82, pp. 99–107, 2015.

[92] E. J. Routh, "Stability of a dynamical system with two independent motions," *Proceedings of the London Mathematical Society*, vol. 5, no. 1, pp. 97–99, 1874.

[93] A. Hurwitz, "On the conditions under which an equation has only roots with negative real parts," *Mathematische Annelen*, vol. 46, pp. 273–284, 1985.

[94] Y. S. Apte, "Routh-Hurwitz stability criterion and its equivalents," *IEE-IERE Proceedings - India*, vol. 7, no. 4, pp. 149–154, 1969.

[95] J. Gough and M. R. James, "The series product and its application to quantum feedforward and feedback networks," *IEEE Trans. Autom. Control*, vol. 54, no. 11, pp. 2530–2544, 2009.

[96] R. L. Hudson and K. R. Parthasarathy, "Quantum Ito's formula and stochastic evolutions," *Commun. Math. Phys.*, vol. 93, no. 3, pp. 301–323, 1984.

[97] D. F. Walls and G. J. Milburn, *Quantum Optics*, 2nd ed. Springer Berlin, 2008.

[98] K. Zhou, J. C. Doyle, and K. Glover, *Robust and Optimal Control*, Upper Saddle River, NJ, USA: Prentice-Hall, 1996.

[99] V. Giovannetti and D. Vitali, "Phase-noise measurement in a cavity with a movable mirror undergoing quantum Brownian motion," *Phys. Rev. A*, vol. 63, no. 2, 2001, Art. no. 023812.

[100] M. H. Wimmer, D. Steinmeyer, K. Hammerer, and M. Heurs, "Coherent cancellation of backaction noise in optomechanical force measurements," *Phys. Rev. A*, vol. 89, no. 5, 2014, Art. no. 053836.

[101] O. Crisafulli, N. Tezak, D. B. S. Soh, M. A. Armen, and H. Mabuchi, "Squeezed light in an optical parametric oscillator network with coherent feedback quantum control," *Opt. Express*, vol. 21, no. 15, pp. 18371–18386, 2013.

[102] M. J. Hartmann and M. B. Plenio, "Steady state entanglement in the mechanical vibrations of two dielectric membranes," *Phys. Rev. Lett.*, vol. 101, no. 20, 2008, Art. no. 200503.

[103] M. Bhattacharya and P. Meystre, "Multiple membrane cavity optomechanics," *Phys. Rev. A*, vol. 78, no. 4, 2008, Art. no. 041801.

[104] W. H. P. Nielsen, Y. Tsaturyan, C. B. Møller, E. S. Polzik, and A. Schliesser, "Multimode optomechanical system in the quantum regime," *Proceedings of the National Academy of Sciences*, vol. 114, no. 1, pp. 62–66, 2017.

[105] S. L. Vuglar and H. Amini, "Design of coherent quantum observers for linear quantum systems," *New J. Phys.*, vol. 16, no. 12, 2014, Art. no. 125005.

[106] Z. Miao, M. R. James, and I. R. Petersen, "Coherent observers for linear quantum stochastic systems," *Automatica*, vol. 71, pp. 264–271, 2016.

[107] A. Kamal, J. Clarke and M. H. Devoret, "Gain, directionality, and noise in microwave SQUID amplifiers: Input-output approach," *Phys. Rev. A*, vol. 86, no. 14, 2012, Art. no. 144510.

[108] J. E. Gough, M. R. James, and H. I. Nurdin, "Squeezing components in linear quantum feedback networks," *Phys. Rev. A*, vol. 81, no. 2, 2010, Art. no. 023804.

[109] I. R. Petersen, "Quantum linear systems theory," *Proceedings of the 19th MTNS*, pp. 2173–2184, 2010.